Combined Action Observation, Motor Imagery and Steady State Motion Visual Evoked Potential Based Brain Computer Interface System

By

Aravind Ravi

A thesis
presented to the University of Waterloo
in fulfillment of the
thesis requirement for the degree of
Doctor of Philosophy
in
Systems Design Engineering

Waterloo, Ontario, Canada, 2024

©Aravind Ravi 2024

Examining Committee Membership

The following served on the Examining Committee for this thesis. The decision of the committee is by majority vote.

External Examiner:	Dr. James Norton Research Scientist, Adjunct Professor, Dept. of Electrical and Computer Engineering National Center for Adaptive Neurotechnologies, University at Albany
Supervisor:	Dr. James Tung Associate Professor, Dept. of Systems Design Engineering University of Waterloo
Co-Supervisor:	Dr. Ning Jiang Adjunct Professor, Dept. of Systems Design Engineering University of Waterloo
Internal Member:	Dr. Shi Cao Associate Professor, Dept. of Systems Design Engineering University of Waterloo
Internal Member:	Dr. Richard Nuckols Adjunct Professor, Dept. of Systems Design Engineering University of Waterloo
Internal-External Member:	Dr. Richard Staines Professor, Dept. of Kinesiology University of Waterloo

Author's Declaration

This thesis consists of material all of which I authored or co-authored: see *Statement of Contributions* included in the thesis. This is a true copy of the thesis, including any required final revisions, as accepted by my examiners.

I understand that my thesis may be made electronically available to the public.

Statement of Contributions

The publications during the doctoral studies that resulted from the work presented in this thesis and outside of the thesis are summarized below. All experimental results, figures, and text are generated from my own work during the Ph.D. research.

Publications and manuscripts presented in the Thesis

1. **Aravind Ravi**, et. al. *Combined Action Observation, Motor Imagery and SSMVEP BCI Enhances Movement Related Cortical Potential.* 11th International IEEE/EMBS Conference on Neural Engineering (NER) (2023) [1].
2. **Aravind Ravi**, et. al. *Signal Characteristics, Motor Cortex Engagement, and Classification Performance of Combined Action Observation, Motor Imagery and SSMVEP (CAMS) BCI.* IEEE Transactions in Neural Systems and Rehabilitation Engineering [Under Revision] (2024).
3. **Aravind Ravi**, et. al. *EEG-Based Gait Phase Decoding from Combined Action Observation and Motor Imagery.* IEEE Transactions in Neural Systems and Rehabilitation Engineering [Under Revision] (2024).
4. **Aravind Ravi**, et. al. *Enhancing the decoding performance of asynchronous visual CAMS BCI.* [In Preparation] (2024).

Other publications and patents during the doctoral studies

1. R.Z. Gao, P. S. Lee, **Aravind Ravi**, et. al. "Hybrid Soft-Rigid Active Prosthetics Laboratory Exercise for Hands-On Biomechanical and Biomedical Engineering Education." Journal of Biomechanical Engineering 146, no. 5 (2024).
2. C. Aimone, G. Moffat, H. J. Banville, SUN Wood, S. Padmanaban, S. Kerr, and **Aravind Ravi**. "System and method for brain modelling." U.S. Patent Application 18/201,502, filed October 5, 2023.
3. M. Abou Jaoude, **Aravind Ravi**, et. al. "Automated Sleep Staging on Wearable EEG Enables Sleep Analysis at Scale." In 2023 11th International IEEE/EMBS Conference on Neural Engineering (NER), pp. 1-4. IEEE, 2023.
4. S. Pearce, **Aravind Ravi**, et. al. "Asynchronous brain computer interface in ar using steady-state motion visual evoked potential." U.S. Patent Application 17/713,622, filed October 13, 2022.
5. **Aravind Ravi**. "Classification of microscopy images of breast tissue: Region duplication based self-supervision vs. off-the shelf deep representations." arXiv preprint arXiv:2202.06073 (2022).
6. **Aravind Ravi**, et. al. "Enhanced system robustness of asynchronous BCI in augmented reality using steady-state motion visual evoked potential." IEEE Transactions on Neural Systems and Rehabilitation Engineering (2022) [2].
7. **Aravind Ravi**, et. al. "Asynchronous SSMVEP BCI and influence of dynamic background in augmented reality." In 2021 27th International Conference on Mechatronics and Machine Vision in Practice (M2VIP) (2021) [3].
8. Y. Gao, **Aravind Ravi**, et. al. "Effect of competing stimuli for steady-state visually evoked potential and steady-state motion visually evoked potential." IEEE Access (2021).
9. Y. Gao, **Aravind Ravi**, et. al. "Does inter-stimulus distance influence the decoding performance of SSVEP and SSMVEP BCI?" In 2021 10th International IEEE/EMBS Conference on Neural Engineering (NER) (2021)
10. X. Zhang, G. Xu, **Aravind Ravi**, et. al. Can a highly accurate multi-class SSMVEP BCI induce sensory-motor rhythm in the sensorimotor area? Journal of Neural Engineering (2021) [4].

11. **Aravind Ravi**, et. al. Comparing user-dependent and user-independent training of CNN for SSVEP BCI. Journal of neural engineering (2020) [5].

Abstract

Stroke is one of the leading causes of long-term acquired disability in adults worldwide. Gait recovery is a major objective in post-stroke rehabilitation programs. Conventional gait therapy encourages patient involvement, but the results can be slow and/or limited, leading to sub-optimal recovery. Active patient involvement, collaboration, and motivation are key factors that promote efficient motor learning. Therefore, there is a need to develop novel rehabilitation strategies to enhance user engagement by utilizing their movement intent. Brain-computer interfaces (BCIs) based on electroencephalography (EEG) offer an attractive approach for rehabilitation as they enable an alternative method for active participation in therapy. Current visual BCIs provide high decoding accuracy but typically do not activate sensorimotor areas critical for motor recovery. Conversely, BCIs based on motor imagery (MI) activate motor areas but suffer from high inter-subject variability and long user training, resulting in poorer movement intent detection accuracy and potentially leading to high cognitive demand.

This thesis proposed a novel BCI paradigm called CAMS—Combined Action Observation (AO), Motor Imagery (MI), and Steady-State Motion Visual Evoked Potentials (SSMVEP). The CAMS paradigm aimed to induce acute changes in movement-related areas of the cortex through the observation and imagery of gait movements, activating both motor and visual cortices to elicit SSMVEP-like responses. Furthermore, the responses elicited by the CAMS paradigm were investigated in two distinct applications to detect user movement intent with the aim of actively engaging the participant. The research conducted across three studies investigates the efficacy of CAMS in enhancing cortical excitability, decoding gait phases, and improving asynchronous visual BCI performance. Twenty-five healthy volunteers

participated in this study wherein they observed and imagined lower limb movements of gait as part of the CAMS intervention, which was compared with an SSMVEP control condition.

Study I aimed to investigate the acute changes in cortical excitability induced by the CAMS intervention. The results demonstrated significant increases in movement-related cortical potential (MRCP) components, indicating enhanced cortical excitability. For instance, the magnitude of BP1 at channel C1 increased from -1.41 ± 0.54 μV pre-intervention to -3.23 ± 0.5 μV post-intervention ($p = 0.009$), highlighting the potential of CAMS to engage motor-related brain areas and promote neuroplasticity. Study II focused on decoding the phases of gait (swing and stance) from EEG responses elicited by the CAMS paradigm. Using Linear Discriminant Analysis (LDA) and Support Vector Machine (SVM), the study achieved a classification accuracy of 75% and 78%, respectively, in decoding the swing and stance phases of gait. Study III introduced a novel detection algorithm based on Complex Convolutional Neural Networks (C-CNN) for asynchronous offline CAMS BCI. The C-CNN method achieved high F1-scores for asynchronous operation. Median F1-scores for C-CNN were 0.88 (W=1s), 0.92 (W=2s), and 0.96 (W=3s), with corresponding False activation rates (FARs) of 0.34, 0.30, and 0.27. Additionally, larger stimulus frequency differences resulted in stronger visual BCI classification performance, with combinations (7.5 Hz, 12 Hz) and (8.57 Hz, 12 Hz) yielding the highest accuracies of 87% and 78%, respectively.

These findings underscore the potential of the CAMS BCI paradigm in enhancing cortical excitability, eliciting responses for decoding gait phases, and improving asynchronous visual BCI performance while simultaneously engaging the movement related areas of the cortex. By providing a comprehensive investigation of the CAMS paradigm, this work contributes to existing knowledge and helps guide future clinical applications in neurorehabilitation.

Acknowledgements

I would like to express my sincere gratitude to my supervisors, Professor James Tung and Professor Ning Jiang, for their constant support, guidance, valuable insights, and patience throughout my Ph.D. journey. I am grateful to be part of two labs, the Engineering Bionics Lab and the Neural and Rehabilitation Engineering Lab, which provided me with the opportunity to interact with a diverse group of students and researchers and explore creative ideas.

I extend my thanks to my co-authors Paul Wolfe, Runze Gao, Nargess Heydari, Yuanpei Gao, Jing Lu, Xin Zhang, and Sarah Pearce for their collaboration in conducting this research. I also thank the members of our lab: Paul, Andrew, Alyson, Christian, Shovon, Naomi, Erica, Jun Song, Ashirbad, Nargess, Fatemeh, Yuanpei, and Amy for their engaging discussions, support in data collection, and research efforts.

Special thanks to Prof. Richard Staines, Prof. Shi Cao, and Prof. Richard Nuckols for being part of my thesis committee, taking the time to review my thesis, and providing valuable suggestions. I also extend my gratitude to Professor James Norton for being an external committee member and for his valuable suggestions.

I extend my heartfelt gratitude to Mr. Sastry Ramachandrula, whose continuous inspiration since my undergraduate days and guidance from afar have been instrumental in my pursuit of academic research.

I would like to acknowledge the scholarship programs offered by Government of Ontario - Ontario Graduate Scholarship (OGS), University of Waterloo - President's Graduate Scholarship (PGS), and Department of Systems Design Engineering for providing the much-needed financial support throughout my Ph.D. Furthermore, this work was partially funded by the Government of Ontario's Early Researcher Award (ERA) program.

I extend my gratitude to the participants who volunteered to take part in my study.

I thank my parents, Mr. Ravi Soundararajan and Mrs. Kalyani Ravi, for raising me to value education and inspiring me throughout my life. I deeply appreciate my sister, Aarthi Ravi, for her encouragement and support, often serving as my pilot subject for many initial trials. I thank my beloved wife, Smrutha Kothanda Raman, for her infinite support and guidance. I also thank all my relatives and friends for their support.

Finally, I pay my obeisance to God, the Almighty, for bestowing upon me good health, strength, courage, inspiration, and guidance.

The following verse from the Bhagavad Gita, Chapter 2, Verse 47, has guided me throughout my academic journey:

"You have the right to work only but never to its fruits.
Let not the fruits of action be your motive, nor let your attachment be to inaction."

Dedication

To my beloved parents, wife, sister, and brother-in-law.

Table of Contents

Examining Committee Membership ii
Author's Declaration iii
Statement of Contributions iv
Abstract vii
Acknowledgements ix
Dedication xi
List of Figures xvi
List of Tables xix
List of Abbreviations xx
Chapter 1 Introduction 1
Chapter 2 Background and Literature Review 7
2.1 Brain Computer Interfaces (BCI) 7
2.1.1 Signal Acquisition and Electroencephalography 7
2.2 BCI Paradigms and EEG Signal Modalities 8
2.2.1 Movement Related Cortical Potentials (MRCP) 9
2.2.2 Action Observation and Motor Imagery Paradigm 11
2.2.3 Visual BCIs: SSVEP, SSMVEP and Hybrid CAMS BCI 12
2.3 Feature Extraction and Classification for EEG based BCIs 13
2.3.1 Feature Extraction 13
2.3.2 Supervised learning and Classification 14
2.4 BCI for Lower Limb Motor Rehabilitation 15
2.4.1 BCIs for Gait Recovery and Decoding Phases of Gait from EEG 15
2.5 Motivation and Thesis Outline 18
2.5.1 Study I 18

2.5.2 Study II 19
2.5.3 Study III 20
Chapter 3 Experiments and Data Collection 21
3.1 Participant Recruitment 21
3.2 Stimulus Design 21
3.2.1 CAMS Stimulus Design 22
3.2.2 Data Acquisition 23
3.2.3 Experimental Protocol 24
Chapter 4 Study I: Combined Action Observation, Motor Imagery and SSMVEP BCI enhances Movement Related Cortical Potentials 27
4.1 Methodology 27
4.1.1 Pre- and Post- Movement Related Cortical Potentials Analysis 27
4.1.2 Visual Stimulus Response Characteristics Analysis 29
4.1.3 Statistical Analysis 30
4.2 Results 31
4.2.1 Pre-/Post- MRCP Measurements CAMS and SSMVEP 31
4.2.2 Visual and Motor Responses for CAMS and SSMVEP 33
4.3 Discussions 35
4.3.1 CAMS BCI Enhances Cortical Excitability 35
4.3.2 CAMS Stimulus Activates Visual and Motor Areas 36
4.3.3 Challenges and Limitations 37
4.3.4 Applications and Conclusions 38
Chapter 5 Study II: EEG-Based Gait Phase Decoding from Combined Action Observation and Motor Imagery 40
5.1 Methodology 40

5.1.1 Pre-processing and Data Labelling 40
5.1.2 Feature Extraction and Decoding phases of Gait 42
5.1.3 Performance Evaluation 44
5.1.4 Statistical Analysis 46
5.2 Results 46
5.2.1 Gait Phase Classification Performance 46
5.2.2 Group-level performance and Frontal Alpha Power 49
5.2.3 Trial-level Performance 50
5.2.4 Spatial Contributions from Cortical Areas 51
5.3 Discussions 52
5.3.1 Gait Phase Decoding from CAMS Stimulus 52
5.3.2 Influence of Attention and Cortical Contributions on Decoding Performance 54
5.3.3 Challenges and Limitations 55
5.3.4 Applications and Conclusions 56
Chapter 6 Study III: Enhancing the Asynchronous Visual BCI Decoding Performance in the CAMS Paradigm 58
6.1 Methodology 58
6.1.1 Dataset Preparation and Pre-processing 58
6.1.2 Canonical Correlation Analysis (CCA) 59
6.1.3 Complex Convolutional Neural Networks (C-CNN) 60
6.1.4 Asynchronous CAMS IC versus NC Detection 65
6.1.5 Performance Evaluation 66
6.1.6 Statistical Analysis 68
6.2 Results 68

6.2.1 Baseline Performance Analysis with Synchronous CCA 68
6.2.2 Enhanced decoding performance with C-CNN..... 69
6.2.3 Asynchronous IC Vs. NC CAMS BCI Performance 71
6.3 Discussions 73
6.3.1 CCA Provides Reasonable Baseline Visual BCI Accuracy..... 73
6.3.2 Comparative Analysis of C-CNN and CCA Performance in Visual BCI..... 74
6.3.3 Asynchronous C-CNN Performance and Pseudo-online Detection 74
6.3.4 Challenges and Limitations..... 75
6.3.5 Applications and Conclusions..... 76
Chapter 7 Conclusions and Future Work 79
7.1 Highlights of Thesis Contributions..... 79
7.1.1 Novel BCI Intervention to Induce Cortical Excitability 79
7.1.2 Decoding Phases of Gait from EEG..... 80
7.1.3 Development of Novel Classification Algorithm for Asynchronous CAMS BCI Operation..... 80
7.2 Future Work..... 81
7.2.1 CAMS in Augmented Reality and Assessing the Signal Characteristics 81
7.2.2 Developing a Closed loop Real-Time System with Feedback..... 81
7.2.3 Translating the CAMS BCI with feedback in Individuals Post-Stroke 82
7.2.4 Conclusions..... 82
References 84
Appendix A 101
A.1 Open Sourced Code Related to the Thesis..... 101

List of Figures

Figure 2-1. The International 10-20 system for EEG. 8
Figure 2-2. Gait phase decoding application, FES denoted by green thunderbolt. 16
Figure 3-1. CAMS stimulus generation and frames used for single gait cycle 22
Figure 3-2. SSMVEP Checkerboard Stimulus..... 22
Figure 3-3. Data Acquisition hardware illustrating the EEG cap with the g.Scarabeo electrodes, the g.GammaBox driver and g.USBAmp Amplifier 23
Figure 3-4. Experiment Protocol..... 24
Figure 3-5. Ankle Dorsiflexion (Pre/Post) Protocol 24
Figure 3-6. Cueing screen and Visual Stimulus Screen (CAMS and SSMVEP) 25
Figure 3-7. Experimental setup showing A. pre/post measurements (left) and B. CAMS intervention (right). 26
Figure 4-1. MRCP components regions of interest: BP1, BP2 and PN..... 28
Figure 4-2 MRCP averages across participants for the channels C1, Cz, C2, CPz and FCz for 'pre' (light blue) and 'post' (dark blue) conditions for CAMS (A) and SSMVEP (B), t = 0 s (movement onset). Significant differences ($p < 0.05$) highlighted in grey. 31
Figure 4-3. Averaged magnitude spectrum for CAMS (A) and SSMVEP (B) responses averaged across channels O1, Oz and O2; all participants for stimulus frequencies: 7.5 Hz, 8.57 Hz, 10 Hz and 12 Hz. Insets for CAMS (A) illustrate responses corresponding to the CAMS step frequency. 34
Figure 4-4. Average ERDS map and temporal dynamics of the ERD index across all participants, channels (C1, Cz, C2) and trials for CAMS (A) and SSMVEP (B) across all stimulus frequencies across the 8 s trial; mu (8 Hz – 12 Hz) and beta (12 Hz – 26 Hz) bands, t = 0 s (onset)..... 35

Figure 5-1. Trialwise Swing/Stance assignment. 41
Figure 5-2. Trial level windowing and segment-wise labeling strategy. 42
Figure 5-3. EEG Processing and Classification Pipeline. 43
Figure 5-4. (A) F1 scores, (B) Stance accuracy and (C) Swing accuracy across participants for stimulus frequencies 7.5 Hz, 8.57 Hz, 10 Hz, 12 Hz for the methods Broad+LDA, Broad+SVM and Delta+LDA. 47
Figure 5-5. Confusion matrices for 'Broad+LDA' for 7.5 and 8.57 Hz. 48
Figure 5-6. Frontal alpha power for 7.5 Hz and 8.57 Hz grouped as responder (A) and non-responder (B). 49
Figure 5-7. F1 score for 7.5 Hz and 8.57 Hz for 'Broad+LDA' grouped as responder (A); non-responder (B). 49
Figure 5-8. Examples of detected gait phases for two trials and two participants for 7.5 Hz (A) and 8.57 Hz (B). 51
Figure 5-9. Region of interest channel contribution to Swing/Stance classification LDA Broad classifier. 51
Figure 6-1. Illustration of the canonical correlation analysis applied on multi-channel EEG [62] 60
Figure 6-2. Convolutional Neural Network Architecture 62
Figure 6-3. Asynchronous classification–Intentional control and no control state. 65
Figure 6-4. CAMS visual BCI classification accuracy for each visual stimulus combination, window lengths [1s, 8s] across all participants using Synchronous CCA. 69
Figure 6-5. CAMS visual BCI accuracy versus stimulus frequency differences using Synchronous CCA. 69
Figure 6-6. Asynchronous CAMS visual BCI accuracy comparing CCA versus C-CNN for W=[1s, 5s]. 70

Figure 6-7. Box-plots of F1-score and False activation rate (FAR) for asynchronous IC versus NC detection for stimulus frequency combination (10 Hz, 12 Hz) and W = [1s, 2s, 3s] with whiskers extending from upper and lower quartile to minimum and maximum values..... 71
Figure 6-8. TPR versus FPR characteristics for asynchronous IC versus NC detection for stimulus frequency combination (10 Hz, 12 Hz) and W = [1s, 2s, 3s]. Dotted line indicates the chance level TPR versus FPR. 72
Figure 6-9. Temporal evolution of the pseudo-online C-CNN classifier of IC and NC states on a single participant's session; W = 1 s. Top: Averaged EEG spectrogram computed across channels POz, O1, O2 and Oz; Bottom: true and predicted labels. 73
Figure 6-10. Asynchronous CAMS visual BCI speed control of a treadmill. 77

List of Tables

Table 4-1. MRCP components averaged amplitude differences (Post – Pre) across the five channels C1, Cz, C2, FCz and CPz across all participants for CAMS (C) and SSMVEP (S) stimulus, * indicates significant difference ($p < 0.05$) based on the Mann-Whitney U test… 32
Table 5-1. CAMS visual stimulus design parameters..... 40

List of Abbreviations

AD	Ankle Dorsiflexion
AO	Action Observation
BCI	Brain Computer Interface
CAMS	Combined Action Observation Motor Imagery and Steady State Visual Evoked Potential
CCA	Canonical Correlation Analysis
CNN	Convolutional Neural Network
EEG	Electroencephalography
ERD/S	Event Related Desynchronization/Synchronization
FFT	Fast Fourier Transform
ITR	Information Transfer Rate
MI	Motor Imagery
SNR	Signal-to-Noise Ratio
SSVEP	Steady State Visual Evoked Potential
SSMVEP	Steady State Motion Visual Evoked Potential

Chapter 1
Introduction

Stroke is one of the leading causes of long-term acquired disability in adults. It is the third largest cause of death and tenth largest contributor to disability in Canada [6]. A stroke occurs when there is a sudden loss of brain function caused by a lack of blood supply (i.e., ischemic), or bleeding (i.e., hemorrhagic), to a part of the brain. This deprives the cells of oxygen and nutrients, ultimately leading to the death of cells in the specific brain region. Some of the common debilitating effects of stroke include impaired motor control, general cognitive deficits, difficulties in generating or processing speech, and altered emotional state [7]. Impaired motor control commonly manifests as hemiplegia and hemiparesis, which leads to loss of motor function on one side of the body, contralateral to the damaged hemisphere of the brain. After stroke, up to 85% of stroke survivors experience impairments in the upper extremity. With respect to impairments of the lower extremity, approximately 20% of the survivors remain dependent on a wheelchair at three months after a stroke and approximately 70% walk with reduced capacity [8].

Post-stroke treatment typically involves restoration of the motor functions through various rehabilitative training protocols. Rehabilitative therapy typically begins in the acute stage within 48 hours after the stroke. Task-specific high intensity restorative exercises are provided to increase mobility and strength in stroke-impaired limbs. Additionally, constraint-induced movement therapy (CIMT) intervention may also be provided as a treatment by constricting the movements of the non-paretic arm with a mitt or sling, while intensively inducing the use of the hemi-paretic arm. Participants must have some residual hand function, high motivation, adequate balance, and adequate walking ability while wearing the restraint to be eligible for the CIMT intervention. This limits the applicability of such protocols in patients with severe motor impairments. Similarly, gait recovery is a major objective in post-stroke rehabilitation programs. High intensity gait training is provided for patients with impairments in lower limb function [9]. In conventional gait therapy, the physiotherapist corrects and

facilitates their movement. Exercise programs are highly customized for each patient and require constant involvement from skilled therapists. These programs encourage patient involvement in the therapy, but the results of the expended effort can be slow and limited leading to sub-optimal recovery [10]. Furthermore, manual handling and reduced availability of human resources make these protocols challenging for patients who are physically dependent [11].

To overcome such limitations, assistive gait devices have been proposed and developed to enable people to walk with the help of external assistance, such as robotics/exoskeletons [12] or functional electrical stimulation (FES) [13], [14]. This allows for high repetition and high intensity with reduced involvement from the therapist. However, robotic-assisted rehabilitation alone has not been shown to be effective compared to conventional therapy [11], [12], [15]. Furthermore, these protocols have been criticized for allowing the patients to be too passive, with reduced effort/intent by the subject, lower metabolic activity [12], and muscle activations. The patient's active involvement [16], [17], collaboration and motivation are key factors that promote efficient motor learning [18]. Previous studies have shown that active training can enhance motor function and cortical excitability compared to passive training [19]. Therefore, there is a need to develop a novel rehabilitation strategy to promote active user engagement by utilizing the movement intent [20].

In conjunction with robotic gait devices, brain computer interfaces (BCIs) based on electroencephalography (EEG) are an attractive approach for rehabilitation as it enables active participation in therapy [7]. BCIs can be especially useful for people with severe disabilities where the central nervous system is intact but are unable to communicate due to damage in the (central or peripheral) nervous and/or musculoskeletal systems. A BCI can obtain the patient's volition explicitly from the neurological signals and utilize them by bypassing the damaged pathways to provide the user with the ability to communicate or interact effectively with their surroundings. BCIs provide novel possibilities for neurorehabilitation for people with

neurological disease such as stroke, amyotrophic lateral sclerosis (ALS) or paralysis [21], [22], [23]. EEG is the most popular non-invasive method for recording neural activity from the surface of the scalp. EEG based BCIs, paired with robotic gait devices or real-time feedback, provide a novel strategy for active rehabilitation by decoding the user's intention to move their affected limb, and the system can provide relevant feedback to enhance user engagement [24].

The most successful EEG based BCI paradigms rely on P300 responses or steady-state visually evoked potentials (SSVEP) [25], [26]. These paradigms are discussed in more detail in Section 2.2. Briefly, SSVEP are steady-state responses elicited, primarily in the occipital cortex, due to a repetitive visual stimulus (flickering at a fixed frequency). Recently, steady state motion visual evoked potential (SSMVEP) based BCIs have gained interest as they reduce visual discomfort and perform like SSVEP BCIs [2]. SSMVEP are responses elicited due to repetitive motion-based stimulus. This paradigm does not require lengthy user training and little-to-no algorithm calibration, in contrast with BCIs based on motor imagery (MI), commonly investigated in BCI studies for stroke rehabilitation [5]. However, while visual BCIs offer high decoding accuracy for communication and control applications, they alone are incapable of activating or stimulating the sensorimotor areas critical for facilitating motor recovery.

BCIs based on sensorimotor rhythm (SMR) and movement related cortical potentials (MRCP) to detect motor imagery (MI) have been applied in the context of stroke rehabilitation [27]. In the case of MI-BCI, the user mentally imagines a limb movement which produces a distinct type of brain activity called sensorimotor rhythm (SMR) [28]. Next, the BCI translates the decoded activity into useful control commands providing relevant sensory-motor feedback to the user in various forms such as functional electrical stimulation (FES) [14] [29], electrical stimulation of the peroneal nerve [30], and/or visual feedback [31]. While the specific role of the primary motor cortex remains to be elucidated, reports indicate the structure is active during imagined movements [32] [33]. Moreover, it has been shown when the decoded motor

intention is paired with properly timed feedback, it can induce efficient neural plasticity [30], [34].

Although several studies have used a MI-BCI approach, some limitations exist. It is estimated that 15-30% of users are unable to elicit a sufficiently clear brain response which is termed as BCI illiteracy [35] [36]. Next, MI-BCI therapies require the patient to maintain sustained attention to the mental imagery task for extended periods of time, which can cause fatigue. MI-BCIs also require a long user training time and calibration before they can be used in real-time [7]. Patients with severe cognitive impairments who are incapable of sustaining attention would become ineligible for such therapies. Finally, MI can be imagined in many ways, which can lead to high inter-subject and inter-session variability. Therefore, there is a need to develop an advanced protocol that provides an intuitive task and elicits stronger and consistent sensorimotor response across subjects.

Action observation (AO) therapy has been demonstrated to have positive rehabilitation outcomes in stroke patients [37], [38]. In this type of intervention, participants are shown videos of limb movements and asked to observe them carefully. The observation of actions has been suggested to activate the same brain regions as those involved in motor imagery and execution [39]. Furthermore, studies have suggested that combined AO + MI (observe and imagine the action) likely produces stronger activations of the sensorimotor areas compared to AO or MI alone [40]. Moreover, providing a visual stimulus during MI will likely enhance user engagement and reduce cognitive demand. Lately, there has been an increased interest in using action observation along with motor imagery as a combined approach for post-stroke therapy [41], [42].

Recently, a novel hybrid BCI was introduced combining the benefits of reduced user training while simultaneously stimulating the sensorimotor area [4]. During combined AO + MI of gait, a significant increase in the event-related desynchronization (ERD) in the mu-band

at Cz was observed along with an SSMVEP BCI accuracy of 90% on four classes using canonical correlation analysis (CCA) [4]. In the current study, this hybrid modality will be referred to as CAMS BCI. CAMS stands for Combined Action observation, Motor imagery and SSMVEP BCI. It is designed to leverage multiple visual stimuli presented on a computer screen, catering towards a multi-class BCI. Previous studies have focused on assessing the efficacy of the visual BCI performance, with emphasis on using occipital EEG electrodes. While this is important for assistive control applications, it is unknown if this BCI can induce changes in the movement-related regions of the cortex when used for an extended period, which would facilitate applications in motor rehabilitation.

Firstly, in this Ph.D. thesis, a novel BCI intervention aimed at inducing acute change in cortical excitability in movement related areas of the cortex based on the CAMS paradigm is proposed. EEG signal characteristics of the visual responses and motor responses during the intervention were quantified using the magnitude spectrum and ERD index, respectively. Changes in signal characteristics pre- and post- intervention are compared to examine short-term changes in cortical excitability.

Secondly, while BCIs decoding motor intent from MI have shown success in upper-limb tasks, their application to gait phase decoding remains underexamined [43]. EEG-based BCIs have shown feasibility in decoding the user's intention such as movement intent [44], [45], [46], walking patterns [43], [47] and gait training via motor imagery [19], [48], [49] and providing congruent feedback to the user. As mentioned previously, providing congruent motor feedback by methods such as FES, robotics, peroneal nerve stimulation, and/or visual feedback, based on BCI detection of movement intent has demonstrated the potential to induce neural plasticity. For this feedback mechanism, the detection of motor intent needs to be accurate and timely to provide feedback to the user. The dataset collected as part of this thesis, specifically, during the CAMS intervention period, was used to develop novel classifiers that can decode the user's intent to provide active feedback during BCI use. Two types of strategies

are examined: 1) a novel gait phase decoder based on EEG and 2) an asynchronous visual CAMS BCI.

The remainder of the thesis is organized as follows: Chapter 2 provides the background and literature review for this project: Sections 2.1 to 2.4 provide the background and literature review, Section 2.5 outlines the motivation, hypotheses and the studies conducted for this project. Chapter 3 describes the participant recruitment, stimulus design and experiments. Chapter 4 focuses on study I: investigating the influence of CAMS on MRCP. Chapter 5 focuses on study II providing a detailed methodology of decoding phases of gait from the responses of CAMS stimulus. Chapter 6 details study III highlighting the design and analysis of a visual BCI based on CAMS responses and provides the methodology for enhancing the overall BCI performance. Finally, Chapter 7 discusses the overall findings, proposes directions for future work and concludes the thesis.

Chapter 2

Background and Literature Review

2.1 Brain Computer Interfaces (BCI)

A brain-computer interface (BCI) is a system that measures brain activity and converts it in (nearly) real-time into functionally useful outputs to replace, restore, enhance, supplement, and/or improve the natural outputs of the brain, thereby changing the ongoing interactions between the brain and its external or internal environments [50]. It may additionally modify brain activity using targeted delivery of stimuli to create functionally useful inputs to the brain. A BCI system consists of five consecutive stages: signal acquisition, pre-processing, feature extraction, classification and control interface or application. The following sections provide an overview of each stage and explain the different BCI modalities and operation strategies.

2.1.1 **Signal Acquisition and Electroencephalography**

Different methods are used to record and monitor brain activity [24]. Brain imaging techniques such as functional magnetic resonance imaging (fMRI) and functional near-infrared spectroscopy (fNIRS) can be used to monitor changes in brain activity at specific parts of the brain. The neuronal activity can also be recorded and monitored by measuring the changes in the electrical activity of the brain with invasive techniques such as: intra-cortical electrode arrays, subdural/epidural from the cortex (also known as Electrocorticography or ECoG) [51], minimally invasive using endovascular implants such as Stentrode [52] , or non-invasively from the scalp of the user (Electroencephalography or EEG). Another non-invasive method is based on measuring the magnetic activity by means of magnetic induction known as Magnetoencephalography (MEG) [53].

BCIs based on EEG are popular as they have the following desirable properties: non-invasiveness, high portability, high temporal resolution, ease of use, low-cost and few risks to users. The first attempt to develop an EEG based BCI system was by Vidal et. al. [54]. An EEG recording system consists of electrodes, amplifiers, analog-to-digital converters and a signal acquisition device. The EEG system measures the potential difference between a signal electrode and a reference electrode. An additional ground electrode is used to measure the differential voltage between the signal electrode and the reference electrode, used for common mode rejection. These electrodes are usually coated with silver-chloride (AgCl) and a conductive gel is used to maintain good electrode-scalp contact (impedance usually between 1 kΩ and 10 kΩ). The electrodes are commonly placed at locations on the scalp based on the International 10-20 system (Figure 2-1).

2.2 BCI Paradigms and EEG Signal Modalities

BCIs can be classified based on the mode of operation by the user: (i) endogenous or exogenous BCIs [55] (ii) synchronous or asynchronous BCIs and (iii) dependent or independent BCIs. Endogenous BCIs allows the user to voluntarily modulate his/her neuronal activity based on intention. The BCI is based on spontaneously generated brain patterns. For example, in Motor Imagery (MI BCI) [28], the user imagines a motor movement such as moving the right/left hand or performs an ankle dorsiflexion [45]. These imagined movements

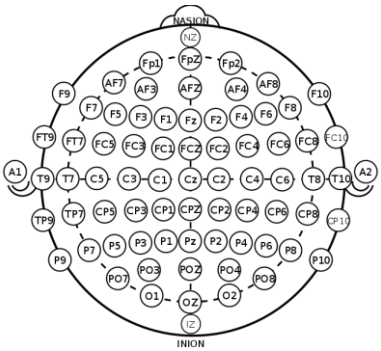

Figure 2-1. The International 10-20 system for EEG.

elicit distinct responses in the EEG which can be detected and translated into a BCI command. Other types of endogenous BCIs include: slow cortical potentials (SCP) and, imagined tactile responses. Exogenous BCIs are based on responses elicited due to an external stimulus. These responses are generated when the user focuses his/her attention on a stimulus associated with a BCI command. Examples include P300, steady-state visual evoked potentials (SSVEP) based BCIs, and steady-state motion visual evoked potential (SSMVEP) [56]. Exogenous BCIs do not require extensive user training compared to endogenous BCIs.

Synchronous and asynchronous BCIs are classified based on the BCI operation strategy and input signal processing modality. Synchronous BCIs analyze the signals at pre-determined time windows and are usually tied to a temporal cue. Therefore, the user is only allowed to send commands during these time periods and the signals outside the window are ignored. On the other hand, asynchronous BCIs continuously monitor and analyze the changes in the neuronal activity offering a more natural mode of interaction [24]. P300 BCIs are tied to a cue/trigger corresponding to the stimulus and are therefore termed synchronous BCI. MI and SSVEP based BCIs do not necessarily need a cue/trigger and are examples of asynchronous BCIs [2] [19], [27].

Dependent BCIs require the user to have some control over their peripheral nerves and muscles (e.g. gaze control of the eyes). For example, SSVEP BCIs that depend on the user's ability to fixate and focus on an external stimulus are Dependent BCIs. In contrast, BCIs that completely rely on volitional control are considered independent. Independent SSVEP BCIs based on user's covert attention [21], [22], [58] have been proposed, but have lower performance compared to the former case.

2.2.1 **Movement Related Cortical Potentials (MRCP)**

The Movement Related Cortical Potential (MRCP) is a low frequency (0 Hz – 5 Hz) negative shift in EEG signal that precedes movement onset. This is often synonymously used

with the Bereitschaftspotential (BP), which is a negative cortical potential that develops 1.5 s prior to the onset of a self-paced movement [59]. The various components of this signal can be attributed to movement preparation and movement execution. Neural generators involved include the pre-motor cortex, cingulate motor areas, (pre-)supplementary motor area (SMA) and primary motor cortex (PMC) [59], [60]. The hypothesis on neural generators suggests that early BP (BP1) activity occurring between 0.5 and 2 seconds prior to movement, is generated by the pre-SMA/SMA. In contrast, late BP (BP2) is associated with the subsequent activation of the contralateral motor cortex. Additionally, BP is thought to reflect the sequential activation of the SMA and M1 prior to self-paced movement, with SMA preceding M1. The components of the MRCP have been used to measure the induction of cortical plasticity [61], skill acquisition and motor training [45], [46], [59], [60], [62], [63], [64], [65]. The study presented by [60] observed an increase in the MRCP amplitude of palmar grasp movements after a single session of motor training and a decrease in MRCP amplitude after six sessions of training. Another study [62] reported an increase in MRCP amplitude after a single bout of aerobic exercise. The increases in negativity of the MRCP were attributed to an increase in cortical excitability. Inline with the observations of [60], Butt et. al, observed a decrease in the MRCP amplitude after multiple training sessions using an upper-limb rehabilitation robot [64], [65], [66]. This reduction in amplitude after repeated sessions could be due to neural efficiency, where less cortical effort is required to perform the task. The study speculated that as learning occurs, the skill becomes more automated, with subcortical structures becoming more active [60]. In summary, an increase in negativity is observed for a single training session, whereas a decrease is observed after multiple training sessions. Furthermore, these studies provide evidence for the use of MRCP as a tool to quantify neurophysiological changes. In the current study, ankle dorsiflexion was used as the task to measure MRCPs pre- and post- the proposed CAMS intervention.

2.2.2 **Action Observation and Motor Imagery Paradigm**

Motor Imagery (MI) can be defined as the mental simulation or rehearsal of an action without any movements. These BCIs work by prompting a user to mentally imagine a limb movement and decodes the sensorimotor rhythm arising from imagination. From the sensorimotor rhythm, the event related-spectral perturbations (ERSPs) and event-related desynchronization/synchronization (ERD/ERS) patterns are decoded in the mu (9 – 11 Hz) and beta (14 – 30 Hz) frequency bands of the EEG. In the case of MI BCI, simultaneous feedback is provided back to the user based on the extent of ERD, for example, the movement of a fixation cross to the left or right depending on the imagined hand [31]. Additionally, the observation of actions (AO) has been shown to activate similar brain regions as those involved in motor imagery and execution [32]. In AO therapy, participants are shown videos of movements and are asked to observe and simultaneously imagine performing the movements mentally. The activity due to AO has been attributed to the activation of the mirror neuron system (MNS) [67], [68]. MI mainly activates the primary motor cortex and supplementary motor area (SMA), whereas AO is associated with activation of the premotor, inferior frontal gyrus (IFG), temporal, posterior parietal, and occipital cortices which are collectively called the action observation network (AON) [43]. Moreover, it has been suggested that AO + MI can produce stronger activation in regions of the brain responsible for movement [40]. Prior studies have shown that congruent AO and MI facilitates corticospinal excitability and produces stronger activation in several movement-related brain regions compared to AO or MI alone [39]. Wright et. al confirmed this by observing an increase in the motor evoked potential (MEP) during combined AO + MI of finger movements [40]. A recent magnetic resonance imaging (MRI) study showed that a 1-hour MI BCI session with neurofeedback can induce structural changes in the brain attributable to increased brain plasticity [31]. The study found an increase in T1-weighted MR signal in the grey matter of the precuneus and sensorimotor

regions following the MI-BCI session. The results from these prior studies motivate the design of novel BCI strategies integrating AO and MI approaches into one system.

2.2.3 **Visual BCIs: SSVEP, SSMVEP and Hybrid CAMS BCI**

When a visual stimulus is presented to a user, light is detected by the photoreceptors in the retina and then transmitted to the retinal ganglion cells. The action potentials generated here propagate through the optic nerves to the visual cortex and other regions of the brain. The visual cortex, which includes multiple areas involved in processing visual information, begins with the primary visual cortex (V1). V1 plays a crucial role in detecting basic features such as edges and orientation, forming the initial stage of visual processing in response to the stimulus. Steady-state visual evoked potentials are responses elicited when a user focuses his/her attention on a repetitive visual stimulus (a light source) flickering at frequencies higher than 6 Hz [69]. These are periodic responses prominently observed in the occipital and occipito-parietal areas of the cortex. SSVEP responses appear as an increase in the amplitude of the signal at the fundamental frequency and its harmonics of the corresponding stimulus with the user's attention. Recently, steady-state motion visually evoked potentials (SSMVEP) based BCI was proposed to address the limitations of conventional SSVEP, such as fatigue, visual discomfort and relatively low interactive performance of the BCI [70] [71]. Different from the flashing style of SSVEP stimuli, the SSMVEP stimuli are designed as an equal-luminance black and white radial checkerboard. The movement of the checkerboard is modulated at a fixed frequency. Specifically, this movement pattern includes a radial contraction and expansion of the stimulus. SSMVEP BCIs share the advantages of SSVEP BCI such as high signal-to-noise ratio, high information transfer rate (ITR) and low participant training time compared to other types of BCIs while minimizing SSVEP-related discomfort for operators [57], [72]. Although visual BCIs based on the flicker or radial motion provide high performance that is beneficial for control applications, these BCI alone cannot activate the sensorimotor areas important for motor recovery.

In this study, a hybrid brain-computer interface (BCI) called CAMS (combined action observation, motor imagery, and SSMVEP) is introduced. This BCI combines the benefits of minimal user training requirements and high detection accuracy, while simultaneously activating the sensorimotor areas. The details of the stimulus design and protocol are detailed in Section 2.6. This is an extension of the BCI proposed in [4], which demonstrated a visual BCI with an accuracy of 90% could produce a significant increase in event-related desynchronization (ERD) at the Cz location. In a follow-up study, an online CAMS BCI for hand movements was implemented with a visual BCI accuracy of 73% in a four-class scenario without algorithm training [73], which outperformed BCIs based on ERD alone. However, it is unknown whether the use of this paradigm for a prolonged period of time can facilitate neuroplastic changes in the areas of the cortex responsible for movement.

2.3 Feature Extraction and Classification for EEG based BCIs

2.3.1 **Feature Extraction**

The performance of a BCI is influenced by the preprocessing, feature extraction and detection algorithms used to analyze and decode the responses. EEG is a non-stationary signal and is prone to interference from several non-brain sources. Sources of noise include ocular artefacts due to eye blinks, muscle artefacts due to movement of the jaw and head, electrocardiogram (ECG) and other sources of noise from the environment. Independent component analysis (ICA) is the most commonly used technique to eliminate such noise artefacts from the EEG data [45], [74]. The multi-channel EEG is decomposed from sensor space into the source space using ICA. Next, the artefact sources are identified via inspection and are removed by zeroing out the corresponding weights. Finally, they are projected back into the sensor space after removing the unwanted noise components. Temporal filtering is applied to eliminate sources of noise such as 60 Hz power line noise, low frequency drifts, etc.

Most commonly used features are based on the changes in the power of the EEG signal at different frequency bands and time point features [75]. The power spectral density (PSD) is commonly employed to measure changes in signal power. A decrease in the power of the signal due to an event is called event-related desynchronization (ERD) and an increase in power is called event-related synchronization (ERS). For example, imagination or execution of a motor action leads to an ERD in the EEG alpha/mu band (8 Hz and 12 Hz) over the PMC and an ERS in the beta band (12 Hz – 26 Hz). Other features for BCIs include band power values, event-related potentials (ERPs), magnitude spectrum features based on Fast Fourier Transform (FFT), and time-frequency features (spectrogram). Feature extraction steps for BCIs usually involve a calibration/training stage to extract the features and are further used to train a machine learning model or classifier to detect the corresponding brain states.

2.3.2 **Supervised learning and Classification**

Supervised classification algorithms such as Linear Discriminant Analysis (LDA) and Support Vector Machines (SVM) are most often used in MI BCI applications [75]. Statistical learning methods such as Canonical Correlation Analysis (CCA) [76], [77] and its variants such as Filter bank CCA (FBCCA) [78], and Task-Related Components Analysis (TRCA) [79] have been used for SSVEP and SSMVEP BCIs. Previous research has demonstrated that CCA can be effective in detecting SSVEP responses in EEG data. CCA is the most widely used baseline classification method for SSVEP and SSMVEP detection [4], [64], [66], [68], [69], [70], [71]. Besides, CCA and FBCCA are calibration free methods that can operate in an asynchronous manner, whereas TRCA is a supervised training-based method that operates in synchronous mode. Recently there has been increased interest in the application of neural networks and deep learning-based algorithms to improve the overall classification performances of EEG based BCIs [71], [84], [85], [86]. A comparison study showed that deep learning-based methods outperformed the classical methods based on CCA and TRCA in asynchronous operation on two SSVEP datasets [5].

Deep learning algorithms are a subset of machine learning algorithms in which the model is trained to learn both the features and the classifier directly from the data. Compared to classical machine learning algorithms that require a sophisticated feature extraction step as input to a classifier, deep learning methods offer the advantage of automatic feature extraction directly from the raw EEG data or in the transform domain of the EEG. A survey on deep learning for EEG indicated that 43% of studies used a specific type of deep learning algorithm known as the Convolutional Neural Network (CNN) for classification tasks [85]. One popular CNN architecture used for BCI applications is the EEGNet [87]. More recently, a combination of CNN with Long Short-Term Memory (LSTM) networks have shown success in EEG based classification tasks [88]. Recent studies showed that CNNs can significantly improve the classification performance in different types of BCI tasks such as motor imagery, P300 and movement-related cortical potentials (MRCP) [87] and SSVEP [71], [89], [90], [91]. The CNN architecture used in this study is same as the one proposed in [5]. This method outperformed several user-dependent training methods for SSVEP BCI and provided higher accuracy for asynchronously processed data than CCA and CNN using magnitude spectrum as input [2], [92] [2]. The application of the C-CNN for the CAMS stimulus is unknown and will be evaluated in this thesis. The C-CNN implemented for this project will be detailed in Chapter 6 of this thesis.

2.4 BCI for Lower Limb Motor Rehabilitation

2.4.1 **BCIs for Gait Recovery and Decoding Phases of Gait from EEG**

While BCIs decoding motor intent from MI have shown to be successful in upper-limb tasks, their application to gait phase decoding remains limited [43]. Prior studies aiming to infer movement intent in gait rehabilitation have used different modalities such as Electromyography (EMG) and EEG, to control exoskeletons or FES neuroprostheses [93]. However, the user's residual muscle function influences the effectiveness of the EMG-based control strategies. In neurological disorders that compromise EMG activity, movement

decoding can be challenging due to a host of factors, including impaired descending motor commands, muscle weakness, and fatigue limiting effectiveness to stimulate motor recovery [94]. In this scenario, EEG-based BCIs have shown feasibility in decoding the user's intention such as movement intent [44], [45], [46], walking patterns [43], [47] and gait training via motor imagery [19], [48], [49]. Figure 2-2 illustrates a concept of an application using the detection of phases of gait from EEG to actuate an FES controller with feedback that is properly timed to the motor intent.

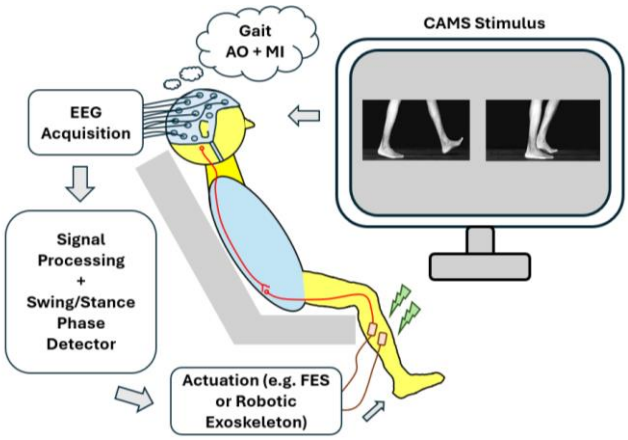

Figure 2-2. Gait phase decoding application, FES denoted by green thunderbolt.

Several studies have investigated the utility of gait phase decoding via EEG in gait rehabilitation post-stroke. One of the earliest studies presented in [19] analyzed EEG activity during robot assisted treadmill walking. The movement intention was decoded from the EEG power spectrum (8 Hz – 30 Hz band) and event related desynchronization (ERD) was used to classify between three states: resting, passive and active walking [19]. The mean classification accuracy between walking and resting state was 94.5% in healthy and 89.9% in stroke patients. Another study trained eight patients with long term paraplegia on both lower limbs to control the locomotor activity by imagining movements of their legs [49]. After twelve months of training, improvements were observed in somatic sensation such as pain localization, touch, and proprioception [49].

Previously, MI BCIs for gait related studies have focused on discriminating brain states between ‘walk’ and ‘rest’ [19] [49], [95]. However, walking, or gait, comprises of two primary phases: swing and stance phase. Gait phase dependent FES of the leg muscles has been reported to enhance walking performance in individuals post-stroke [96]. Coordinating the timing of FES feedback with voluntary or imagined intent can induce efficient neurological recovery [97]. The association between the intent to move, descending from the cortex, needs to be accurately paired with the afferent volley from the movement [30], [98]. Consequently, decoding phases of gait has attracted interest for the development of novel gait rehabilitation BCIs and remains relatively less explored. Furthermore, few studies on hybrid BCIs, combining several signal modalities have shown promising results in gait phase detection, supporting the need for hybrid approaches [94] [99].

Phase dependent modulation of cortical activity during combined AO + MI has gained interest for neurorehabilitation applications [43], [100]. An EEG study in [100] showed the combinatory effects of AO + MI could induce phase-dependent activation of the sensorimotor cortex during walking even without actual movement. Furthermore, a decrease in the EEG band powers in alpha and beta bands from the sensorimotor areas were observed, including modulation with phase of gait. This suggests combining AO and MI may enhance the specificity and effectiveness of neurorehabilitation interventions by closely emulating the neural activation patterns observed during actual walking. Such findings underscore the potential impact of accurate gait phase detection for developing practical BCIs.

Few studies have examined decoding phases of gait from EEG signals. One study employed a long short-term memory (LSTM) network on EEG when participants walked on a treadmill and reported an accuracy of 90% in decoding two phases of gait (swing and stance) [47]. A recent study proposed neural decoding of gait phases during combined AO + MI [43]. The authors demonstrated that the stance and swing phases can be decoded with improved accuracy when MI and AO are used concurrently than using each alone. They developed a

linear discriminant analysis (LDA) based classifier to classify between swing and stance phases from EEG with an overall accuracy of 72% for 2-classes. However, the methodology used for AO + MI involved the participants to view a live performer walking on a treadmill, presenting challenges for practical real-world applications for BCI control.

In this thesis, the CAMS visual stimulus consisted of lower limb movements displayed at four different speeds and will be detailed in Chapter 2. Therefore, the feasibility of decoding the two phases of gait (Swing and Stance) from the responses elicited by the CAMS paradigm in the EEG was investigated in this thesis. These will be detailed in subsequent sections.

2.5 Motivation and Thesis Outline

The overall aim of this thesis was to study the signal characteristics and influence of CAMS on motor cortical excitability. Specifically, we explored the effect of using CAMS BCI as an intervention to induce cortical excitability measured using MRCP. Next, we also investigated the feasibility of decoding the phases of gait from the CAMS BCI responses. Finally, we developed an asynchronous visual BCI capable of decoding the CAMS stimulus frequency from the visual responses. These are presented in the following three studies.

2.5.1 **Study I**

Visual BCIs provide high performance that is beneficial for control applications, but these alone cannot activate the sensorimotor area, which is crucial for motor recovery. Furthermore, it is unknown whether the prolonged use of visual BCI paradigms can lead to changes in the cortical areas responsible for movement. In this study, a hybrid BCI called CAMS is introduced. While previous studies have demonstrated high visual BCI decoding accuracy, it remains unclear whether prolonged use of this paradigm can induce changes in the cortical regions responsible for movement. In this thesis, we hypothesized that the CAMS BCI intervention will enhance cortical excitability in the movement-related areas of the cortex, as

indicated by an increase in negativity in the MRCP recorded before and after the intervention. To test this hypothesis, a 40-minute intervention was conducted in which participants engaged in congruent AO and MI of gait movements. MRCP was recorded before and after the intervention to determine whether changes in cortical excitability have occurred. For a control condition, the same protocol with an SSMVEP checkerboard stimulus was used as the intervention. The effects of the intervention on several MRCP components were analyzed, including the Bereitschaftspotential (BP1, BP2), peak negativity (PN) and the slope of BP1and BP2. The MRCP was recorded on five EEG channels placed on the scalp around the primary motor cortex (C1, Cz, C2, FCz and CPz). The experiments, stimulus design, methodology, results, and discussions for this study I are presented in Chapters 3 and 4 of this thesis.

2.5.2 **Study II**

Gait phase decoding via EEG allows for the precise identification of different phases of the gait cycle (e.g., heel strike, toe-off). This precision is crucial in designing interventions that can be timed accurately to specific gait events, enhancing the effectiveness of the rehabilitation process. The dataset collected during the CAMS intervention phase of Study I was used to develop a novel decoding algorithm for identifying the phases of gait from EEG of simultaneous gait AO + MI. The two phases of gait, swing phase and stance phase, were identified from EEG based on the labels generated by the CAMS stimulus. The feasibility of decoding the two phases of gait from each of the four gait frequencies used in the CAMS stimulus was investigated. Our hypothesis predicts the proposed classifier for a 2-class problem will exceed the chance level accuracy of 50% by at least 15%, with an average accuracy of 65% or above. The results were compared and benchmarked with the methodology presented by the study in [43]. Chapter 5 presents the methodology, results and discussions of gait phase decoding using the CAMS stimulus data.

2.5.3 **Study III**

In this study, we proposed a novel detection algorithm based on C-CNN to develop an offline asynchronous CAMS BCI. Previous studies have shown that the CAMS stimulus can induce SSVEP-like activity in the occipital area and simultaneously induce sensorimotor rhythm in the motor area [4]. Our prior study on AO + MI stimulus of gait achieved an average accuracy of 55% for a 2-second window length across four classes using CCA [4]. For real-time BCI operation, low latency and high response accuracy are essential. Therefore, this study focused on a 2-class scenario to establish a baseline with CCA. The proposed C-CNN was compared with the baseline CCA to evaluate its effectiveness in classifying the two classes. Additionally, the study aimed to improve decoding accuracy with shorter window lengths to promote low latency, using the C-CNN algorithm for detecting visual responses. The goal was to develop methods that enhance CAMS BCI performance, potentially leading to real-time systems with congruent feedback to boost user engagement. Chapter 6 details the implementation of the algorithm, methodology, results and discussions for this study.

Chapter 3

Experiments and Data Collection

The dataset collected for this thesis was used in all three studies listed in the thesis outline. The following sections describe the participant recruitment, stimulus design, data acquisition and experiment protocol.

3.1 Participant Recruitment

Twenty-five healthy adults (8 Females and 17 Males, aged 19-46 years, naïve BCI users) with normal or corrected-to-normal vision volunteered for the experiment. Before starting the experiment, all participants signed a written informed consent. The experiment was approved by the Office of Research Ethics of the University of Waterloo (ORE # 31850).

3.2 Stimulus Design

For this study, two types of repetitive visual stimuli were designed. These two stimuli were the radial checkerboard SSMVEP stimulus and a repetitive gait CAMS stimulus. The repetitive movement frequencies for the SSMVEP stimulus were: 7.5 Hz, 8.57 Hz, 10 Hz and 12 Hz, and its detailed implementation can be found in [70]. This stimulus contained a periodic expansion and contraction movement of a checkerboard as shown in Figure 3-2. Supplementary material in [70] provides a detailed video of the process of the contraction and expansion of the equal-luminance checkerboard stimulus. This will be referred to as checkerboard/SSMVEP stimulus interchangeably. Next, the CAMS stimulus was designed with a repetitive gait pattern and will be detailed in the next section. Overall, the CAMS was used as the condition under investigation, and the SSMVEP was used as the control condition.

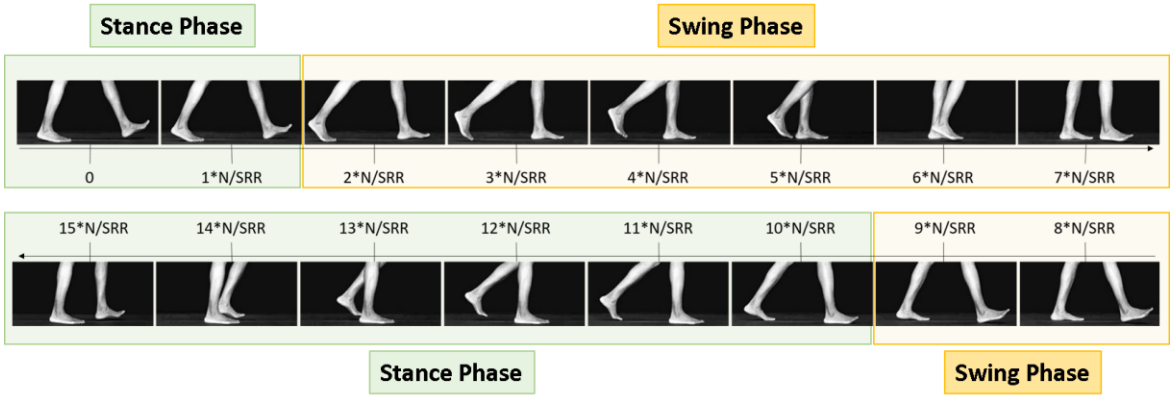

Figure 3-1. CAMS stimulus generation and frames used for single gait cycle

3.2.1 **CAMS Stimulus Design**

A sequence of sixteen frames corresponding to a single cycle were extracted from a video (open source) of gait and were presented successively at a fixed controllable inter-frame interval. The 16 images used to generate the gait cycle are illustrated in Figure 3-1 and its detailed implementation can be found in [4]. All stimuli were presented on an LCD screen with a refresh rate of 60 Hz. Each image would last a duration of N frames, before presenting the next frame. The stride frequency (STF) was defined as the reciprocal of the time taken to present one full cycle of gait (3.1). The stimulus frequency (SF) was defined as a function of the screen refresh rate (3.2). Four values of the parameter N were implemented: 8, 7, 6 and 5. Consequently, the stride frequencies were: 0.47 Hz, 0.54 Hz, 0.62 Hz and 0.75 Hz, and the

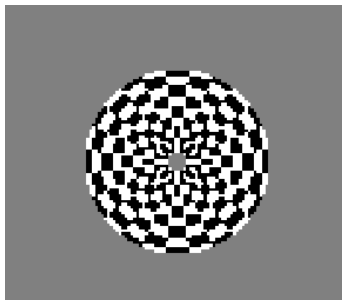

Figure 3-2. SSMVEP Checkerboard Stimulus

corresponding stimulus frequencies were: 7.5 Hz, 8.57 Hz, 10 Hz and 12 Hz. The stimulus frequencies were kept consistent with the SSMVEP stimulus.

$$STF = \frac{\mathrm{SRR}}{(\mathrm{N} * \mathrm{NF})} \qquad \mathrm{NF} = 16;\ \mathrm{SRR} = 60;\ \mathrm{N} = \{5,6,7,8\} \tag{3.1}$$

$$SF = \frac{\mathrm{SRR}}{(\mathrm{N})} \qquad \mathrm{SRR} = 60;\ \mathrm{N} = \{5,6,7,8\} \tag{3.2}$$

3.2.2 **Data Acquisition**

The EEG signals from each participant was acquired using the g.USBamp and Gammabox (g.tec Guger Technologies, Austria) wet electrode (g.Scarabeo) system with a sampling rate of 1200 Hz. Twelve active EEG electrodes, F3, Fz, F4, FCz, C1, Cz, C2, CPz, POz, O1, O2 and Oz, were used to record the EEG from the frontal, central, occipital and occipito-parietal areas according to the International 10-20 system, FPz was used as the ground, and an electrode on the left ear lobe was used as the reference. Additionally, two surface electrodes (720 Series 30*22mm Ag/AgCl, AMBU) were used to record the EMG activity over the Tibialis Anterior (TA) muscle of the right leg with the ground and reference placed over the malleoli of the ankle. These channels were added as auxiliary channels to the

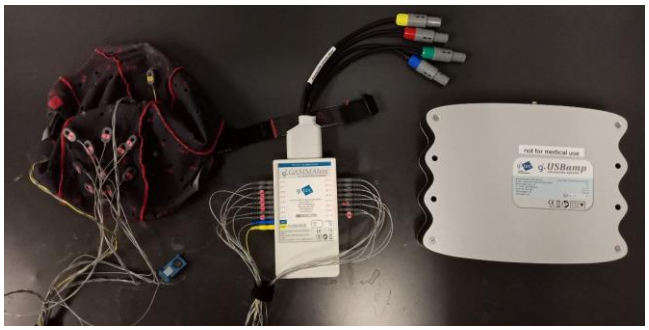

Figure 3-3. Data Acquisition hardware illustrating the EEG cap with the g.Scarabeo electrodes, the g.GammaBox driver and g.USBAmp Amplifier

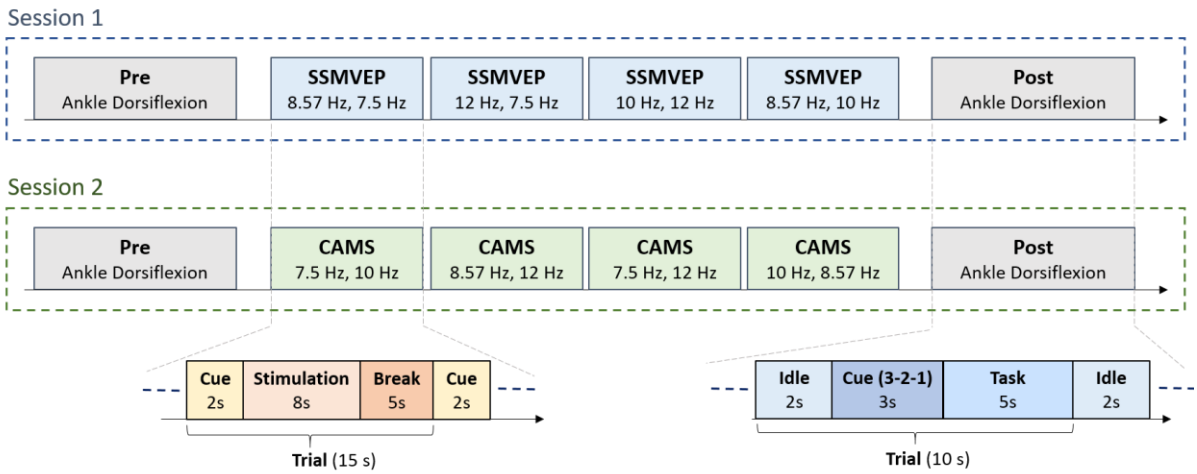

Figure 3-4. Experiment Protocol

same amplifier sampling at 1200 Hz. The apparatus used for this experiment are shown in Figure 3-3.

3.2.3 **Experimental Protocol**

Figure 3-4. illustrates the overall schema of the experiment protocol. Each participant was required to participate in two sessions, with a minimum 24-hour separation. A single experiment session consisted of three phases of measurements: pre, intervention, and post. The phases of pre- and post- measurements were identical, consisting of forty ankle dorsiflexions (AD) each, and the intervention-phase consisted of four blocks of the visual stimulus either CAMS or SSMVEP randomly assigned across participants.

Figure 3-5. Ankle Dorsiflexion (Pre/Post) Protocol

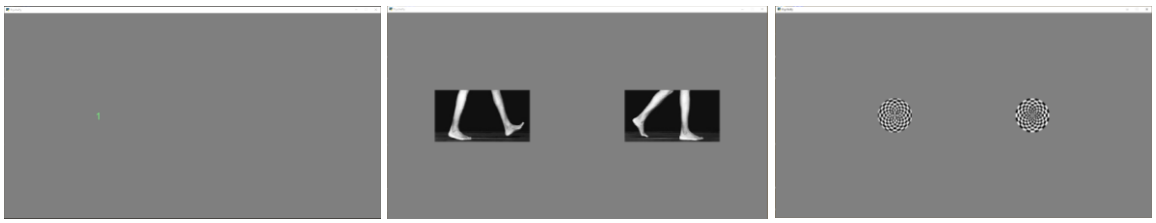

Figure 3-6. Cueing screen and Visual Stimulus Screen (CAMS and SSMVEP)

3.2.3.1 Pre/Post phase

In both pre- and post-phases of the session, the participants received a visual cue that instructed them to perform one self-paced AD during the trial. A single trial comprised of an idle period of 2 s, cue period of 3 s and task period of 5 s. During the cue period, the participant was provided a countdown from three to one every 1 s as illustrated in Figure 3-5. They were instructed to perform a single AD anytime during the 5 s task period in a self-paced manner. This protocol was consistent for both sessions across all participants.

3.2.3.2 Intervention phase

During the intervention phase (CAMS or SSMVEP), two visual stimuli were presented on the screen, and the participant was directed by a visual cue to gaze at one at a time. The stimulus frequencies for these two stimuli were randomly selected from the four frequencies defined earlier. Four paired stimulus frequency combinations out of the six combinations were randomly assigned for each participant. Each trial consisted of a 2 s cue period during which the participant was directed to focus on one of two stimuli displayed on the screen. An 8 s stimulation period followed, where participants were instructed to observe the stimulus for the entire period. Finally, a 5 s break was provided before the start of the next trial. The cueing screen is illustrated in Figure 3-6.

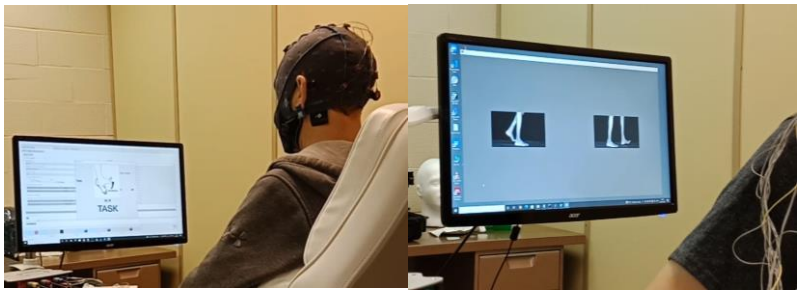

Figure 3-7. Experimental setup showing A. pre/post measurements (left) and B. CAMS intervention

Each block consisted of 40 stimulus presentations. Each stimulus was presented 20 times during the entire block. Each block lasted 10 minutes. A total of four blocks were performed. In each block, two of four stimulus frequencies were presented in random order, with each frequency presented twice during the entire intervention period. Approximately 3 minutes of resting period was provided between blocks. The stimulus presentation sequence was randomized. The order of the two stimulus conditions was randomized for each participant.

During the CAMS session, participants were instructed, "Observe the gait video as directed by the visual cue and mentally imagine as if you were walking in synchrony with the video; try to synchronize your left and right leg movements with the gait shown in the video." During the SSMVEP session, participants were instructed to focus on the respective checkerboard stimuli. To reduce movement and ocular artefacts, participants were asked to avoid sudden jerky movements and eye blinks during each trial. The monitor was placed at 55 cm measured between the screen and the eyes of the participant. They were seated in a comfortable chair with both legs rested in a reclined position. Additionally, resting state EEG was collected for 30 s before and after each block. In total, a single session consisted of approximately 40 minutes of intervention-phase, and 15 minutes of pre- and post-measurements, excluding breaks between blocks. The complete experimental protocol was designed and developed in a custom python-based user-interface tool [44]. All data were recorded, stored in comma separated values files and were analyzed offline using Python tools and are illustrated in Figure 3-7.

Chapter 4

Study I: Combined Action Observation, Motor Imagery and SSMVEP BCI enhances Movement Related Cortical Potentials

In this study, a novel BCI intervention aimed at inducing acute change in cortical excitability based on the CAMS paradigm was proposed. It was hypothesized that the proposed CAMS intervention would increase cortical excitability in the movement related areas of the cortex. Specifically, an increase in negativity in the components of the MRCP was expected to be observed after a single experiment session of CAMS. Furthermore, this was compared with the SSMVEP checkerboard as a control condition. Next, the signal characteristics of the visual responses and motor responses during the intervention were quantified using the magnitude spectrum and ERD index, respectively. The following sections of Study 1 have been submitted to IEEE TNSRE and are under revision.

4.1 Methodology

4.1.1 **Pre- and Post- Movement Related Cortical Potentials Analysis**

EEG and EMG recordings were carefully screened for noisy EEG channels, abrupt changes in peak-to-peak EEG amplitude and MRCP morphology. Three of twenty-five participants were removed from the analysis due to noisy Cz channel, particularly participants with longer hair. Two more participants were removed from the analysis as the number of good MRCP trials, defined as those that contained a peak-to-peak amplitude of less than 100 µV, were less than 30%. Finally, twenty participants were used in the subsequent analysis.

Movement onset of the AD was first detected using a threshold-based approach applied to two EMG channels. First, temporal filtering was applied between 100 Hz and 200 Hz using a 4th order Butterworth band-pass filter on both EMG channels. Next, the mean of the signal was subtracted from the filtered signal. To improve the signal-to-noise ratio for movement onset detection, the Teager-Kaiser energy operator (TKEO) [101] was applied on the derived signal. Next, a signal rectification step was applied by taking its absolute value. Finally, through visual inspection, a threshold was empirically identified for each recording, and the first time point that exceeded the threshold was retained as the movement onset time for each AD epoch. The median threshold across sessions and participants for detecting an AD event was 20 mV. Furthermore, the onsets were visually inspected and validated. These movement onsets were subsequently used to select the corresponding AD epochs in the multi-channel EEG signal.

The EEG data from the pre- and post- phases were pre-processed using Independent Component Analysis (ICA) to remove ocular artefacts related to eye movements and blinks [74] using the MNE Python toolbox [102]. After applying ICA, the signals were filtered between 0.01 Hz and 5 Hz using a fourth order zero-phase Butterworth band-pass filter to extract the MRCP activity [45], [103]. The signals were segmented into epochs from 3 s prior to movement onset up to 2 s after. The MRCP was extracted from the channels: C1, C2, Cz, FCz and CPz. Epochs containing an amplitude greater than 105 µV (peak-to-peak) were

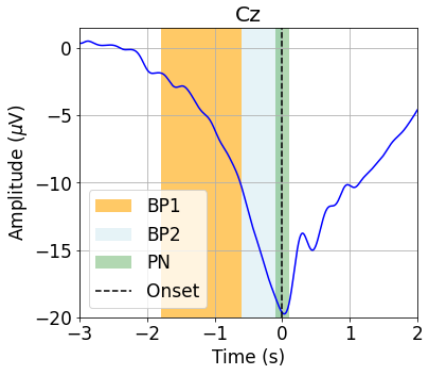

Figure 4-1. MRCP components regions of interest: BP1, BP2 and PN

rejected. Baseline correction was applied to all trials in the period between -3 s and -2 s relative to the movement onset. The MRCP was segmented into three regions similar to [60]. From the pre- and post- epochs the following components were extracted from each trial: 1) BP1 - the mean amplitude of the readiness potential between -1800 milliseconds (ms) and -600 ms, 2) BP2 - the mean amplitude of the potential between -600 ms and movement onset, and 3) PN - the peak amplitude of the negativity corresponding to the motor potential between -100 ms and 100 ms with respect to the movement onset. Additionally, the slopes of BP1 and BP2 were calculated by linear regression to estimate the slope as Slope1 and Slope2, respectively. These regions are illustrated in Figure 4-1.

4.1.2 **Visual Stimulus Response Characteristics Analysis**

Responses in the EEG during the intervention phase for both types of visual stimulus were characterized based on activity elicited in the occipital and motor areas. The magnitude spectrum and signal-to-noise ratio (SNR) were estimated for occipital channels containing steady state visual responses on channels O1, Oz and O2. The motor responses were quantified based on the event related desynchronization (ERD) index on channels C1, Cz and C2.

First, EEG signals were filtered between 0.5 Hz and 40 Hz using a 4th order zero-phase Butterworth band-pass filter. Next, the magnitude spectrum was computed using the Fast Fourier Transform (FFT) applied on the entire 8 s visual stimulation trial at a resolution of 0.09 Hz. The average magnitude spectrum for the four stimulus frequencies (7.5 Hz, 8.57 Hz, 10 Hz and 12 Hz) were each averaged across all participants, trials and channels (O1, Oz, O2). Next, the SNR was calculated from the magnitude spectrum with respect to the fundamental stimulus frequency for both types of stimuli. For each stimulus frequency f, SNR was computed as the ratio of the maximum frequency amplitude in the band [f − 0.3 Hz, f + 0.3 Hz] to the mean amplitude of the band [f − 2 Hz, f − 0.3 Hz) and (f + 0.3 Hz, f + 2 Hz], similar to the method used in [2].

To quantify the extent of activity induced in the motor area, the ERD index was computed. The event related spectral perturbation (ERSP) was computed on the EEG trials from channel C1, Cz and C2 based on the multi-taper time frequency approach using the MNE Python toolbox with a time window of 500 ms [104]. The relative changes in spectral power during the trial were obtained by taking the log-ratio between the power in each frequency band to the power during the baseline period (-1 s to 0 s). Similar to previous studies, the ERD index was calculated and defined in equation (4.1),

$$ERD\ Index = 10\ \times\ log_{10}\frac{P}{R} \tag{4.1}$$

where P is the power during the trial task period and R is the power in the reference baseline period. This index was used to quantify the degree of EEG band power reduction resulting from a desynchronization of cortical neurons during motor task execution [104], [105]. The frequency bands mu (8 Hz – 12 Hz) and beta (12 Hz to 26 Hz) were quantified in this study.

4.1.3 **Statistical Analysis**

Statistical analysis was performed across participants, trials and stimulus types to compare changes between the pre- and post- measurements. For each stimulus condition, EEG components BP1, BP2, PN, Slope1 and Slope2 were extracted per trial from the pre- and post-measurements. These were compared individually for each of the five channels: C1, Cz, C2, FCz and CPz, and stimulus types: SSMVEP and CAMS. The comparisons were evaluated with a Mann-Whitney U test with the significance level set to 5%. Furthermore, the temporal differences of the individual MRCP time series between pre- and post- measurements were analyzed using a cluster-based permutation test [106] [107] using the built-in MNE function. This was performed on the epoched trials across all participants for each channel and stimulus

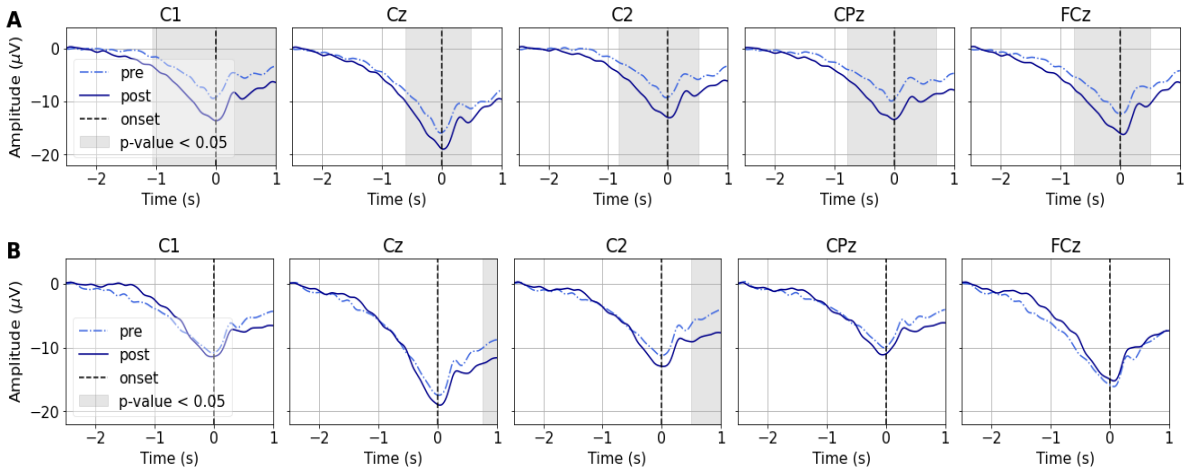

Figure 4-2 MRCP averages across participants for the channels C1, Cz, C2, CPz and FCz for 'pre' (light blue) and 'post' (dark blue) conditions for CAMS (A) and SSMVEP (B), t = 0 s (movement onset). Significant differences (p < 0.05) highlighted in grey.

type. The cluster forming threshold was automatically identified as 3.85 based on α significance threshold of 0.05 and the number of permutations was set to 1000.

4.2 Results

4.2.1 **Pre-/Post- MRCP Measurements CAMS and SSMVEP**

Figure 4-2a and Figure 4-2b illustrates the grand average MRCP across all participants and trials for all the five channels around Cz along with the pre- and post- phases for the CAMS and SSMVEP stimuli, respectively. An overall increase in negativity can be observed following the intervention phase across all channels for the CAMS stimulus. Moreover, this increase is consistent across the entire trial duration between -1500 ms to 500 ms with respect to movement onset. An increase in negativity was observed for the components BP1, BP2 and PN for all channels placed over the primary motor cortex (C1, Cz and C2) with the greatest differences found for the BP2 component. In contrast, MRCP components had no significant changes between the pre- and post- measurements for the SSMVEP stimulus condition in most

Table 4-1. MRCP components averaged amplitude differences (Post – Pre) across the five channels C1, Cz, C2, FCz and CPz across all participants for CAMS (C) and SSMVEP (S) stimulus, * indicates significant difference ($p < 0.05$) based on the Mann-Whitney U test.

Channel	BP_1 (µV)		BP_2 (µV)		PN (µV)		$Slope_1$ (µV/s)		$Slope_2$ (µV/s)	
	C	S	C	S	C	S	C	S	C	S
C_1	-1.82*	1.5	-4.15*	-0.1	-4.4*	-0.6	-1.85*	0.16	-1.47	-3.9*
C_z	-0.96*	0.46	-2.9*	-1.0	-3*	-1.5	-1.05*	-0.45	-1.88	-3.5*
C_2	-1.51*	0.29	-3.7*	-1.1	-3.7*	-1.7	-1.7*	-0.51	-1.29	-3.7*
FC_z	-1.7*	1.66	-3.64*	1.1	-3.6*	0.8	-1.68*	0.9	-1.05	-3.03*
CP_z	-1.35*	0.29	-3.6*	-0.9	-3.68*	-1.1	-1.45*	-0.51	-1.42	-2.6*

channels; the early components in C1 and FCz showed pre- measurements to be more negative than post- measurements.

Table 4-1 summarizes the amplitude differences (post - pre) between the measurements from the pre- and post- phases across the five channels and participants for each MRCP component; C indicates CAMS and S indicates SSMVEP stimulus. An increase in negativity can be readily observed post- intervention across all channels and components for the CAMS stimulus condition. Statistical analyses revealed a significant difference in all five channels C1, C2, Cz, FCz and CPz for the components BP1, BP2 and PN for the CAMS stimulus. BP1 was (average pre-, post- in µV ± standard error) C1: (-1.41 ± 0.54, -3.23 ± 0.5; $p = 0.009$), Cz: (-3.74 ± 0.54, -4.7 ± 0.5; $p = 0.04$), and C2: (-1.15 ± 0.6, -2.66 ± 0.5; $p = 0.04$). BP2 was significantly higher for channels C1: (-6.8 ± 0.72, -10.95 ± 0.71; p < 10-3) and Cz: (-11.9 ± 0.74, -14.8 ± 0.73; p = p < 10-3), C2 (-6.5 ± 0.7, -10.2 ± 0.75; p < 10-3). Finally, there was a significant increase in the motor potential PN in channels C1 (-9.8 ± 0.8, -14.2 ± 0.8; p < 10-3), Cz: (-16.6 ± 0.8, -19.6 ± 0.8; p < 10-3), and C2 (-9.9 ± 0.8, -13.6 ± 0.8; p = p < 10-3). Significant changes were identified in the Slope1 across all channels for CAMS, and no significant changes were observed for Slope2. For the SSMVEP stimulus, no significant

increase in negativity was observed in the MRCP components. The results of cluster-based permutation test comparing the epoched trials between the pre- and post- conditions for CAMS revealed significant differences across the channels C1, C2, Cz, FCz and CPz, particularly in the regions between -1000 ms and 250 ms relative to movement onset. No significant changes in negativity were observed in the measurements for the SSMVEP control condition. Furthermore, no significant differences were observed when comparing the time series of the pre- conditions between CAMS and SSMVEP for all channels except FCz.

4.2.2 **Visual and Motor Responses for CAMS and SSMVEP**

4.2.2.1 Visual Response Characteristics

Figure 4-3a and Figure 4-3b illustrates the averaged magnitude spectrum of the visual steady-state responses recorded during the 8 s visual stimulation phase of the CAMS and SSMVEP stimuli, respectively. The average magnitude spectrum for the stimulus frequencies 7.5, 8.57, 10 and 12 Hz were computed across subjects, trials and channels (O1, O2, Oz) for both stimulus types. Figure 4-3a shows the magnitude responses corresponding to the fundamental frequency across all participants for the CAMS stimulus. The average amplitude of the dominant peaks were (μV): 0.88 ± 0.33 (7.5 Hz), 0.87 ± 0.31 (8.57 Hz), 0.82 ± 0.27 (10 Hz) and 0.72 ± 0.40 (12 Hz). The insets in Figure 4-3b illustrate the responses observed in the lower frequency range in the proximity of the respective step frequencies for the CAMS stimulus. These responses averaged across participants were (μV): 1.65 ± 0.46 (7.5 Hz), 1.8 ± 0.46 (8.57 Hz), 1.6 ± 0.41 (10 Hz) and 1.54 ± 0.61 (12 Hz). A strong magnitude response was observed

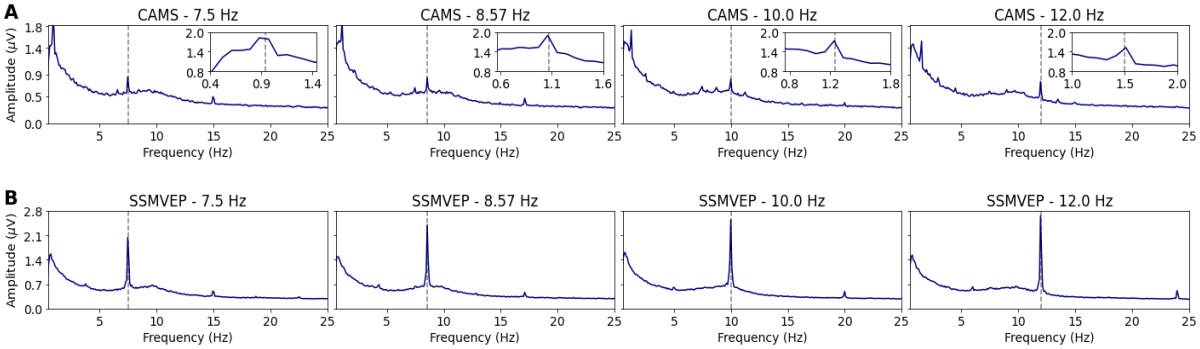

Figure 4-3. Averaged magnitude spectrum for CAMS (A) and SSMVEP (B) responses averaged across channels O1, Oz and O2; all participants for stimulus frequencies: 7.5 Hz, 8.57 Hz, 10 Hz and 12 Hz. Insets for CAMS (A) illustrate responses corresponding to the CAMS step frequency.

for all four stimulus frequencies for SSMVEP stimulus with average magnitude responses (μV): 1.98 ± 0.86 (7.5 Hz), 2.35 ± 1.04 (8.57 Hz), 2.48 ± 1.3 (10 Hz) and 2.63 ± 1.13 (12 Hz). Furthermore, the mean SNR for CAMS were (dB): 4.07 ± 2.3 (7.5 Hz), 4.01 ± 2.25 (8.57 Hz), 4.05 ± 1.8 (10 Hz) and 4.03 ± 2.7 (12 Hz). The SNR for SSMVEP stimulus was (dB): 10.6 ± 4.45 (7.5 Hz), 12.14 ± 4.83 (8.57 Hz), 12.43 ± 5.04 (10 Hz) and 14.95 ± 3.8 (12 Hz).

4.2.2.2 Motor Responses – Event Related Desynchronization

Figure 4-4a (top) displays the averaged event-related desynchronization (ERD) map for the CAMS stimulus averaged across the four stimulus frequencies, participants, trials and channels (C1, Cz and C2). The median ERD index computed throughout the trial for the mu band was -1.5, beta band was -1.8 and combined mu + beta was -1.7 for CAMS. Figure 4-4b (bottom) illustrates the averaged temporal dynamics of the ERD index calculated across the 8 second trial during the SSMVEP intervention. The median ERD index calculated for the mu band was -0.83, beta was -1.4, and mu + beta was -1.25. Comparing the ERD indexes between CAMS and SSMVEP, it can be observed that CAMS has a greater ERD index compared to the SSMVEP stimulus in the mu (-1.5 vs -0.83), beta (-1.8 vs -1.5) and combined (-1.7 vs -1.25) bands, respectively.

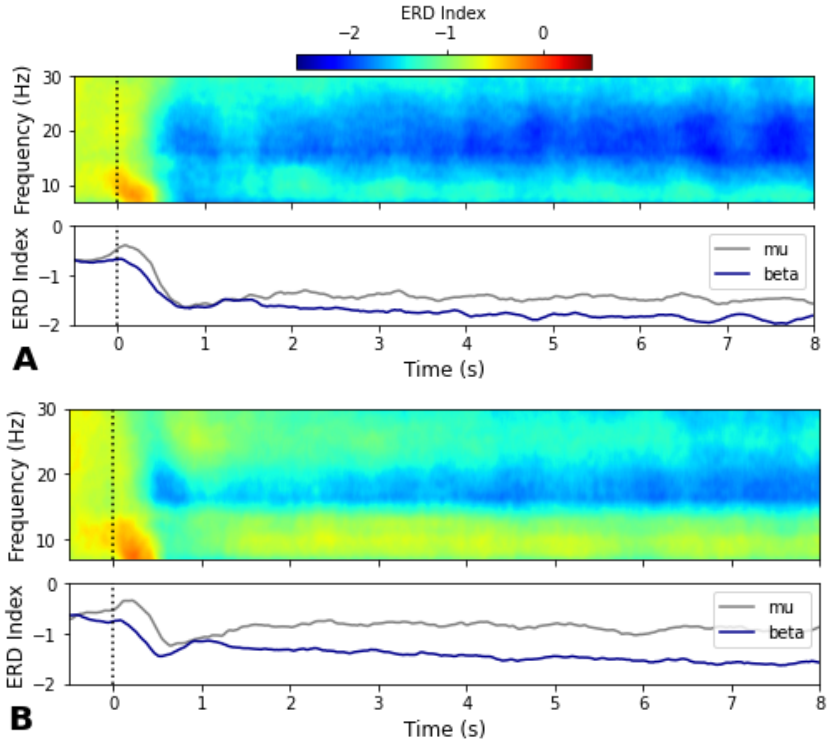

Figure 4-4. Average ERDS map and temporal dynamics of the ERD index across all participants, channels (C1, Cz, C2) and trials for CAMS (A) and SSMVEP (B) across all stimulus frequencies across the 8 s trial; mu (8 Hz – 12 Hz) and beta (12 Hz – 26 Hz) bands, t = 0 s (onset).

4.3 Discussions

4.3.1 **CAMS BCI Enhances Cortical Excitability**

The results of the pre- and post- measurements clearly indicated that the CAMS BCI intervention enhanced the MRCP components across all channels evident by the increased negativity. This finding can be attributed to an increase in cortical excitability, similar to previous research reporting association between MRCP negativity and cortical excitability [59]. The effects of AO + MI on enhancing the short-term MRCP components is qualitatively similar to the effects reported following aerobic exercise [62]. The morphological changes observed in the BP1, BP2 and PN suggest changes in contributing cortical regions such as

SMA and M1 [59]. To the authors' best knowledge, this is the first study to examine measures of MRCP in an AO + MI paradigm (CAMS), supporting stronger cortical excitability compared to MI or AO alone.

4.3.2 **CAMS Stimulus Activates Visual and Motor Areas**

The evidence from this study supports the hypothesis that CAMS elicits stronger activation of the motor areas of the CNS compared to SSMVEP alone, and simultaneously activates both visual and motor areas. Firstly, a clear fundamental peak and a second harmonic of lower amplitude can be observed in all occipital channels for the CAMS stimulus for all four stimulus frequencies. Next, an interesting and unexpected result was the occurrence of peaks at the lower frequencies between 0.4 Hz and 2 Hz. On further investigation, the peaks illustrated within the insets of Figure 4-3a were equal to twice the stride frequencies derived from the CAMS stimulus design. This result indicates manifestation of the step frequency from repetitive movement observation on the occipital EEG electrodes. The results of the averaged SSMVEP magnitude spectrum responses indicated a clear peak at the fundamental frequency of the stimulus and a smaller peak at the second harmonic. No other prominent peaks were identified at other frequencies.

The SNR for the CAMS stimulus frequencies were lower than the SSMVEP responses, as expected. Interestingly, the mean SNR was consistent across all frequencies for the CAMS responses. As a result, there is a need to investigate stimulus parameters such as higher frequencies of gait, size, color and contrast influencing the overall SNR of CAMS visual responses. Moreover, this provides opportunities to develop robust and accurate detection algorithms to detect the CAMS response in a visual BCI application.

The motor responses due to the CAMS intervention showed a large ERD, indicating an overall decrease in the power in the mu and beta frequency bands for the entire duration of the trial. This is likely due to cortical activation of M1 and associated areas during congruent action

observation and imagination of gait. Although ERD was observed in the SSMVEP intervention, it is lower than the ERD during the CAMS stimulus. Moreover, the ERD during CAMS was sustained throughout the trial for both the mu and beta bands. Overall, these results confirm the simultaneous activation of the motor and occipital cortices evidenced by the ERD and steady state visual responses observed for the CAMS stimulus. Furthermore, the step frequency observed in Figure 4-3a in the lower end of the magnitude spectrum of CAMS can be beneficial for enhancing the decoding performance of the BCI in future studies.

4.3.3 **Challenges and Limitations**

The experiment protocol for the pre- and post- measurements comprised of ~40 trials of AD to measure MRCP, with component calculations performed on a per-trial basis. However, more accurate estimates of MRCP components on an individual subject level can be attained by increasing the number of AD trials. Furthermore, due to the slow frequency nature of the signal, it is susceptible to noise interference. Consequently, up to 30% of trials were rejected for some participants in this study. Hence, future investigations may consider increasing the number of trials to up to 100 for both pre- and post- measurements, while being mindful of the extended experiment duration for participants. The post- measurements were performed within a timeframe of less than four minutes following the conclusion of the last CAMS block. The duration of the observed increase in cortical excitability does not necessarily reflect persistence of these effects over a longer time span.

In this study, recording of MRCPs was performed using only five channels positioned around the Cz electrode. Further investigations to investigate source localization and signal coherence with more channels would provide deeper insight into specific effects. The MRCP was used as a measure to quantify changes in cortical excitability in this study. Although EEG offers a cost-effective and simple setup, it is also highly variable and user dependent. Complementary to the EEG-based approach, future studies replicating the CAMS intervention

with transcranial magnetic stimulation (TMS) evoked motor evoked potentials is warranted [108]. Currently, there are few studies that have correlated TMS-elicited metrics with EEG-based measurements, highlighting the necessity for such a comparison study in the future [61], [109].

An interesting characteristic of the CAMS stimulus is the multi-network nature of the elicited activity. This presents challenges in pinpointing specific neurophysiologic mechanisms at play. Considering the observed changes in the BP and peak negativity components of MRCP, it is likely that cortical excitability changes occurred in the SMA and M1 contralateral to limb movement. The integration of AO + MI in the CAMS stimulus introduced additional modulation of the MRCP by influencing the PN, but also potentially the preparatory components. AO is expected to engage the mirror neuron networks [68], while MI is likely to target networks closely related to those involved in motor planning and execution. Given this close relationship, it is expected that they induce changes in M1, as observed.

The CAMS stimulus is a relatively new stimulus design introduced in the literature. Previous studies combining AO with MI have demonstrated increased involvement of the motor cortex when AO is performed from a first-person view compared to a third-person view [110]. However, in the present study, we implemented a third-person view of gait for the CAMS stimulus. Subsequent investigations can explore the effects of the intervention using a first-person view stimulus. Furthermore, the proposed experiment protocol can be extended to upper limb movements [73] and study influence of the CAMS stimulus on cortical regions associated with upper limb movements.

4.3.4 **Applications and Conclusions**

The results from this study indicate that the proposed CAMS BCI paradigm provides multiple benefits including the ability to enhance cortical excitability within the primary and supplementary motor areas and providing reliable BCI classification performance. Firstly, the

CAMS intervention resulted in an increase in negativity across all MRCP components associated with movement preparation and execution. These findings have implications for motor recovery in individuals with neurological damage affecting the motor cortex [32]. The obtained results substantiate our initial hypothesis that a brief 40-minute intervention employing congruent AO and MI within a BCI can augment motor cortical involvement linked to movement preparation and execution. This paradigm holds promise for neuro-rehabilitation applications and helps inform future BCI designs. These findings contribute to understanding the combined AO and MI paradigm in enhancing cortical excitability for motor rehabilitation. Further research is warranted to explore clinical applications and optimize the personalized CAMS BCI paradigm for neurorehabilitation interventions.

Chapter 5 Study II: EEG-Based Gait Phase Decoding from Combined Action Observation and Motor Imagery

This study investigated the feasibility of decoding the two phases of gait (swing and stance) from EEG responses elicited by the CAMS paradigm. Two linear classifiers, based on Linear Discriminant Analysis (LDA) and Support Vector Machine (SVM), were implemented on two different frequency bands of interest. The results were compared and benchmarked against the methodology presented in [13]. To the best of the author's knowledge, this is the first study to explore EEG-based gait phase decoding using the CAMS BCI paradigm. The findings and results of Study 2 have been submitted to the IEEE TNSRE journal and are currently under review.

5.1 Methodology

5.1.1 **Pre-processing and Data Labelling**

For this investigation, the EEG recorded during the stimulus presentation period was analyzed for gait phase decoding, as described in Section 3.2. The sixteen frames

Table 5-1. CAMS visual stimulus design parameters.

N	Stim. Freq. (Hz)	Stride Freq. (Hz)	Swing/Stance Dur. (s)	Inter-frame Interval (s)
5	12	0.75	0.67	0.083
6	10	0.625	0.80	0.1
7	8.57	0.54	0.93	0.116
8	7.5	0.47	1.06	0.133

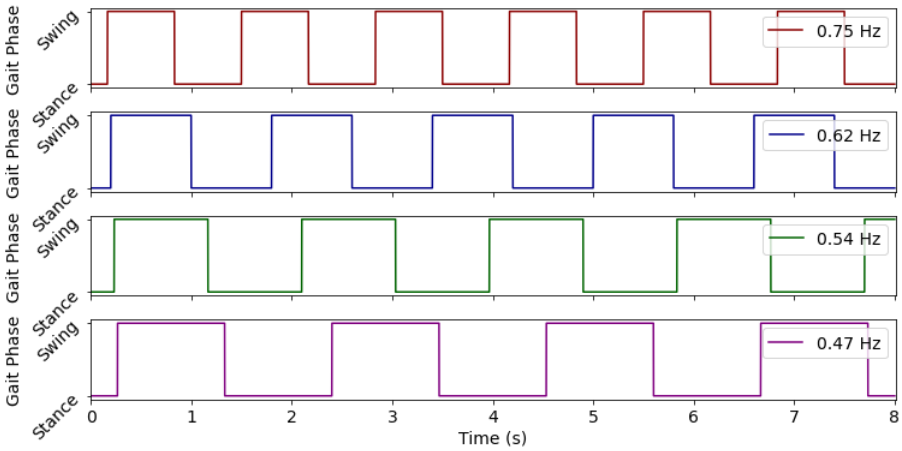

Figure 5-1. Trialwise Swing/Stance assignment.

corresponding to a single cycle of gait were broadly labelled into the Swing and Stance phase as illustrated in Figure 3-1 with respect to the right leg. The labels for the frames were manually assigned based on the movement of a single leg. Consequently, eight frames were designated as Swing, followed by eight frames designated as Stance. Table 5-1 presents the inter-frame intervals and the duration of Swing and Stance phase for each stimulus frequency. For example, for eight consecutive frames, the duration of Swing/Stance for the frequencies 7.5 Hz and 8.57 Hz were 1066 ms and 933 ms, respectively.

Next, the 8-second EEG trial corresponding to the CAMS visual stimulation period was labeled as Swing or Stance based on these precise timings illustrated in Figure 5-1. Figure 5-3 illustrates an overview of the EEG signal processing steps and the machine learning pipeline. The EEG signals were pre-processed by bandpass filtering, epoching, segmenting and down sampling each 8-second trial corresponding to the CAMS visual stimulation period. For the detection of gait phases, a previous study analyzed slow cortical potentials in the delta band (0.1 Hz to 4 Hz) [43]. In this study, the delta band processing was used as a baseline for comparison. Consequently, two different frequency bands were analyzed in this study: the delta band and a broad band (0.1 Hz to 20 Hz) for temporal feature extraction. These were

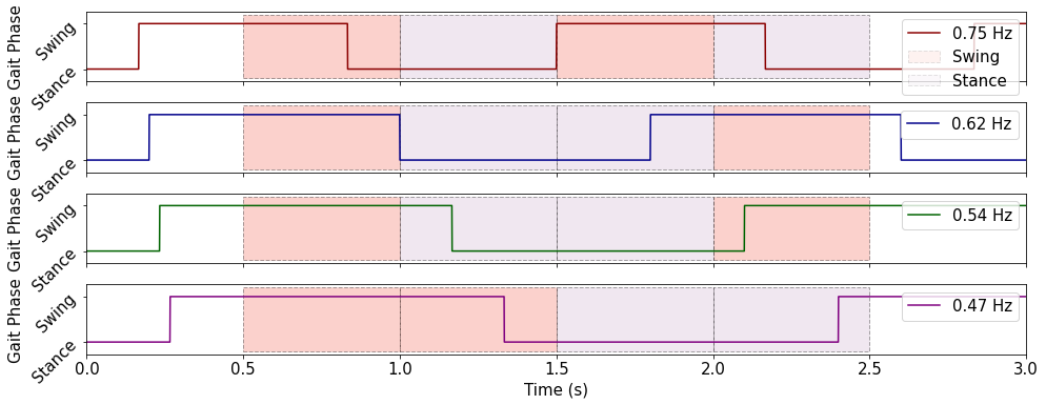

Figure 5-2. Trial level windowing and segment-wise labeling strategy.

implemented using a 4th order Butterworth bandpass filter. Next, the signals were down sampled to 120 Hz for analysis.

Each 8-second trial was segmented into non-overlapping windows of 500 milliseconds (ms) for gait phase decoding. Figure 5-2 illustrates the windowing operation for each trial and stimulus frequency. Next, each non-overlapping window was assigned a label of either Swing or Stance based on the corresponding set of frames that were displayed as part of the CAMS gait stimulus. Difficulties in labeling may emerge when the 500 ms windows do not coincide with the onset of a gait phase. Such misalignment could result in windows that spans the end of one phase and the beginning of another, which could pose a challenge for the classification task. Therefore, each window was assigned a label based on a majority vote; for example, if the percentage of Swing duration was equal to or greater than 60% in that window, then it was labeled as Swing. A similar strategy was used to label the Stance segments. Windows that had a class duration occupying less than 60% of the segment were not included in the training set.

5.1.2 **Feature Extraction and Decoding phases of Gait**

The windowing and feature extraction approaches were inspired by [43] and modified for the current study. Each 500 ms segment consisted of 12 EEG channels and 60 temporal

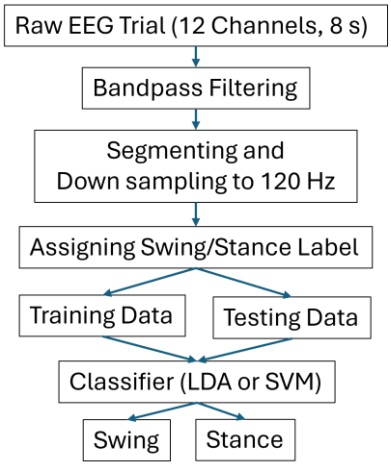

Figure 5-3. EEG Processing and Classification Pipeline.

samples. A feature vector was constructed by concatenating the time points for each channel into a single feature vector of length $60 \times N_{ch} = 720$, where N_{ch} is the number of EEG channels. Finally, the vectors were labeled with class 0 (Stance) and class 1 (Swing).

The two phases of gait from the CAMS responses were classified using three different methods. The first approach, inspired by [43], involved applying a Linear Discriminant Analysis (LDA) classifier to the features extracted from the delta band filtered signals. This method will be referred to as 'Delta+LDA'. This method was used as a baseline to compare other feature extraction methods proposed in this study. In this study, we proposed to expand the frequency band in the feature set to a wider range, which included activities of the alpha band up to the lower beta band from 0.1 Hz to 20 Hz. This extension was inspired by prior studies that demonstrated a relationship between alpha and beta spectral power and various gait parameters, including gait phase and speed [111]. Subsequently, the LDA applied on this feature set was called 'Broad+LDA'. The LDA was implemented using the scikit-learn toolbox in Python, utilizing the least squares solver (lsqr), and an automatic shrinkage setting provided by the toolbox to determine the optimal parameter [112]. Shrinkage is a type of regularization that enhances the estimation of covariance matrices when the number of training samples is relatively small compared to the number of features. Under these conditions, the empirical

sample covariance is not a reliable estimator, and shrinkage contributes to better generalization performance of the classifier [113]. Class prior probabilities were computed and provided as input to the classifier to handle class imbalances.

Additionally, a Linear Support Vector Machine (SVM) classifier was implemented as a binary classifier to detect Swing versus Stance phase on the proposed feature set called 'Broad+SVM'. The LinearSVC library in Python was employed to implement the SVM with the parameter C = 0.05. The class imbalance was handled by automatically adjusting class weights to be inversely proportional to the class frequencies in the input training data. A grid search was performed on the set C = {0.01, 0.05, 0.1, 0.5, 1, 10, 100} to determine the best parameter that maximized the overall accuracy across participants. Overall the three approaches, namely: 'Delta+LDA', 'Broad+LDA' and 'Broad+SVM' were compared for their effectiveness in classifying the two phases of gait.

These methods were trained and validated using a five-fold cross-validation applied to the 40 trials of 8 s duration. Care was taken to ensure there was no overlap in the windows between the training and test folds. Furthermore, the training was designed to be rigorous by ensuring that windows from the same trial were not included in both the training and testing folds, thereby enhancing the generalization capability. Each classifier was trained for each of the four stimulus frequencies in a user-dependent manner.

5.1.3 **Performance Evaluation**

Performance of the classifiers in decoding the Swing and Stance phase were quantified based on the F1 score and classification accuracy. Individual class accuracies for Swing phase and Stance phase were derived from the confusion matrix shown in Figure 5-5. From the confusion matrices, a true positive (TP) was defined as any window that the classifier correctly labelled as Swing phase. A false positive (FP) was defined if a window of Swing was misclassified as Stance class. If a window of Stance was incorrectly classified as Swing, it was

considered a false negative (FN). If a window labelled Stance was correctly classified as Stance, this was considered a true negative (TN). Finally, the F1-score was defined as (5.1):

$$\mathrm{F1} = \frac{\mathrm{TP}}{\mathrm{TP} + 0.5 * (\mathrm{FP} + \mathrm{FN})} \tag{5.1}$$

Next, the individual Swing and Stance accuracies were computed from the confusion matrices as per (5.2) and (5.3), respectively:

$$\text{Swing Accuracy} = \frac{\mathrm{TP}}{\mathrm{TP} + \mathrm{FN}} \tag{5.2}$$

$$\text{Stance Accuracy} = \frac{\mathrm{TN}}{\mathrm{TN} + \mathrm{FP}} \tag{5.3}$$

The spatial contributions of the cortical regions in decoding the phases of gait were evaluated based on the trained 'Broad+LDA' model. The contribution of each EEG electrode was computed from the weights of the LDA classifier and was implemented based on previous studies [43]. The channel contribution was calculated as per (5.4):

$$Weight_k = \frac{\sum_{j=1}^{L} |W_{kj}|}{\sum_{i=1}^{N} \sum_{j=1}^{L} |W_{ij}|} \tag{5.4}$$

for all k from 1 to N, where N is number of electrodes (N = 12), $Weight_k$ is the normalized contribution of each EEG electrode k against the sum of all the weights, L is the number of concatenated time points in the feature vector (L = 60). Based on the 12 EEG electrodes used in this study, three regions of interest (ROI) were assigned corresponding to a cortical area. The ROIs defined were: frontal (F3, F4, Fz), central (FPz, C1, Cz, C2, CPz) and occipital (POz, O1, Oz, O2). For each ROI, the contributions were computed as the average of the normalized weights obtained from (5.4).

Furthermore, the frontal alpha band power activity was measured and correlated with performance to evaluate if attention related measures modulated the overall classification accuracy. The average magnitude spectrum was computed across channels (F3, Fz, F4) for each stimulus frequency and participant. The alpha band power from the lower alpha band (7 to 10 Hz) was calculated from the magnitude spectrum [114] [115].

5.1.4 **Statistical Analysis**

Statistical analysis was performed to compare the classification performances of the three methods: 'Delta+LDA,' 'Broad+SVM,' and 'Broad+LDA'. The overall performance measured as F1-score was analyzed using a mixed-effects model ANOVA. The response variable was the F1-score. The participant was a random factor, the stimulus frequencies was a fixed factor with four levels (7.5, 8.57, 10 and 12 Hz); the classification algorithm was a fixed factor with three levels. The null hypothesis was that the average F1-score were same across all classification algorithms. The significance level for all tests was set at $\alpha = 0.05$. A similar test was performed to compare the individual Swing and Stance accuracies. Additionally, the spatial contributions from the cortical areas derived from the weights of the classifier were compared using a mixed effects ANOVA. The stimulus frequencies was a fixed factor with four levels; the participant was a random factor and the ROI was a fixed factor with three levels. The channel contribution was the response variable tested with the significance level set at $\alpha = 0.05$.

5.2 Results

5.2.1 **Gait Phase Classification Performance**

Figure 5-4a illustrates the overall performance quantified by the F1-scores computed across all participants for the three methods 'Broad+LDA', 'Broad+SVM', and 'Delta+LDA' at four different stimulus frequencies. For the four frequencies, the median F1 scores for

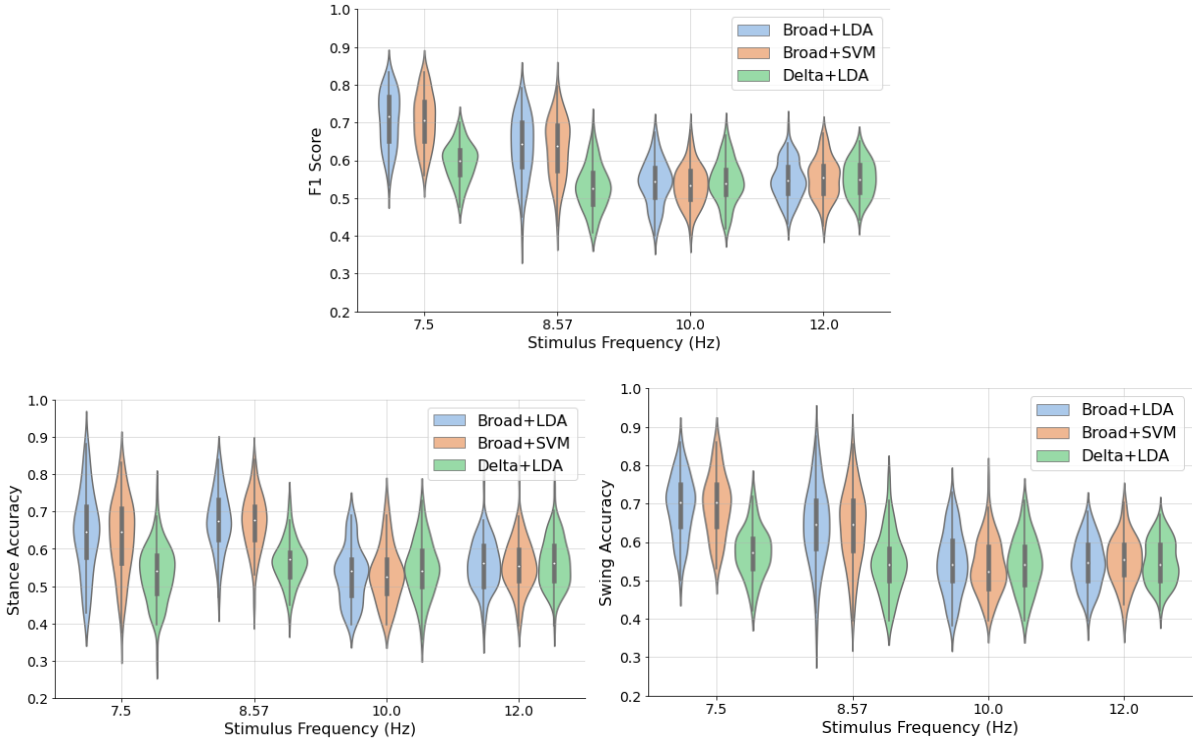

Figure 5-4. (A) F1 scores, (B) Stance accuracy and (C) Swing accuracy across participants for stimulus frequencies 7.5 Hz, 8.57 Hz, 10 Hz, 12 Hz for the methods Broad+LDA, Broad+SVM and Delta+LDA.

'Broad+LDA,' 'Broad+SVM,' and 'Delta+LDA' methods were observed as follows (7.5 Hz): 0.72 ± 0.07, 0.7 ± 0.07, 0.6 ± 0.05, (8.57 Hz): 0.64 ± 0.06, 0.64 ± 0.06, 0.53 ± 0.06, (10 Hz): 0.54 ± 0.06, 0.53 ± 0.06, 0.54 ± 0.06, (12 Hz): 0.65 ± 0.06, 0.55 ± 0.06, 0.55 ± 0.06 respectively. The analyses indicated that lower stimulus frequencies, specifically 7.5 Hz and 8.57 Hz, resulted in the highest F1 scores. The mixed-effects model ANOVA revealed that all main effects were significant ($p < 10^{-3}$). The main factors were stimulus frequency, F (1, 285) = 298.51, $\eta_p^2 = 0.51$, $p < 10^{-3}$; classification algorithm, F (2, 285) = 207.01, $\eta_p^2 = 0.59$, $p < 10^{-3}$; and interaction between stimulus frequency and classification algorithm was F (2, 285) = 12.0, $\eta_p^2 = 0.078$, $p < 10^{-3}$. Specifically, Broad+LDA' and 'Broad+SVM' showed significantly higher F1 scores compared to 'Delta+LDA' ($p < 10^{-3}$). No significant differences were noted between 'Broad+LDA' and 'Broad+SVM' ($p > 0.05$). The two-way interactions between the

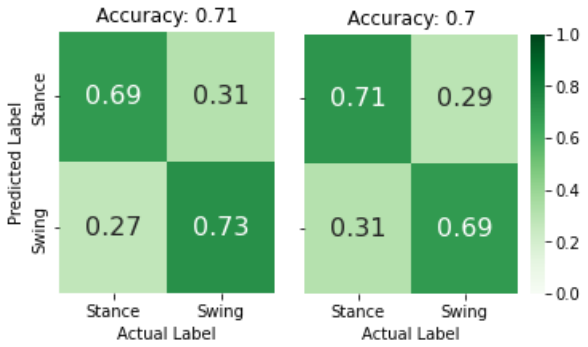

Figure 5-5. Confusion matrices for 'Broad+LDA' for 7.5 and 8.57 Hz.

method and stimulus frequencies were also significant ($p < 10^{-3}$). Post-hoc simultaneous comparisons applied a Bonferroni correction on the interaction term, revealing that F1 scores for 7.5 Hz and 8.57 Hz were significantly higher compared to 10 Hz and 12 Hz for both 'Broad+LDA' ($p < 10^{-3}$) and 'Broad+SVM ($p < 10^{-3}$) methods.' No significant differences were observed between 10 Hz and 12 Hz for all methods ($p > 0.05$).

Figure 5-4b and Figure 5-4c illustrates the individual Swing and Stance phase accuracies across all participants for the three methods and four stimulus frequencies, respectively. The median Swing accuracies for 'Broad+LDA', 'Broad+SVM', 'Delta+LDA', were (7.5 Hz): 0.7 ± 0.08, 0.7 ± 0.08, 0.57 ± 0.1, (8.57 Hz): 0.65 ± 0.05, 0.65 ± 0.07, 0.54 ± 0.08, (10 Hz): 0.54 ± 0.1, 0.52 ± 0.08, 0.54 ± 0.1, (12 Hz): 0.55 ± 0.1, 0.55 ± 0.08, 0.54 ± 0.08, respectively. The Stance phase accuracies were (7.5 Hz): 0.65 ± 0.11, 0.65 ± 0.1, 0.54 ± 0.1, (8.57 Hz): 0.67 ± 0.05, 0.68 ± 0.07, 0.57 ± 0.08, (10 Hz): 0.54 ± 0.1, 0.52 ± 0.08, 0.54 ± 0.08, (12 Hz): 0.56 ± 0.1, 0.55 ± 0.08, 0.56 ± 0.06, respectively. The mixed effects model revealed both individual Swing and Stance accuracies using the 'Broad+LDA' and 'Broad+SVM' were significantly higher than 'Delta+LDA' ($p < 10^{-3}$). These were significantly different for 7.5 Hz and 8.57 Hz compared to 10 Hz and 12 Hz stimulus frequencies. Overall, the 'Broad+LDA' method showed higher average performance in individual Swing and Stance phase classification, as also evident in the balanced accuracies presented in the aggregated median confusion matrix for both 7.5 Hz and 8.57 Hz as illustrated in Figure 5-5.

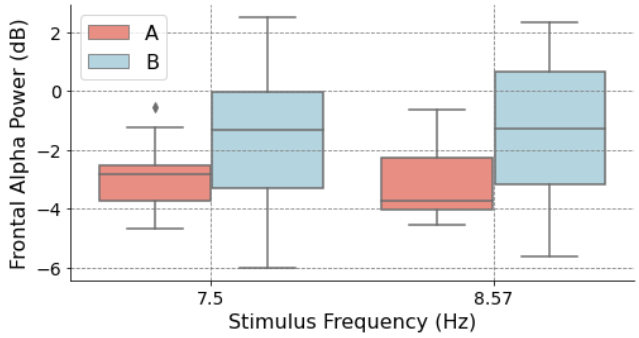

Figure 5-6. Frontal alpha power for 7.5 Hz and 8.57 Hz grouped as responder (A) and non-responder (B).

5.2.2 **Group-level performance and Frontal Alpha Power**

Furthermore, a participant-wise analysis separated the participants into two groups: responders (Group A) and non-responders (Group B) based on the classification accuracy related to BCI illiteracy [116]. In the present study, participants scoring above 70% accuracy were grouped into Group A (n=11) and the remaining in Group B (n=9). Figure 5-7 illustrates the grouping results for F1 score 7.5 Hz and 8.57 Hz with 'Broad+LDA' method. The median F1 scores for Group A vs. Group B with 'Broad+LDA' was: (7.5 Hz): 0.77 ± 0.06 vs. 0.65 ± 0.05 and (8.57 Hz): 0.68 ± 0.07 vs. 0.6 ± 0.06, respectively. Group A scored significantly higher than Group B for 7.5 Hz ($p < 10^{-3}$) and 8.57 Hz ($p = 0.004$), respectively.

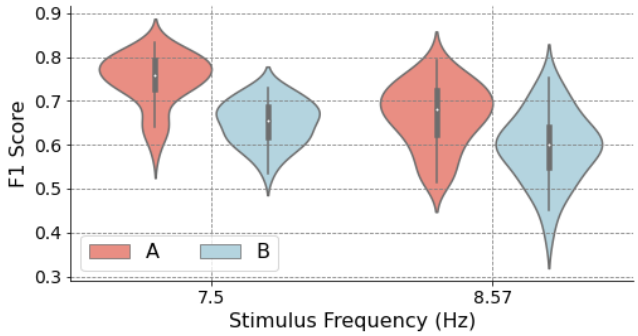

Figure 5-7. F1 score for 7.5 Hz and 8.57 Hz for 'Broad+LDA' grouped as responder (A); non-responder (B).

The group level differences in performance were investigated further by considering frontal alpha power computed from the average spectrum (F3, Fz, F4). A Pearson's correlation test between the frontal alpha power and f1-score revealed significant and moderate negative correlations for stimulus frequencies 7.5 Hz ($r = -0.38$, $p < 10^{-3}$) and 8.57 Hz ($r = -0.33$, $p < 10^{-3}$). The correlations for 10 Hz ($r = -0.12$, $p > 0.05$) and 12 Hz ($r = -0.01$, $p > 0.05$) were not significant. Therefore, subsequent analysis was performed to group the average frontal alpha power across the two Groups A and B. Figure 5-6 illustrates the frontal alpha power during the CAMS stimulation phase for Group A and B. The median alpha power (dB) for Group A versus B was: (7.5 Hz): -2.9 ± 1.2 vs. -1.3 ± 2.7 and (8.57 Hz): -3.8 ± 1.2 vs. -1.3 ± 2.5.

5.2.3 **Trial-level Performance**

The individual trial-level performance was visually investigated to identify regions of misclassifications. Figure 5-8 illustrates the alignment between the actual and predicted gait phases for two separate trials from the testing fold. The figure is divided into two panels, each representing a trial from a distinct participant for stimulus frequency 7.5 Hz Figure 5-8a) from participant P3 and 8.57 Hz Figure 5-8b) from P7. This graph allows for a direct comparison of the model's performance in predicting the timing of gait phase transitions. A high similarity between the actual and predicted phases of gait can be observed indicating the model's ability to capture the gait phase timings. However, instances of misclassifications highlight potential areas for improving the classifier's performance. Furthermore, within the same participant, inter-trial variability in detection performance can also be observed.

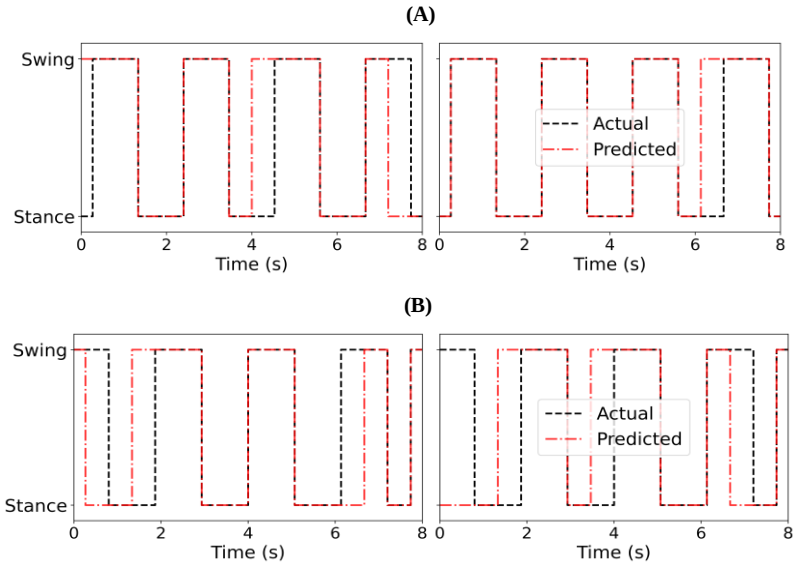

Figure 5-8. Examples of detected gait phases for two trials and two participants for 7.5 Hz (A) and 8.57 Hz (B).

5.2.4 **Spatial Contributions from Cortical Areas**

To examine the spatial contributions of cortical activities, the percentage contribution of each electrode was calculated from the weights of the 'Broad+LDA' model. Each cortical region was quantitatively analyzed by defining three ROIs (frontal, central and occipital).

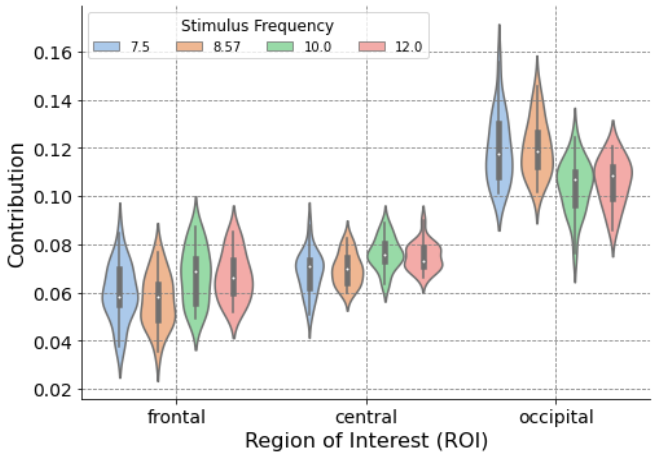

Figure 5-9. Region of interest channel contribution to Swing/Stance classification LDA Broad classifier.

Figure 5-9 illustrates distributions of the average contributions of the three ROIs for the trained gait phase decoder for each of the four stimulus frequencies. Across all frequencies, the occipital region has the highest contribution to the decoding performance followed by central and frontal electrodes, respectively.

The mixed-effects ANOVA revealed that the ROI and interaction between stimulus frequency and ROIs were significant ($p < 10^{-3}$). Post-hoc tests with Bonferroni correction revealed overall significant differences between the three ROIs with the highest to lowest contribution: occipital > central > frontal ($p < 10^{-3}$). The median contributions for stimulus frequency 7.5 Hz and 8.57 Hz were: (7.5 Hz): occipital (0.12) > central (0.07, $p < 10^{-3}$) and frontal (0.05, $p < 10^{-3}$); (8.57 Hz): occipital (0.19) > central (0.07, $p < 10^{-3}$) > frontal (0.06, $p < 10^{-3}$). There were significant differences between frontal and central ROIs for 8.57 Hz ($p = 0.003$) whereas, no significant differences for 7.5 Hz ($p > 0.05$).

5.3 Discussions

5.3.1 **Gait Phase Decoding from CAMS Stimulus**

The preliminary results presented in this study demonstrate the successful decoding of gait phases from the CAMS responses, validating the feasibility of this task using the novel CAMS BCI paradigm. The highest F1-scores were achieved by the 'Broad+LDA' and 'Broad+SVM' methods compared to the 'Delta+LDA' method proposed by [43]. This result underscores the potential benefit of utilizing a broader frequency range as input features to the classifier. Furthermore, the overall balanced accuracy of 71% for the 7.5 Hz and 8.57 Hz frequencies is consistent with existing literature on gait phase decoding, such as [43] which reported 72%. Similarly, the individual Swing and Stance phase accuracies for 7.5 Hz and 8.57 Hz on 'Broad+LDA' outperformed the 'Delta+LDA' approach with Stance and Swing accuracies reported at 70% and 73%, respectively. These results also align with previous work

on gait phase detection using AO + MI [43]. Notably, our approach achieves similar performance using the CAMS stimulus on a computer screen with just 12 EEG channels, in contrast to the earlier study that utilized a live human performer for gait presentation employing 46 EEG channels.

The group-level analysis of responders and non-responders, defined by BCI literacy in [116], showed that over 55% of the participants in this study achieved high BCI decoding performance. In this study, we set a stricter threshold for responders at 70%, compared to the 60% threshold used in the prior work [116] for MI-BCI. While both studies involve MI, the tasks differ; the current study employs AO + MI with CAMS whereas the previous study was MI. The responder group achieved a significantly higher F1-score of 0.77, compared to the non-responder group, further demonstrating the potential of an effective gait decoder. Additionally, observations from Figure 5-6 highlight the influence of attention on overall BCI decoding performance, as evidenced by the observed negative correlation between the frontal alpha activity and the F1-score.

In this study, four different stimulus speeds were investigated, with higher performances observed at the slower frequencies of 7.5 Hz and 8.57 Hz. In contrast, poorer performances at 10 Hz and 12 Hz can likely be attributed to two factors. Firstly, the study utilized 500 ms windows for segmenting the data. At frequencies of 7.5 Hz and 8.57 Hz, the swing/stance durations, being close to 1 s, likely allowed for capture of relevant features for effective decoding and provided more windows for training the classifiers. Conversely, for the 10 Hz and 12 Hz, where the swing/stance durations were less than 800 ms, these windows may not have captured sufficient details, provided fewer training examples and led to lower decoding accuracy. Secondly, the influence of frontal alpha power on accuracies was investigated. A significant moderate negative correlation was observed between frontal alpha power and F1-scores at 7.5 Hz and 8.57 Hz, whereas no significant correlations were noted at 10 Hz and 12 Hz. This suggests that, at slower speeds, the more intentional MI of swing and stance phases

requires greater cognitive engagement, likely resulting in stronger modulation of alpha power and clearer phase representation in the EEG compared to that at higher speeds.

The temporal evolution of the predictions at the single trial level highlights the model's ability to capture gait phases, though some errors are observed in the transition regions between phases. Despite these challenges, the high similarity between the actual and predicted phases at the trial-level emphasizes the promise of the proposed methods for real-world applications. Further investigations are required to improve the decoding accuracy of the gait phases at the transition regions. Subsequent studies could explore classifiers such as those that incorporate the temporal sequence [117] and temporal context [118] from the EEG to capture the gait dynamics and non-linear relationships.

5.3.2 **Influence of Attention and Cortical Contributions on Decoding Performance**

In this study, the observed decrease in frontal alpha power can be attributed to increased attentional demands and enhanced visual processing during the CAMS stimulus presentation. These findings are consistent with previous research, such as those by [114] and [115], which have noted that reductions in alpha power, particularly in the frontal and occipital areas, are associated with improved attentional focus and visual target detection. These findings suggest a neural mechanism whereby suppression of the alpha power may enhance sensory awareness and cognitive processing [119]. In our study, a larger decrease in frontal alpha power among responders suggests that participants were likely more engaged and attentive during the CAMS AO + MI task, contributing to higher gait phase decoding performance. This is also supported by another study that found an increase in the SSMVEP BCI classification performance when frontal alpha features were combined with features from the occipital electrodes [120].

Analysis of the cortical contributions revealed a predominant contribution from the occipital region to the decoder, emphasizing the role of visual processing in the CAMS paradigm. This finding is consistent with previous research on AO + MI, which have also noted substantial contributions from left and right occipital regions [43]. This likely reflects the visual-motor imagery process that involves visualizing movements of the lower limbs/gait, and the repetitive nature of the CAMS stimulus eliciting a visual steady state response, thereby enhancing the BCI decoding performance. Additionally, a notable contribution was also observed from the motor cortex, indicating that CAMS engages both occipital and motor areas, effectively integrating AO + MI. A previous study indicated that combining AO + MI might produce a synergistic effect, with the MI component serving as a mental simulation of motor actions, and the AO component, acting as an external visual scaffold [121]. Consequently, this integrated approach in the CAMS paradigm reinforces the mental simulation of gait, thereby enhancing the gait decoding performance.

5.3.3 **Challenges and Limitations**

To the best of the authors' knowledge, this study is the first to successfully decode gait phases from the responses to the CAMS stimulus. While the results are promising, they also highlight several challenges and provide opportunities for further research.

Although the study demonstrated promising offline decoding accuracies, translating these results into real-time applications, such as FES requires precise timing synchronization between detection and feedback, introducing additional challenges. It is crucial to test these implementations in real-time to evaluate their accuracy and latency effectively. Additionally, the fixed analysis window length of 500 ms may be reasonable for capturing the dynamics of gait at lower CAMS stimulus frequencies, such as 7.5 Hz and 8.57 Hz, where it corresponds to half the swing/stance duration. However, at higher gait speeds, this fixed window length

may result in decreased decoding performance. Future studies should explore adaptive window lengths or different analysis techniques to improve performance at higher gait speeds.

Significant differences in gait decoding performance between responders and non-responders highlight the challenge of BCI illiteracy. The current study design does not fully capture this effect, suggesting the need for further investigation into whether enhanced decoding algorithms can improve outcomes for non-responders. Subsequent research should aim to differentiate between the impacts of BCI illiteracy and algorithm performance for the CAMS BCI.

The median decoding F1-score for the responder group was 0.77, indicating robust gait decoding performance at slower speeds such as 7.5 Hz and 8.57 Hz for the unilateral leg. However, the performance may be lower when decoding for both legs, which warrants further exploration. While linear models with simple features have provided effective performance, there is potential to explore more sophisticated deep learning models that could offer improved detection capabilities [47], [88]. Additionally, expanding and augmenting the dataset could enhance the robustness and generalizability of the models. Besides, the model proposed in this study is a user-dependent model; therefore, developing user-independent models could facilitate faster calibration and training, benefiting real-time applications.

5.3.4 **Applications and Conclusions**

Decoding specific gait phases (Swing and Stance) with high precision using EEG data is less explored in the literature, with most studies targeting broader categories of movement [19], [49], [95]. Accurately decoding these phases is crucial for developing targeted rehabilitation interventions, such as gait phase-specific FES. The findings from this study on the CAMS BCI highlight a promising opportunity for applying the classifier outputs to enhance gait phase-dependent FES systems such as the one illustrated in Figure 2-2. By synchronizing FES with the classifier outputs, stimulation can be customized to trigger with each user's movement

intent, potentially increasing the effectiveness of gait training and accelerating motor recovery. Furthermore, the combination of visual and motor imagery with sensory feedback through FES, driven by precise gait phase detection, may promote neuroplasticity, resulting in significant and enduring recovery outcomes. The ability to decode gait phases could significantly enhance the development of control interfaces for exoskeletons [95], [122], and robot-assisted gait therapy [123].

This study successfully demonstrated the feasibility of using a CAMS BCI paradigm to decode swing and stance phases of gait from EEG data. Notably, the 'Broad+LDA' and 'Broad+SVM' methods achieved high F1-scores, indicating effective classification performance that compares favorably with existing methods in the literature. These findings provide valuable insights for the development of novel BCI feedback mechanisms specifically targeting different phases of gait. Implementing them in future designs can potentially enhance gait recovery outcomes in post-stroke rehabilitation.

Chapter 6 Study III: Enhancing the Asynchronous Visual BCI Decoding Performance in the CAMS Paradigm

Our previous study on AO + MI stimulus of gait achieved an average accuracy of 55% for a 2-second window length across four classes using CCA [4]. The objective of this study was to classify CAMS stimulus targets into one of two visual frequencies and enhance visual BCI performance, specifically low latency and high response accuracy towards real-time BCI operation. Primarily using features extracted from the occipital electrodes (POz, O1, Oz, O2), this study first aimed to investigate the classification performance in a 2-class scenario and establish a baseline with CCA. Additionally, the study sought to improve decoding accuracy at lower window lengths (to reduce latency) by proposing the use of the C-CNN algorithm for detecting visual responses.

6.1 Methodology

6.1.1 **Dataset Preparation and Pre-processing**

For this study, the dataset collected as part of Study 1 intervention phase was used to investigate visual BCI performance enhancements. As described in Chapter 3, each visual stimulation trial was presented to the participants for 8 s. EEG responses to the CAMS stimulus during this 8 s stimulation period were employed for analysis and enhancement.

Briefly, the channels POz, O1, O2 and Oz were used for this analysis. All the signals were filtered using a 4th order Butterworth band-pass filter between 0.1 Hz and 40 Hz. The CCA was used as a baseline to study the initial decoding performance of the CAMS response and establish a benchmark for comparison. To achieve this, CCA was applied to windows

processed both synchronously and asynchronously. In synchronous processing, segments for each window length were time-locked to the onset of the stimulus without sliding windows. For instance, if W = 2 s and the stimulus frequency was 7.5 Hz, the first 2 s of all 20 trials, time-locked to the onset, were extracted between [0s, 2s]. In asynchronous processing, each 8-second trial was segmented into sliding windows of various lengths (1 s, 2 s, 3 s, 4 s, 5 s, 6 s, 7 s, 8 s) with a 100 ms step size to increase the number of training epochs for the algorithm. The asynchronous method also served as a data augmentation step to increase the number of training examples required to train the C-CNN algorithm. The following sections provide a detailed explanation of the methods CCA and C-CNN, used to decode the CAMS responses.

6.1.2 **Canonical Correlation Analysis (CCA)**

Canonical Correlation Analysis (CCA) is the most widely used statistical method to detect SSVEP/SSMVEP responses [70], [81], [124]. In the context of BCI, CCA is used to estimate the underlying correlation between multi-channel EEG data X and a set of predefined reference templates Y of the same length to decode the user's intent. CCA aims to find the vectors w_x and w_y based on the transformations: $x = X^T w_x$ and $y = Y^T w_y$that maximize the correlation between x and y by solving (6.1):

$$\rho(x, y) = max_{w_x, w_y} \frac{\mathrm{E}\left[w_x^T X Y^T w_y\right]}{\sqrt{\mathrm{E}[w_x^T X X^T w_x]\mathrm{E}\left[w_y^T Y Y^T w_y\right]}}. \tag{6.1}$$

$$Y_n = \begin{bmatrix} sin(2\pi f_n t) \\ cos(2\pi f_n t) \\ sin(4\pi f_n t) \\ cos(4\pi f_n t) \end{bmatrix}, \qquad t = \left[\frac{1}{f_s}, \frac{2}{f_s}, \ldots, \frac{N_s}{f_s}\right], \tag{6.2}$$

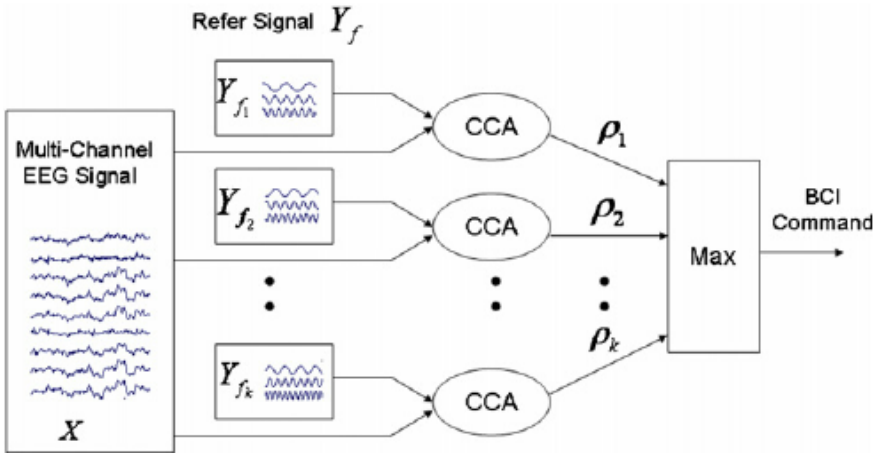

Figure 6-1. Illustration of the canonical correlation analysis applied on multi-channel EEG [62]

Where $Y_n \in \mathbb{R}^{4\times N_s}$ are the reference templates, f_n were the stimulus frequencies, N_s defines the number of samples, and f_s denotes EEG sampling frequency. The preprocessed data segments were input into the CCA algorithm. Each segment was analyzed to find the linear combinations of EEG channels that best correlate with the reference signals representing the visual stimulus frequency. To classify one of the two CAMS stimuli, the class was assigned as: C = argmax (ρ_{fi}), $i = 1, 2$ where ρ_{fi} were the canonical features extracted for each segment of the EEG. Figure 6-1 provides a visual illustration of the CCA method applied to multi-channel EEG.

6.1.3 **Complex Convolutional Neural Networks (C-CNN)**

In this study, the C-CNN architecture and methodology are adapted from our previous studies using C-CNN for SSVEP stimulus classification [5], [125], [126]. This method has shown superior performance in decoding the visual stimulus compared to other methods for SSVEP BCI [2], [5]. However, the performance of the C-CNN on the CAMS stimulus response classification has yet to be examined. In this study, we evaluated its effectiveness in decoding

the CAMS frequency responses, particularly in the low latency regime. The subsequent sections have been developed based on definitions provided in our prior work [126].

6.1.3.1 Feature Extraction

The complex FFT representation, including both magnitude and phase information, was employed as classifier inputs. First, the time-domain signal was converted to its complex FFT form using the standard FFT with a resolution of 0.2930 Hz. Frequency components from the real part and the imaginary parts were extracted for each channel between 0.1 Hz and 35 Hz, producing two vectors, each of length 120. These vectors were combined into a single feature vector as: $\mathrm{I} = Re(X) \mid\mid Im\ (X)$, forming a 240-length vector with the real part in the first half and imaginary part in the second half. This feature vector was stacked together to form a matrix with dimensions $N_{ch} \times 2 * N_{fc}$, where $N_{fc} = 120$ frequency components and N_{ch} = 4, number of channels. This method, which uses the complex FFT as input to the CNN, is known as the C-CNN approach. An example of the input I_{C-CNN} is defined as (6.3):

$$I_{C-CNN} = \begin{bmatrix} Re\{FFT(x_{POz})\}, Im\{FFT(x_{POz})\} \\ Re\{FFT(x_{O1})\}, Im\{FFT(x_{O1})\} \\ Re\{FFT(x_{Oz})\}, Im\{FFT(x_{Oz})\} \\ Re\{FFT(x_{O2})\}, Im\{FFT(x_{O2})\} \end{bmatrix} \tag{6.3}$$

6.1.3.2 Network Architecture

The CNN architecture used in this analysis was adapted from the one proposed in [5], [126]. Figure 6-2 illustrates the CNN architecture used in this investigation. CNN consists of four main layers: an input layer, two convolutional layers, and a fully connected output layer. The input layer of the CNN, $I_{p.j}$, had dimensions $N_{ch} \times 2 * N_{fc}$, where $1 \leq p \leq N_{ch}$ and $1 \leq j \leq 2 * N_{fc}$. This was followed by the convolutional layer C1 was designed based on the spatial filtering concept. The kernel dimensions of $N_{ch} \times 1$ were used for this layer and performed 1D

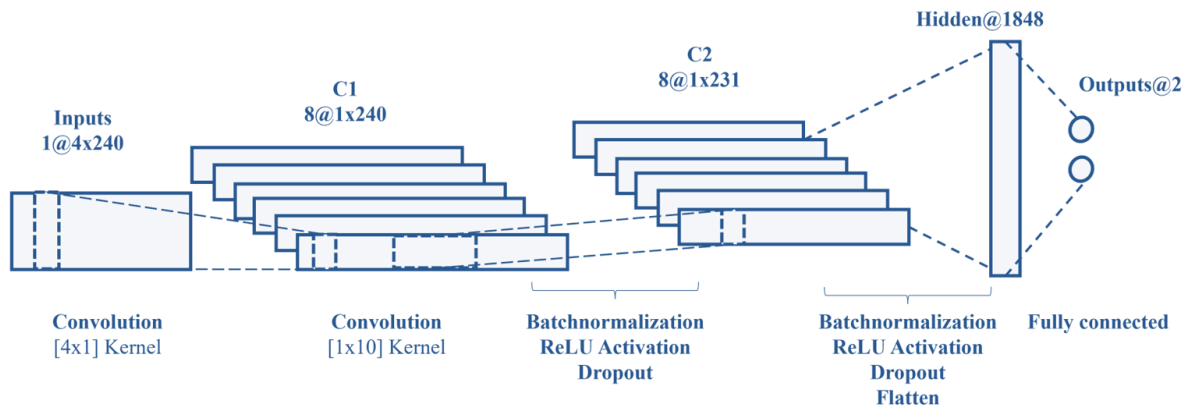

Figure 6-2. Convolutional Neural Network Architecture

convolutions across the channel dimension (N_{ch}) of the input; $N_{ch} = 4$. The objective for this layer was to learn representations applying different weights to each input channel. The number of feature maps in the C1 layer was $2 * N_{ch}$ (i.e., 8), with dimensions $1 \times 2 * N_{fc}$. The C2 layer was designed to operate on the spectral representation dimension (N_{fc}) of the previous layer. The kernel dimension for this layer was 1×10. The number of feature maps in this layer were $2 * N_{ch}$ (i.e., 8). As a result of the convolution, the feature maps in this layer had the dimensions equal to $1 \times (2 * N_{fc} - 10 + 1)$, i.e. 231. Batch normalization which has been shown to reduce the internal covariance within input samples resulting in the samples having zero mean and unit variance [127], was performed on the outputs of layers C1 and C2. The rectified linear unit (ReLU) (6.5) was used as the activation function. To prevent overfitting, Dropout was added to the network as a regularization technique. Dropout and batch normalization have been shown to improve the generalization performance and training speed of neural networks [127]. After flattening the output of the previous layer, the number of units in the output layer (K) were kept equal to the number of classes in the input data, i.e. K = 2. The output layer was equipped with the *softmax* function to output the probability that a given input segment belonged to a particular class. The following section details the network learning procedure. The style of notation is similar to the one used in [89].

6.1.3.3 Network Learning

A unit in the network is defined by $x_k^l(p)$ where l is the layer, k is the feature map and p is the position of the unit in the feature map. Therefore, the output of a specific unit is defined as:

$$x_k^l(p) = f\big(BN(\sigma_k^l(p))\big), \tag{6.4}$$

where f is the ReLU activation function defined as:

$$f(\sigma) = max\ (\sigma, 0). \tag{6.5}$$

$\sigma_k^l(p)$ represents the scalar product of a set of input units and the weight connections between these units and the pth unit in map k and layer l. BN represents the batch-normalization step. This will be explained in the subsequent sections. The computations performed by each layer are described as follows. The Conv_1 layer performs the following operation:

$$\sigma_k^1(p) = \sum_{j=1}^{N_{ch}} I_{p,j} w_k^1(j) + b_k^1 \tag{6.6}$$

where $w_k^1(j)$ is a set of weights with $1 \leq j \leq N_{ch}$ and b_k^1 is a bias. k indexes the feature map with $1 \leq k \leq 2 * N_{ch}$. In this layer, there are a total of $2 * N_{ch}$ feature maps and the size of the convolution kernel is $N_{ch} \times 1$. The output of each σ_k^1 is a $1 \times 2 * N_{fc}$ vector, where N_{fc} denotes the samples in the frequency domain. Next, batch normalization (BN) is performed on this output and passed through the ReLU activation function.

$$x_k^1 = f(BN(\sigma_k^1) \tag{6.7}$$

The output of C1 layer, x_k^1 , is fed as input to C2 layer.

$$\sigma_k^2(p) = \sum_{i=1}^{2*N_{ch}} \sum_{j=1}^{10} x_i^1(p+j-1)w_i^2(j) + b_k^2 \tag{6.8}$$

This layer is similar to C1, the output of each σ_k^2 is a $1 \times (2 * N_{fc} - 10 + 1)$ vector. BN and ReLU are applied to this output respectively. The output layer performs the following operation:

$$\sigma^3(p) = \sum_{k=1}^{2*N_{ch}} \sum_{i=1}^{2*N_{fc}-10+1} x_k^2 w_k^3(i) + b_k^3 \tag{6.9}$$

The softmax function is used as the activation function at the output layer:

$$S = \frac{\exp\,(x_p^3)}{\sum_{j=1}^{K} \exp\,(x_j^3)} \tag{6.10}$$

The output S is a vector of length K and each element in this vector corresponds to a probability score that a given sample belonged to a particular class.

6.1.3.4 Training Parameters

The weights of the CNN were initialized based on a Gaussian distribution $\sim N(0, 0.01)$. The network was trained using the backpropagation technique by minimizing the categorical cross-entropy loss L:

$$L_i = \sum_{j=1}^{K} t_{i,j} log(S_{i,j}) \tag{6.11}$$

where $t_{i,j}$ is the ground truth probability score and $S_{i,j}$ is the predicted probability score for the ith training example and j^{th} class. The stochastic gradient descent with momentum was used as the optimization algorithm to train the network. A grid search was employed as the hyper-parameter search strategy to find the best training parameters. The search space was defined as follows: Learning Rate (α) : $\{10^{-3}, 2 \times 10^{-3}, 5 \times 10^{-3}, 10^{-2}, 10^{-1}\}$, Mini Batch size

(B) : 2^b; $b \epsilon \{5, 6, 7, 8, 9, 10\}$, Dropout Ratio (D) : $\{0.25, 0.3, 0.35, 0.4, 0.45, 0.5\}$, L2 Regularization (L) : $\{10^{-4}, 5 \times 10^{-4}, 10^{-3}, 5 \times 10^{-3}\}$, Number of Epochs (E) : $\{20, 30, 40, 50, 60\}$, and parameters that led to the best average accuracy across all participants were chosen. The hyper-parameter optimization was performed for all pipelines. Within each pipeline, the same hyper-parameters were used for all participants and window sizes.

6.1.4 **Asynchronous CAMS IC versus NC Detection**

In practical applications, it is preferable to allow users to interact with the BCI asynchronously, meaning the BCI operates independently of specific stimulus timings or predefined intervals. Unlike cue-paced or synchronous BCIs, asynchronous operation involves continuous decoding and analysis of responses, which is more technically challenging but provides a more natural interaction. This mode includes two states: intentional control (IC) and no control (NC). For the CAMS stimulus, the time when the user gazes at the stimulus is called an IC state. The NC state or rest state is defined when the user does not gaze at the stimulus.

To evaluate the performance of the asynchronous BCI, the EEG data was labelled as IC state and NC state. The 8 s stimulation period was labelled as the IC state, and the combined 7 s duration of the cue (2 s) and rest period (5 s) was labelled as the NC state. This is illustrated in Figure 6-3. The multi-channel EEG signals were segmented with a fixed window (W = [1s, 2s, 3s]) and a step size of 100 ms. For training, the user-dependent C-CNN, the final softmax layer was modified to include a third NC class, resulting in a total of three neurons: two IC = (C1, C2) states and one NC = C3 state. The convolutional layers and kernels were kept same as the two-class architecture. A 5-fold cross-validation scheme was used to evaluate the IC vs.

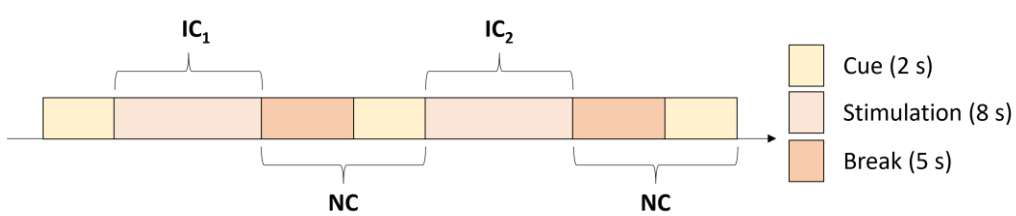

Figure 6-3. Asynchronous classification–Intentional control and no control state.

NC detection. Since each stimulus frequency consisted of 20 trials for every stimulus combination block; 20 NC trials were randomly sampled from the pre-defined time regions to ensure balanced training examples for the classifier.

6.1.5 **Performance Evaluation**

The two class classifier performance for CCA and C-CNN were analyzed for each of the six two-class stimulus frequency combinations used in the CAMS BCI paradigm: (7.5 Hz, 8.57 Hz), (7.5 Hz, 10 Hz), (7.5 Hz, 12 Hz), (8.57 Hz, 10 Hz), (8.57 Hz, 12 Hz), (10 Hz, 12 Hz). The overall classification accuracy was calculated for each stimulus frequency combination. Furthermore, baseline analysis with synchronous CCA compared the influence of stimulus frequency difference in each intervention block on the overall classification accuracy.

The C-CNN classifier was evaluated based on the five-fold cross-validation. The classifier was trained individually for each participant, stimulus frequency combination and window length (W = [1 s, 5 s]). Each stimulus combination block consisted of 20 trials presented for each stimulus frequency; therefore, the five folds were selected over the trials i.e. the training fold consisting of 16 trials and testing fold consisting of 4 trials. The validation accuracy from each fold was averaged to derive the overall accuracy for each stimulus combination, participant, and window length.

To evaluate the asynchronous IC versus NC detection of the three class C-CNN, the confusion matrix was used to derive the performance metrics. The two stimulus frequency predictions belonging to IC_1 and IC_2 were combined into a single category IC class or class 1. Next, the NC was defined as the second class or class 2. From the confusion matrices, a true positive (TP) was defined during the IC state when the participant looked at the CAMS targeted frequency and the classifier predicted this segment correctly as an IC state. A false positive (FP) was defined when the classifier predicted an NC state as IC state. If the classifier misclassified an IC state as NC, this was defined as a false negative (FN). The F1-score was

calculated as (5.1). The true positive rate (TPR) and false positive rate (FPR) were calculated as per (6.12), (6.13):

$$\mathrm{TPR} = \frac{\mathrm{TP}}{\mathrm{TP} + \mathrm{FN}} \tag{6.12}$$

$$\mathrm{FPR} = \frac{\mathrm{FP}}{\mathrm{FP} + \mathrm{TN}} \tag{6.13}$$

Furthermore, for nearly real-time applications, classifying an active (IC) state into a different active state usually has more negative effect than misclassifying it as an inactive (NC) state. Therefore, a false activation rate (FAR) was defined as the rate of misclassifications within the different IC states, *i.e.* misclassification between one IC state and another IC state. Consider $CM \in \mathbb{R}^{N_c+1 \times N_c+1}$ to be the resultant confusion matrix of the three-class classification, where $N_c = 2$, is the number of IC states [2]. After normalizing the CM by the number of test examples in each class, the FAR per class (F_j) was defined as per (6.14). Finally, the average FAR across all stimulus frequencies was calculated according to (6.15):

$$F_j = 1 - \frac{CM_{jj}}{\sum_{i=1}^{N_c} CM_{ji}}; j = \{1, 2, \dots, N_c\} \tag{6.14}$$

$$\mathrm{FAR} = \frac{1}{N_c} \sum_{j=1}^{N_c} F_j, j = \{1, 2, \dots, N_c\} \tag{6.15}$$

Additionally, for a qualitative evaluation of the pseudo-online performance of the asynchronous BCI classifier, the trained three class C-CNN extracted from one of the cross-validation folds was applied on the entire training session. Specifically, this was applied in a continuous decoding scenario which included segments of data containing the transition segments between IC and NC. This step emulated an online asynchronous BCI.

6.1.6 **Statistical Analysis**

Statistical analyses were performed across participants, detection algorithms, and stimulus frequency combinations for their overall classification accuracy. The performance of CCA and C-CNN were evaluated for their ability to classify CAMS visual stimuli as a binary problem. Accuracies were calculated for each frequency combination and the overall performance was analysed using a mixed-effect model ANOVA. The classification accuracy was the response variable. Participant and window length (W=[1 s, 5 s], 5 levels) were treated as random factors, classification algorithm was a fixed factor with two levels (CCA and C-CNN), and the stimulus frequency combination was a fixed factor with six levels. The null hypothesis was that the average classification accuracies were the same for all algorithms. The significance level was set as α=0.05.

6.2 Results

6.2.1 **Baseline Performance Analysis with Synchronous CCA**

Figure 6-4 illustrates the CAMS visual BCI performance for the different two class stimulus frequency combinations for window lengths W=1s to W=8s across all participants using CCA. The median accuracies for W < 4 s were less than 65%, whereas for W ≥ 4 s, the accuracies were greater than 70%. The highest classification accuracies were achieved for W

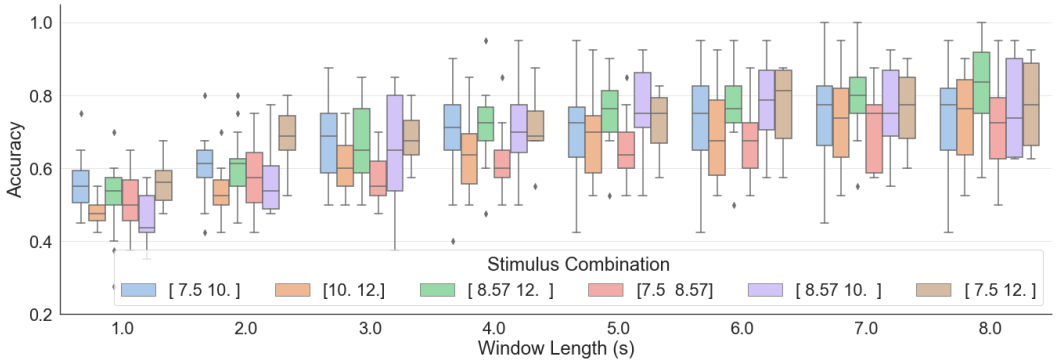

Figure 6-4. CAMS visual BCI classification accuracy for each visual stimulus combination, window lengths [1s, 8s] across all participants using Synchronous CCA.

= 8 and stimulus combinations (Hz): (8.57, 12) and (7.5, 12). Figure 6-5 presents the classification accuracy considering the frequency differences between the six different stimulus frequency combinations used in this study for W = 8 s. It is evident that higher classification accuracies were achieved for the stimulus frequencies with greater differences such as (8.57, 12) and (7.5, 12), corresponding to differences 3.43 Hz and 4.5 Hz, respectively. The highest decoding accuracy of 83.8% was achieved for the combination (8.57, 12).

6.2.2 **Enhanced decoding performance with C-CNN**

Figure 6-6 illustrates the CAMS visual BCI performance for C-CNN method compared to CCA for the different two class stimulus frequency combinations for window lengths W=1s to W=5s across all participants. The median accuracies for W < 4 s were higher than 68% for

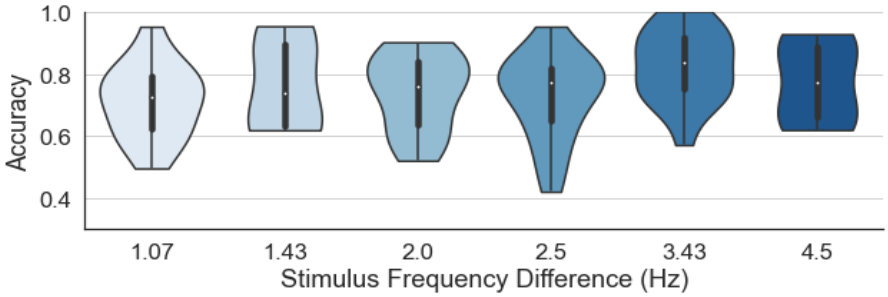

Figure 6-5. CAMS visual BCI accuracy versus stimulus frequency differences using Synchronous CCA.

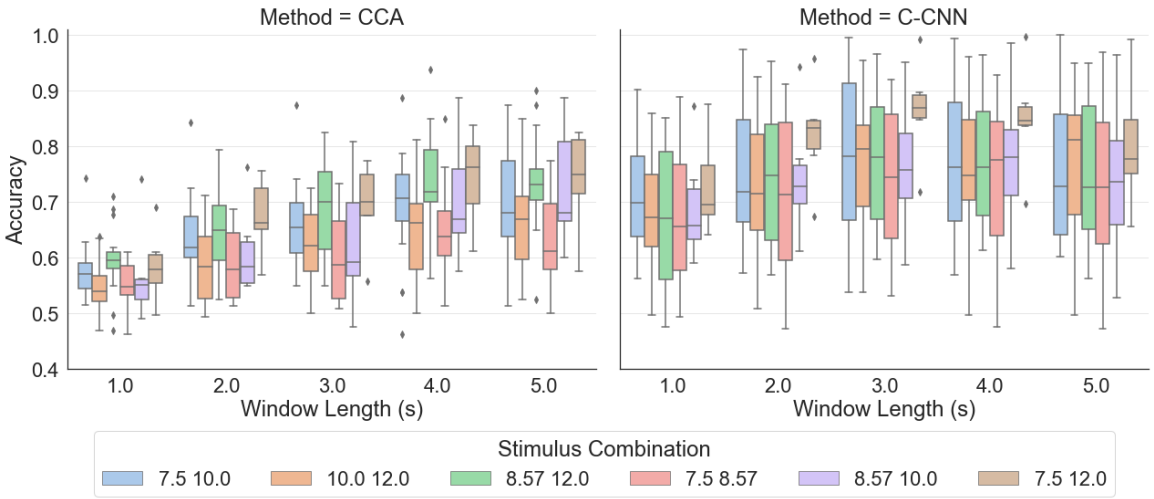

Figure 6-6. Asynchronous CAMS visual BCI accuracy comparing CCA versus C-CNN for W=[1s, 5s].

C-CNN compared to CCA. The highest classification accuracies were achieved for W = 3 s and stimulus combinations (Hz): (7.5, 12) and (8.57, 12), similar to the results of the synchronous CCA baseline. The median accuracies for W = 3 s for C-CNN versus CCA for different stimulus frequency combinations were (Hz): (7.5, 12): (0.87 ± 0.089 vs. 0.7 ± 0.078); (8.57, 12): (0.78 ± 0.114 vs. 0.7 ± 0.085); (10, 12): (0.8 ± 0.13 vs. 0.62 ± 0.06); (7.5, 10): (0.78 ± 0.142 vs. 0.65 ± 0.07); (8.57, 10): (0.76 ± 0.12 vs. 0.59 ± 0.12); (7.5, 8.57): (0.75 ± 0.12 vs. 0.58 ± 0.07).

Statistical analysis revealed that all the main effects including the classification algorithm and stimulus frequency combination, were significant ($p \leq 10^{-3}$). Furthermore, the two-way interaction term between the algorithm and stimulus frequency combination were significant ($p = 0.002$). Simultaneous comparisons with Bonferroni correction indicated significant differences between C-CNN and CCA, with C-CNN performing significantly better than CCA ($p = 0.001$). Comparisons between the algorithm and stimulus frequency combination revealed that C-CNN outperformed CCA across all stimulus frequency combinations ($p \leq 10^{-3}$).

The accuracy was significantly higher for (7.5, 12) and (8.57, 12) combinations compared to the other frequency combinations ($p < 0.028$) across classification algorithms. For C-CNN, the accuracy for each stimulus frequency combination, in descending order of performance, was (Hz): (7.5, 12), (10, 12), (7.5, 10), (8.57, 12), (7.5, 8.57), (8.57, 10), across all window lengths. The effect of window length on the classification performance revealed that the C-CNN significantly outperformed CCA at W < 3 s ($p \leq 0.017$), was marginally better than CCA at W = 4 s ($p = 0.06$) and showed no significant difference CCA at W = 5 s ($p = 0.142$). The highest accuracy for C-CNN was achieved for the window length W = 3 s with a mean accuracy of 78 % averaged across all combinations and highest accuracy of 88% for (7.5, 12) combination.

6.2.3 **Asynchronous IC Vs. NC CAMS BCI Performance**

Figure 6-7a and Figure 6-7b illustrates the average F1-score and FAR calculated across the five folds from training the C-CNN offline for windows lengths W = [1s, 2s, 3s] on the (10 Hz, 12 Hz) stimulus frequency combination. The median F1-scores were: (W=1s, F1=0.88), (W=2s, F1=0.92) and (W=3s, F1=0.96). The corresponding median FAR scores were: (W=1s, FAR=0.34), (W=2s, FAR=0.3) and (W=3s, FAR=0.27). A 9% increase in median F1-score

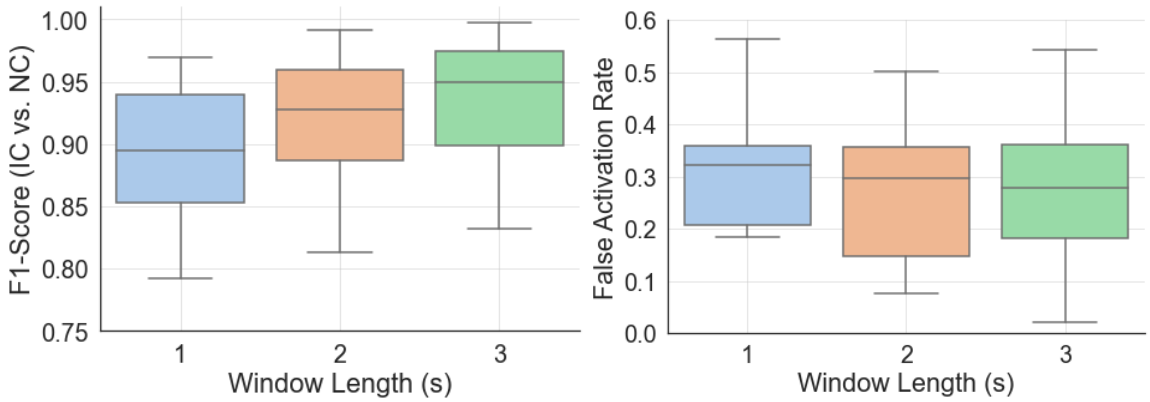

Figure 6-7. Box-plots of F1-score and False activation rate (FAR) for asynchronous IC versus NC detection for stimulus frequency combination (10 Hz, 12 Hz) and W = [1s, 2s, 3s] with whiskers extending from upper and lower quartile to minimum and maximum values.

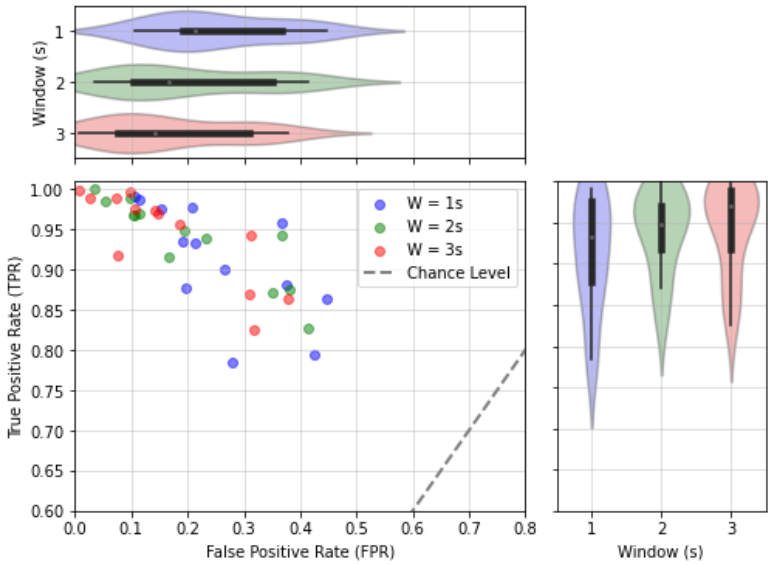

Figure 6-8. TPR versus FPR characteristics for asynchronous IC versus NC detection for stimulus frequency combination (10 Hz, 12 Hz) and W = [1s, 2s, 3s]. Dotted line indicates the chance level TPR versus FPR.

can be achieved from W=1s to W=3s; and a median decrease of 20% in FAR can be achieved with W = 3s. Furthermore, the TPR and FPR for the three window lengths were analyzed. Figure 6-8 presents the TPR versus FPR characteristics for the asynchronous IC versus NC detection for the stimulus frequency combination of (10 Hz, 12 Hz) and W = [1s, 2s, 3s]. The median TPR and FPR were: (W=1, TPR=0.94, FPR=0.22), (W=2, TPR=0.95, FPR=0.17), (W=3, TPR=0.98, FPR=0.14). Overall, as expected, increase in window length leads to improved performance. The asynchronous BCI was analyzed further for its behavior in a pseudo-online detection scenario.

Figure 6-9 illustrates the temporal evolution of the pseudo-online C-CNN predictions on one of the sessions between 4 and 6.5 minutes from the start of the session for one of the participants. The ground truth and predicted labels for the three classes: IC1 (10 Hz), IC2 (12 Hz) and NC, are shown along with the average EEG spectrogram calculated across POz, O1,

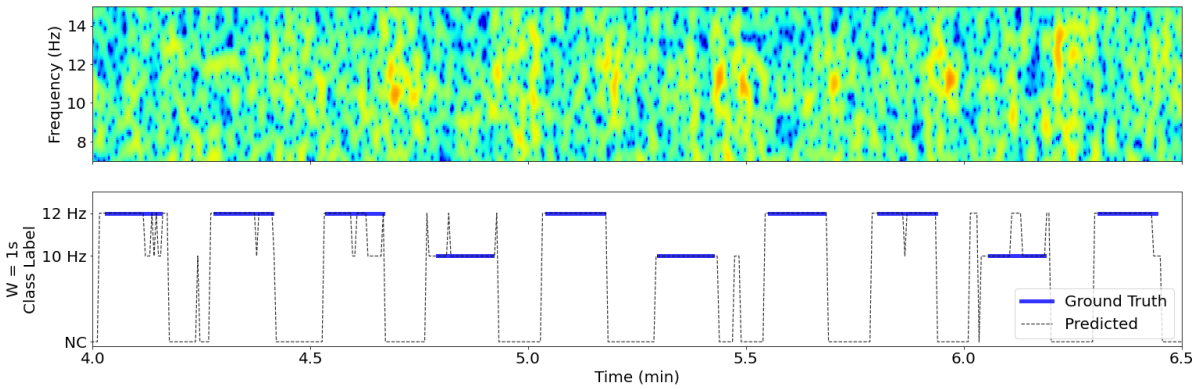

Figure 6-9. Temporal evolution of the pseudo-online C-CNN classifier of IC and NC states on a single participant's session; W = 1 s. Top: Averaged EEG spectrogram computed across channels POz, O1, O2 and Oz; Bottom: true and predicted labels.

O2 and Oz channels. Furthermore, the pseudo-online predictions calculated at W = 1s and step of 100 ms was smoothed with a majority vote of 3 consecutive values.

6.3 Discussions

6.3.1 **CCA Provides Reasonable Baseline Visual BCI Accuracy**

The CAMS stimulus, characterized by its repetitive gait pattern, notably induces a steady-state response observed in the occipital electrodes (illustrated in Figure 4-3), allowing for reliable classification using CCA. While the decoding accuracy was 83.8% (for W = 8s), practical considerations prioritize lower latency and higher speed for effective BCI control applications. These results provide a baseline and motivate future studies to improve the classification performance for lower window lengths, typically corresponding to faster detection speeds. Interestingly, the presentation of two gait speeds at a larger frequency difference resulted in higher accuracy and vice versa. Future inquiry into the effects of frequency differences between stimuli is required for improving the multi-class CAMS BCI paradigm.

6.3.2 **Comparative Analysis of C-CNN and CCA Performance in Visual BCI**

The findings indicate offline decoding performance of the asynchronous two-class BCI with C-CNN outperformed the CCA. This was expected, given the C-CNN was trained on user specific data, whereas CCA was an unsupervised, generic method used as a baseline for comparison. However, the superior performance of C-CNN, particularly at shorter window lengths, suggests that it is more effective in capturing the frequency domain features of the CAMS stimulus. This likely results from the C-CNN's ability to utilize both magnitude and phase information present in the signal [5].

The significant performance differences across stimulus frequency combinations indicate that certain stimulus frequency combinations may be more conducive to eliciting strong, detectable responses, which are crucial for optimizing BCI performance. Particularly, the highest performances were observed for the frequency combinations with the largest difference between the stimulus frequency (E.g. (10, 12) and (12, 7.5)). This observation suggests that smaller frequency differences between stimuli may lead to reduced discriminability in the EEG responses. Nevertheless, a high accuracy of 87% at W = 3 s makes C-CNN a promising candidate for practical implementations where low latency and reliable response detection are critical. Future research should investigate the effects of varying frequency differences between stimuli to enhance the performance of the multi-class CAMS BCI paradigm. Understanding these effects could lead to optimized stimulus designs that improve classification accuracy and overall BCI effectiveness.

6.3.3 **Asynchronous C-CNN Performance and Pseudo-online Detection**

The asynchronous three-class C-CNN provides high decoding performance without requiring windows to be precisely aligned with stimulus onset, unlike synchronous BCIs. Increasing the window length from 1s to 3s improved the F1 score by 9% and decreased the FAR by 20%. However, shorter window lengths are preferable for low latency applications

due to the trade-off between window length and accuracy. Despite this, an F1-score of 0.88 is reasonable for decoding IC versus NC states in the CAMS BCI. The system achieved a high TPR of 0.94 and reasonably low FPR of 0.22 indicating reliable performance in detecting user intent (visual). These metrics suggest that while shorter windows may slightly reduce accuracy, the system provides reliable performance suitable for practical applications where timely feedback is essential.

The example on the pseudo-online results indicated a high similarity between the predicted and ground truth labels of IC and NC states. A higher number of misclassifications were observed at the transition regions between states, i.e., at the onset and offset of the stimulation periods. This is likely due to the nature of the labeling of windows for asynchronous detection; windows at the transitions were not included in the training set while training the C-CNN. These windows contain a mix of steady-state activity and transition-state data, which closely resembles the errors that would likely occur in an online system. To address these challenges, majority vote-based windowing and increasing the detection window length can reduce errors and improve overall performance.

6.3.4 **Challenges and Limitations**

The study highlights that shorter window lengths, while preferable for low latency, may reduce accuracy. Ensuring a balance between window length and performance is crucial for practical applications, where both accuracy and low latency are essential for user engagement and effective rehabilitation outcomes. Therefore, subsequent work needs to validate the proposed algorithm's effectiveness in a real-time setting and then decide whether further improvements can be made to increase the accuracy for shorter windows. The current investigation focused on the occipital channels targeted towards assessing the visual BCI performance. Including frontal channels may further enhance asynchronous BCI performance by leveraging features related to attention [120].

Currently, the CAMS stimulus is presented on a computer screen, which may not fully engage users or simulate real-world conditions. Developing an augmented reality (AR) environment for the CAMS BCI can provide a more immersive and interactive experience, potentially enhancing user engagement and improving BCI performance. AR can simulate more realistic scenarios, making the system easy to use and portable. Previous studies have successfully implemented SSMVEP checkerboard stimulus in AR and shown high decoding performance [2], [3].

Another challenge identified in the study is the finding that larger stimulus frequency differences improved classification accuracy. Smaller frequency differences resulted in lower accuracy, suggesting that better separation and discrimination of EEG responses require optimizing stimulus parameters. Future research should systematically investigate the optimal frequency differences and other stimulus parameters, such as color, contrast, distance, and size, to maximize classification performance.

This study implemented user-dependent training of C-CNN for detecting the CAMS responses. As user-dependent systems require individual calibration and user-training, they can be time-consuming and expensive. A more practical approach would involve the development of user-independent systems or collecting extensive training data upfront across many users, which can then be fine-tuned for each individual [5], [125]. Improving calibration efficiency is crucial for broader adoption and ease of use in clinical settings.

6.3.5 **Applications and Conclusions**

The CAMS BCI system, with its high accuracy and low latency, has significant potential for various control applications beyond traditional uses. Its ability to decode user intent from EEG signals in real-time enables it to be adapted for a wide range of tasks, providing intuitive and seamless control interfaces.

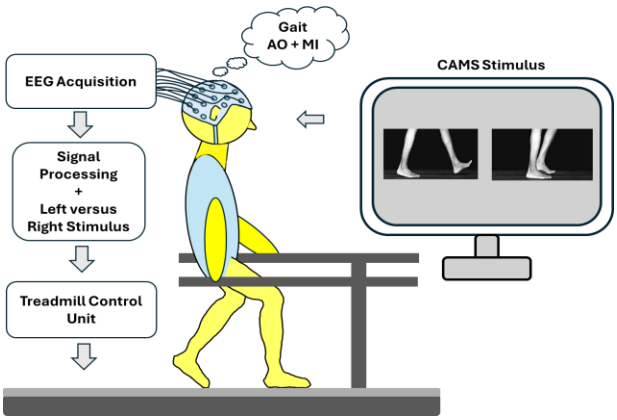

Figure 6-10. Asynchronous CAMS visual BCI speed control of a treadmill.

One promising application is controlling the speed of a treadmill in an asynchronous manner, as illustrated in Figure 6-10. This application leverages the high accuracy and low latency achieved by the C-CNN algorithm, making it suitable for real-time BCI control in rehabilitation settings. The CAMS BCI system can be integrated into a treadmill to allow users to adjust the speed depending on which speed of gait/visual stimulus they are attending to. For example, in the case of the stimulus frequency combination (10 Hz, 12 Hz), the 10 Hz stimulus could be mapped to a slower speed of the treadmill, while the 12 Hz stimulus could be mapped to a higher speed of the treadmill. By decoding the CAMS responses associated with different gait speeds, the system can provide the user with intuitive control of the treadmill. While this could be achieved with a simple SSVEP/SSMVEP BCI, the advantage of CAMS lies in its ability to simultaneously activate and engage regions of the motor cortex during the session. As users observe and imagine the movement, the motor cortex remains engaged, which could lead to enhanced neuroplasticity and better rehabilitation outcomes [39]. This feedback also provides a means for the user to be actively involved in the therapy, leading to improved results compared to passive involvement in therapy.

This study successfully demonstrated the use of the adapted C-CNN algorithm in decoding the responses from the CAMS stimulus. The C-CNN method achieved high F1-

scores, significantly outperforming CCA method, particularly at shorter window lengths. The median F1-scores for C-CNN were 0.88 (W=1s), 0.92 (W=2s), and 0.96 (W=3s), with corresponding FARs of 0.34, 0.30, and 0.27. These results indicate that C-CNN provides superior classification performance, making it a promising tool for real-time BCI applications and future rehabilitation strategies.

Chapter 7 Conclusions and Future Work

7.1 Highlights of Thesis Contributions

This thesis proposed and explored a novel BCI paradigm called CAMS: Combined Action Observation, Motor Imagery, and Steady-State Visual Evoked Potentials. Through three distinct studies, we advanced our understanding of this paradigm's effects on cortical excitability, its application in decoding gait phases, and enhancing asynchronous visual BCI decoding performance. Below are the key contributions and findings from each study, followed by discussion on next steps towards generating a closed-loop system for motor rehabilitation.

7.1.1 **Novel BCI Intervention to Induce Cortical Excitability**

The first study demonstrated that the CAMS BCI intervention enhanced cortical excitability within the primary and supplementary motor areas. The intervention resulted in increased negativity across all MRCP components associated with movement preparation and execution. The effects of AO + MI on enhancing the short-term MRCP components is qualitatively similar to the effects reported following aerobic exercise [62]. These findings support the CAMS paradigm's ability to effectively engage the movement related areas of the cortex offering a new approach for improving neuroplasticity and motor recovery in individuals with neurological damage. To the authors' best knowledge, this is the first study to examine measures of MRCP in an AO + MI paradigm (CAMS). The ability to measure acute changes in cortical excitability using EEG—a method known for its ease of use and non-invasiveness—provides a promising new avenue for understanding and enhancing neuroplasticity in motor rehabilitation.

7.1.2 **Decoding Phases of Gait from EEG**

This thesis presents novel methods for decoding the phases of gait (swing and stance) from EEG signals during congruent AO + MI of gait via the CAMS approach. This study highlighted the importance of accurately decoding gait phases for developing targeted rehabilitation interventions such as phase-specific functional electrical stimulation. The overall balanced accuracy of 71% for the 7.5 Hz and 8.57 Hz frequencies aligns with existing literature on gait phase decoding, such as [43], which reported an accuracy of 72%. The successful classification of gait phases with high precision underscores the potential of CAMS BCI to enhance FES gait systems by detecting phase timing, promoting neuroplasticity and improving motor recovery outcomes. The ability to decode phases of gait with a simple visual stimulus makes this approach particularly valuable. Additionally, a relatively latency with a 500 ms detection window demonstrated excellent performance, making it suitable for (near) real-time applications. This system not only facilitates phase-level control, but also promotes active patient involvement in their therapy, thereby enhancing user engagement and participation. This contribution of a novel BCI paradigm with ability of decoding the phases of gait advances the field of neurorehabilitation by providing effective tools for gait recovery.

7.1.3 **Development of Novel Classification Algorithm for Asynchronous CAMS BCI Operation**

This thesis introduced an adapted complex convolutional neural network algorithm and demonstrated its effectiveness in decoding the visual responses from the CAMS stimulus. The C-CNN method achieved superior classification performance, particularly at shorter window lengths, significantly outperforming the CCA method. Notably, the C-CNN achieved an accuracy above 95% for W = 3 s using occipital electrodes, surpassing the 88% accuracy reported in another study utilizing CNN on a CAMS-like stimulus [120]. With high F1-scores and low false activation rates, this contribution establishes the C-CNN as a robust tool for real-time decoding of CAMS BCI responses, enhancing the reliability and effectiveness in

rehabilitation settings. The high accuracy and low latency of the C-CNN algorithm ensure that the system can provide timely and precise feedback to users. The ability to offer rapid feedback not only improves the system's functionality, but also actively involves patients in their rehabilitation process. This combination of accuracy, low latency, and active user participation makes the CAMS BCI system a promising tool in advancing neurorehabilitation.

7.2 Future Work

7.2.1 **CAMS in Augmented Reality and Assessing the Signal Characteristics**

One promising direction for future research involves implementing the CAMS BCI in an augmented reality (AR) environment. AR can provide a more immersive and engaging experience, potentially enhancing the effectiveness of the BCI intervention. By incorporating AR, users can interact with a virtual environment that closely mimics real-world scenarios, making the rehabilitation process more relevant and motivating. To thoroughly assess the signal characteristics of the CAMS BCI in an AR environment, it is essential to test various background conditions. These conditions could include different visual complexities, moving backgrounds, and varying levels of ambient light. By examining how these factors influence the EEG signals and BCI performance, we can optimize the AR environment to maximize user engagement and system accuracy. Previous studies have explored the integration of AR with SSMVEP BCIs, demonstrating the feasibility and benefits of such an approach [2], [128]. These findings provide a valuable foundation for integrating CAMS BCI with AR, highlighting the potential for improved signal characteristics and user experience.

7.2.2 **Developing a Closed loop Real-Time System with Feedback**

Another crucial area for future research is the development of a closed-loop real-time system incorporating feedback. Such a system would provide immediate, contextually relevant feedback to the user, enhancing the effectiveness of the BCI intervention and promoting

neuroplastic changes [129], [130]. To develop a comprehensive rehabilitation tool, the closed-loop system should include the decoding and integration of gait phases. By accurately identifying and responding to phases of the gait cycle (swing and stance), the system can provide precise and timely feedback, facilitating motor learning and recovery [43]. Incorporating the visual BCI detection within the closed-loop system can further enhance its functionality. For example, adjusting the difficulty of a task or real-time control of treadmill speed based on the user's neural responses can create a more adaptive and personalized rehabilitation experience.

7.2.3 **Translating the CAMS BCI with feedback in Individuals Post-Stroke**

Translating the CAMS BCI system into clinical practice for individuals post-stroke is a critical next step. This translation involves validating the system in clinical populations, including examining specific effects of CAMS BCI. A proposed avenue is incorporating Transcranial Magnetic Stimulation (TMS) based motor evoked potential (MEP) measurements into the protocol to provide deeper insights underlying the observed MRCP changes [61], [109] [108], [131]. By correlating changes in MEP with MRCP alterations, we can gain a deeper understanding of the neuroplastic effects facilitated by the CAMS BCI intervention. An essential factor is to explore the longevity of the intervention's effects, as the current thesis only explored short-term effects from a single session. By conducting follow-up assessments over extended periods, we can investigate how long the beneficial effects of the CAMS BCI last and whether booster sessions or maintenance protocols are necessary to sustain these effects. Understanding the long-term impact of the intervention will inform the design of more effective and durable rehabilitation programs.

7.2.4 **Conclusions**

The research presented in this thesis highlights the potential of the CAMS BCI paradigm in enhancing cortical excitability, decoding gait phases, and improving asynchronous

visual BCI performance. By providing a comprehensive analysis of the CAMS paradigm, this work contributes to existing knowledge and helps guide future clinical applications in neurorehabilitation. The promising results indicate potential for BCI applications that can enhance the quality of life for individuals with motor impairments, establishing CAMS paradigm as a valuable tool in the field of neurorehabilitation.

References

[1] A. Ravi, J. Tung, and N. Jiang, "Combined Action Observation , Motor Imagery and SSMVEP BCI Enhances Movement Related Cortical Potential," in *11th International IEEE EMBS Conference on Neural Engineering*, 2023.

[2] A. Ravi, J. Lu, S. Pearce, and N. Jiang, "Enhanced System Robustness of Asynchronous BCI in Augmented Reality Using Steady-State Motion Visual Evoked Potential," *IEEE Transactions on Neural Systems and Rehabilitation Engineering*, vol. 30, pp. 85–95, 2022, doi: 10.1109/TNSRE.2022.3140772.

[3] A. Ravi, J. Lu, S. Pearce, and N. Jiang, "Asynchronous SSMVEP BCI and Influence of Dynamic Background in Augmented Reality," in *2021 27th International Conference on Mechatronics and Machine Vision in Practice, M2VIP 2021*, Institute of Electrical and Electronics Engineers Inc., 2021, pp. 340–343. doi: 10.1109/M2VIP49856.2021.9665078.

[4] X. Zhang, G. Xu, A. Ravi, S. Pearce, and N. Jiang, "Can a highly accurate multi-class SSMVEP BCI induce sensory-motor rhythm in the sensorimotor area?," *J Neural Eng*, vol. 18, no. 3, 2021, doi: 10.1088/1741-2552/ab85b2.

[5] A. Ravi, N. H. Beni, J. Manuel, and N. Jiang, "Comparing user-dependent and user-independent training of CNN for SSVEP BCI," *J Neural Eng*, vol. 17, no. 2, Apr. 2020, doi: 10.1088/1741-2552/ab6a67.

[6] W. Johnson, O. Onuma, M. Owolabi, and S. Sachdev, "Stroke: A global response is needed," *Bull World Health Organ*, vol. 94, no. 9, pp. 634A-635A, 2016, doi: 10.2471/BLT.16.181636.

[7] R. Mane, T. Chouhan, and C. Guan, "BCI for stroke rehabilitation: Motor and beyond," *J Neural Eng*, vol. 17, no. 4, 2020, doi: 10.1088/1741-2552/aba162.

[8] O. Lennon *et al.*, "A systematic review establishing the current state-of-the-art, the limitations, and the desired checklist in studies of direct neural interfacing with robotic

gait devices in stroke rehabilitation," *Front Neurosci*, vol. 14, no. June, pp. 1–18, 2020, doi: 10.3389/fnins.2020.00578.

[9] J. M. Belda-Lois *et al.*, "Rehabilitation of gait after stroke: A review towards a top-down approach," *J Neuroeng Rehabil*, vol. 8, no. 1, p. 66, 2011, doi: 10.1186/1743-0003-8-66.

[10] R. Bogey and T. G. Hornby, "Gait training strategies utilized in poststroke rehabilitation: Are we really making a difference?," Nov. 2007. doi: 10.1310/tsr1406-1.

[11] F. Dierick *et al.*, "Hemorrhagic versus ischemic stroke: Who can best benefit from blended conventional physiotherapy with robotic-assisted gait therapy," *PLoS One*, vol. 12, no. 6, Jun. 2017, doi: 10.1371/journal.pone.0178636.

[12] N. Postol *et al.*, "The Metabolic Cost of Exercising with a Robotic Exoskeleton: A Comparison of Healthy and Neurologically Impaired People," *IEEE Transactions on Neural Systems and Rehabilitation Engineering*, vol. 28, no. 12, pp. 3031–3039, Dec. 2020, doi: 10.1109/TNSRE.2020.3039202.

[13] C. E. King, P. T. Wang, C. M. McCrimmon, C. C. Y. Chou, A. H. Do, and Z. Nenadic, "Brain-computer interface driven functional electrical stimulation system for overground walking in spinal cord injury participant," in *2014 36th Annual International Conference of the IEEE Engineering in Medicine and Biology Society, EMBC 2014*, Institute of Electrical and Electronics Engineers Inc., Nov. 2014, pp. 1238–1242. doi: 10.1109/EMBC.2014.6943821.

[14] C. E. King, P. T. Wang, C. M. McCrimmon, C. C. Chou, A. H. Do, and Z. Nenadic, "The feasibility of a brain-computer interface functional electrical stimulation system for the restoration of overground walking after paraplegia," *J Neuroeng Rehabil*, vol. 12, no. 1, pp. 1–11, 2015, doi: 10.1186/s12984-015-0068-7.

[15] J. Hidler *et al.*, "Multicenter randomized clinical trial evaluating the effectiveness of the Lokomat in subacute stroke," *Neurorehabil Neural Repair*, vol. 23, no. 1, pp. 5–13, 2009, doi: 10.1177/1545968308326632.

[16] F. A. S. Bright, N. M. Kayes, L. Worrall, and K. M. McPherson, “A conceptual review of engagement in healthcare and rehabilitation,” *Disabil Rehabil*, vol. 37, no. 8, pp. 643–654, Apr. 2015, doi: 10.3109/09638288.2014.933899.

[17] A. H. Lequerica, C. S. Donnell, and D. G. Tate, “Patient engagement in rehabilitation therapy: Physical and occupational therapist impressions,” *Disabil Rehabil*, vol. 31, no. 9, pp. 753–760, 2009, doi: 10.1080/09638280802309095.

[18] A. Pennycott, D. Wyss, H. Vallery, V. Klamroth-Marganska, and R. Riener, “Towards more effective robotic gait training for stroke rehabilitation: a review,” *Journal of Neuroengineering and Rehabilitation (JNER)*, vol. 9, p. 65, 2012, doi: 10.3929/ethz-b-000163684.

[19] E. García-Cossio *et al.*, “Decoding sensorimotor rhythms during robotic-assisted treadmill walking for brain computer interface (BCI) applications,” *PLoS One*, vol. 10, no. 12, pp. 1–21, 2015, doi: 10.1371/journal.pone.0137910.

[20] G. Bartur, K. Joubran, S. Peleg-Shani, J. J. Vatine, and G. Shahaf, “An EEG Tool for Monitoring Patient Engagement during Stroke Rehabilitation: A Feasibility Study,” *Biomed Res Int*, vol. 2017, 2017, doi: 10.1155/2017/9071568.

[21] B. Z. Allison, D. J. McFarland, G. Schalk, S. D. Zheng, M. M. Jackson, and J. R. Wolpaw, “Towards an independent brain-computer interface using steady state visual evoked potentials,” *Clinical Neurophysiology*, vol. 119, no. 2, pp. 399–408, 2008, doi: 10.1016/j.clinph.2007.09.121.

[22] D. Lesenfants *et al.*, “An independent SSVEP-based brain-computer interface in locked-in syndrome,” *J Neural Eng*, vol. 11, no. 3, p. 035002, 2014, doi: 10.1088/1741-2560/11/3/035002.

[23] X. Zhang, G. Xu, J. Xie, M. Li, W. Pei, and J. Zhang, “An EEG-driven Lower Limb Rehabilitation Training System for Active and Passive Co-stimulation,” *Proceedings of the Annual International Conference of the IEEE Engineering in Medicine and Biology*

Society, EMBS, vol. 2015-Novem, no. August, pp. 4582–4585, 2015, doi: 10.1109/EMBC.2015.7319414.

[24] L. F. Nicolas-Alonso and J. Gomez-Gil, "Brain computer interfaces, a review," *Sensors*, vol. 12, no. 2, pp. 1211–1279, 2012, doi: 10.3390/s120201211.

[25] X. Chen, Y. Wang, M. Nakanishi, X. Gao, T.-P. Jung, and S. Gao, "High-speed spelling with a noninvasive brain–computer interface," *Proceedings of the National Academy of Sciences*, vol. 112, no. 44, pp. E6058–E6067, 2015, doi: 10.1073/pnas.1508080112.

[26] Y. Wang, X. Gao, B. Hong, C. Jia, and S. Gao, "Brain-computer interfaces based on visual evoked potentials: Feasibility of practical system designs," Sep. 2008. doi: 10.1109/MEMB.2008.923958.

[27] R. Xu *et al.*, "A closed-loop brain-computer interface triggering an active ankle-foot orthosis for inducing cortical neural plasticity," *IEEE Trans Biomed Eng*, vol. 61, no. 7, pp. 2092–2101, 2014, doi: 10.1109/TBME.2014.2313867.

[28] G. Pfurtscheller and C. Neuper, "Motor imagery and direct brain-computer communication," *Proceedings of the IEEE*, vol. 89, no. 7, pp. 1123–1134, 2001, doi: 10.1109/5.939829.

[29] L. G. Hernandez-Rojas *et al.*, "Brain-Computer Interface Controlled Functional Electrical Stimulation: Evaluation With Healthy Subjects and Spinal Cord Injury Patients," *IEEE Access*, vol. 10, pp. 46834–46852, 2022, doi: 10.1109/ACCESS.2022.3170906.

[30] N. Mrachacz-Kersting *et al.*, "Efficient neuroplasticity induction in chronic stroke patients by an associative brain-computer interface," *J Neurophysiol*, vol. 115, no. 3, pp. 1410–1421, 2016, doi: 10.1152/jn.00918.2015.

[31] T. Nierhaus, C. Vidaurre, C. Sannelli, K. R. Mueller, and A. Villringer, "Immediate brain plasticity after one hour of brain–computer interface (BCI)," *Journal of Physiology*, vol. 599, no. 9, pp. 2435–2451, 2021, doi: 10.1113/JP278118.

[32] T. Mulder, “Motor imagery and action observation: Cognitive tools for rehabilitation,” *J Neural Transm*, vol. 114, no. 10, pp. 1265–1278, 2007, doi: 10.1007/s00702-007-0763-z.

[33] P. Barhoun *et al.*, “The role of the primary motor cortex in motor imagery: A theta burst stimulation study,” *Psychophysiology*, vol. 59, no. 10, Oct. 2022, doi: 10.1111/psyp.14077.

[34] N. Mrachacz-Kersting, S. R. Kristensen, I. K. Niazi, and D. Farina, “Precise temporal association between cortical potentials evoked by motor imagination and afference induces cortical plasticity,” *Journal of Physiology*, vol. 590, no. 7, pp. 1669–1682, 2012, doi: 10.1113/jphysiol.2011.222851.

[35] C. Vidaurre and B. Blankertz, “Towards a cure for BCI illiteracy,” *Brain Topogr*, vol. 23, no. 2, pp. 194–198, 2010, doi: 10.1007/s10548-009-0121-6.

[36] A. Singh, A. A. Hussain, S. Lal, and H. W. Guesgen, “A comprehensive review on critical issues and possible solutions of motor imagery based electroencephalography brain-computer interface,” *Sensors*, vol. 21, no. 6, pp. 1–35, 2021, doi: 10.3390/s21062173.

[37] L. R. Borges, A. B. Fernandes, L. P. Melo, R. O. Guerra, and T. F. Campos, “Action observation for upper limb rehabilitation after stroke,” *Cochrane Database Syst Rev*, vol. 10, no. 10, p. CD011887, 2018, doi: 10.1002/14651858.CD011887.pub2.

[38] G. Buccino and P. T. R. S. B, “Action observation treatment: a novel tool in neurorehabilitation,” *Phil. Trans. R. Soc. B*, no. April, 2014.

[39] D. L. Eaves, M. Riach, P. S. Holmes, and D. J. Wright, “Motor imagery during action observation: A brief review of evidence, theory and future research opportunities,” *Front Neurosci*, vol. 10, no. NOV, pp. 1–10, 2016, doi: 10.3389/fnins.2016.00514.

[40] D. J. Wright, J. Williams, and P. S. Holmes, “Combined action observation and imagery facilitates corticospinal excitability,” *Front Hum Neurosci*, vol. 8, no. November, pp. 1–9, 2014, doi: 10.3389/fnhum.2014.00951.

[41] J. R. Emerson, J. A. Binks, M. W. Scott, R. P. W. Kenny, and D. L. Eaves, "Combined action observation and motor imagery therapy: a novel method for post-stroke motor rehabilitation," *AIMS Neurosci*, vol. 5, no. 4, pp. 236–252, 2018, doi: 10.3934/neuroscience.2018.4.236.

[42] A. Hioka *et al.*, "Activation of mirror neuron system during gait observation in sub-acute stroke patients and healthy persons," *Journal of Clinical Neuroscience*, vol. 60, pp. 79–83, 2019, doi: 10.1016/j.jocn.2018.09.035.

[43] H. Yokoyama, N. Kaneko, K. Watanabe, and K. Nakazawa, "Neural decoding of gait phases during motor imagery and improvement of the decoding accuracy by concurrent action observation," *J Neural Eng*, vol. 18, no. 4, p. 46099, 2021, doi: 10.1088/1741-2552/ac07bd.

[44] J. Niu and N. Jiang, "Pseudo-online detection and classification for upper-limb movements," *J Neural Eng*, vol. 19, no. 3, Jun. 2022, doi: 10.1088/1741-2552/ac77be.

[45] F. Karimi, J. Kofman, N. Mrachacz-Kersting, D. Farina, and N. Jiang, "Detection of movement related cortical potentials from EEG using constrained ICA for brain-computer interface applications," *Front Neurosci*, 2017, doi: 10.3389/fnins.2017.00356.

[46] I. K. Niazi, N. Jiang, M. Jochumsen, J. F. Nielsen, K. Dremstrup, and D. Farina, "Detection of movement-related cortical potentials based on subject-independent training," *Med Biol Eng Comput*, vol. 51, no. 5, pp. 507–512, 2013, doi: 10.1007/s11517-012-1018-1.

[47] S. Tortora, S. Ghidoni, C. Chisari, S. Micera, and F. Artoni, "Deep learning-based BCI for gait decoding from EEG with LSTM recurrent neural network," *J Neural Eng*, vol. 17, no. 4, Aug. 2020, doi: 10.1088/1741-2552/ab9842.

[48] N. Tang, C. Guan, K. K. Ang, K. S. Phua, and E. Chew, "Motor imagery-assisted brain-computer interface for gait retraining in neurorehabilitation in chronic stroke," *Ann Phys Rehabil Med*, vol. 61, p. e188, 2018, doi: 10.1016/j.rehab.2018.05.431.

[49] A. R. C. Donati *et al.*, “Long-Term Training with a Brain-Machine Interface-Based Gait Protocol Induces Partial Neurological Recovery in Paraplegic Patients,” *Sci Rep*, vol. 6, no. August, pp. 1–16, 2016, doi: 10.1038/srep30383.

[50] J. R. Wolpaw, N. Birbaumer, D. J. McFarland, G. Pfurtscheller, and T. M. Vaughan, “Brain-computer interfaces for communication and control,” *Clinical Neurophysiology*, vol. 113, no. 6, pp. 767–791, 2002, doi: 10.1016/S1388-2457(02)00057-3.

[51] G. Schalk and E. C. Leuthardt, “Brain-computer interfaces using electrocorticographic signals,” *IEEE Rev Biomed Eng*, vol. 4, pp. 140–154, 2011, doi: 10.1109/RBME.2011.2172408.

[52] S. E. John, D. B. Grayden, and T. Yanagisawa, “The future potential of the Stentrode,” Oct. 03, 2019, *Taylor and Francis Ltd*. doi: 10.1080/17434440.2019.1674139.

[53] J. Mellinger *et al.*, “An MEG-based Brain-Computer Interface (BCI),” 2007.

[54] J. J. Vidal, “Toward Direct Brain-Computer Communication,” *Annu Rev Biophys Bioeng*, vol. 2, no. 1, pp. 157–180, 1973, doi: 10.1146/annurev.bb.02.060173.001105.

[55] Y. Jiang, X. Zhao, R. Abiri, S. Borhani, and E. W. Sellers, “A comprehensive review of EEG-based brain–computer interface paradigms,” *J Neural Eng*, vol. 16, no. 1, p. 011001, 2018, doi: 10.1088/1741-2552/aaf12e.

[56] W. Yan, G. Xu, J. Xie, M. Li, and Z. Dan, “Four novel motion paradigms based on steady-state motion visual evoked potential,” in *IEEE Transactions on Biomedical Engineering*, 2018. doi: 10.1109/TBME.2017.2762690.

[57] C. Guger *et al.*, “How many people could use an SSVEP BCI?,” *Front Neurosci*, vol. 6, no. NOV, pp. 2–7, 2012, doi: 10.3389/fnins.2012.00169.

[58] S. P. Kelly, E. Lalor, C. Finucane, and R. B. Reilly, “A comparison of covert and overt attention as a control option in a steady-state visual evoked potential-based brain computer interface,” pp. 4725–4728, 2005, doi: 10.1109/iembs.2004.1404308.

[59] H. Shibasaki and M. Hallett, “What is the Bereitschaftspotential?,” *Clinical Neurophysiology*, vol. 117, no. 11, pp. 2341–2356, 2006, doi: 10.1016/j.clinph.2006.04.025.

[60] M. Jochumsen *et al.*, “Quantification of movement-related EEG correlates associated with motor training: A study on movement-related cortical potentials and sensorimotor rhythms,” *Front Hum Neurosci*, vol. 11, no. December, pp. 1–12, 2017, doi: 10.3389/fnhum.2017.00604.

[61] A. L. Smith and W. R. Staines, “Externally cued inphase bimanual training enhances preparatory premotor activity,” *Clinical Neurophysiology*, vol. 123, no. 9, pp. 1846–1857, Sep. 2012, doi: 10.1016/j.clinph.2012.02.060.

[62] J. S. Thacker, L. E. Middleton, W. E. McIlroy, and W. R. Staines, “The influence of an acute bout of aerobic exercise on cortical contributions to motor preparation and execution,” *Physiol Rep*, vol. 2, no. 10, pp. 1–11, 2014, doi: 10.14814/phy2.12178.

[63] O. Yilmaz *et al.*, “Movement related cortical potentials change after EEG-BMI rehabilitation in chronic stroke,” *International IEEE/EMBS Conference on Neural Engineering, NER*, pp. 73–76, 2013, doi: 10.1109/NER.2013.6695874.

[64] M. Butt, G. Naghdy, F. Naghdy, G. Murray, and H. Du, “Assessment of Neuroplasticity Using EEG Signal in Rehabilitation of Brain Stem Stroke Patients,” *Canadian Conference on Electrical and Computer Engineering*, vol. 2020-Augus, no. c, pp. 22–25, 2020, doi: 10.1109/CCECE47787.2020.9255731.

[65] M. Butt, G. Naghdy, F. Naghdy, and G. Murray, “Effect of Post-Stroke Motor Training on EEG Movement-Related Cortical Potentials,” pp. 1–25, 2020, [Online]. Available: https://doi.org/10.21203/rs.3.rs-50667/v1

[66] M. Butt, G. Naghdy, F. Naghdy, G. Murray, and H. Du, “Effect of Robot-Assisted Training on EEG-Derived Movement-Related Cortical Potentials for Post-Stroke Rehabilitation-A Case Series Study,” *IEEE Access*, vol. 9, pp. 154143–154155, 2021, doi: 10.1109/ACCESS.2021.3127939.

[67] G. Rizzolatti and L. Craighero, “The mirror-neuron system,” *Annu Rev Neurosci*, vol. 27, pp. 169–192, 2004, doi: 10.1146/annurev.neuro.27.070203.144230.

[68] J. J. Q. Zhang, K. N. K. Fong, N. Welage, and K. P. Y. Liu, “The activation of the mirror neuron system during action observation and action execution with mirror visual feedback in stroke: A systematic review,” *Neural Plast*, vol. 2018, no. December 2019, 2018, doi: 10.1155/2018/2321045.

[69] D. Regan, “Some Characteristics of Average Steady-State,” *Electroencephalogr Clin Neurophysiol*, pp. 238–248, 1965.

[70] W. Yan *et al.*, “Steady-State Motion Visual Evoked Potential (SSMVEP) based on equal luminance colored enhancement,” *PLoS One*, vol. 12, no. 1, pp. 1–18, 2017, doi: 10.1371/journal.pone.0169642.

[71] X. Zhang *et al.*, “A Convolutional Neural Network for the Detection of Asynchronous Steady State Motion Visual Evoked Potential,” *IEEE Transactions on Neural Systems and Rehabilitation Engineering*, vol. PP, no. c, pp. 1–1, 2019, doi: 10.1109/TNSRE.2019.2914904.

[72] I. Volosyak, D. Valbuena, T. Lüth, T. Malechka, and A. Gräser, “BCI demographics II: How many (and What Kinds of) people can use a high-frequency SSVEP BCI?,” *IEEE Transactions on Neural Systems and Rehabilitation Engineering*, vol. 19, no. 3, pp. 232–239, 2011, doi: 10.1109/TNSRE.2011.2121919.

[73] X. Zhang, W. Hou, X. Wu, S. Feng, and L. Chen, “A Novel Online Action Observation-Based Brain-Computer Interface That Enhances Event-Related Desynchronization,” *IEEE Transactions on Neural Systems and Rehabilitation Engineering*, vol. 29, pp. 2605–2614, 2021, doi: 10.1109/TNSRE.2021.3133853.

[74] L. Huang, H. Wang, and Y. Wang, “Removal of Ocular Artifact from EEG Using Constrained ICA,” *Advanced Engineering Forum*, vol. 2–3, pp. 105–110, 2011, doi: 10.4028/www.scientific.net/aef.2-3.105.

[75] F. Lotte *et al.*, “A Review of Classification Algorithms for EEG-based Brain-Computer Interfaces: A 10-year Update,” *J Neural Eng*, pp. 0–20, 2018, doi: 10.1088/1741-2552/aab2f2.

[76] Zhonglin Lin, Changshui Zhang, Wei Wu, and Xiaorong Gao, “Frequency Recognition Based on Canonical Correlation Analysis for SSVEP-Based BCIs,” *IEEE Trans Biomed Eng*, vol. 53, no. 12, pp. 2610–2614, 2006, doi: 10.1109/TBME.2006.886577.

[77] G. Bin, X. Gao, Z. Yan, B. Hong, and S. Gao, “An online multi-channel SSVEP-based brain-computer interface using a canonical correlation analysis method,” *J Neural Eng*, vol. 6, no. 4, p. 046002, 2009, doi: 10.1088/1741-2560/6/4/046002.

[78] X. Chen, Y. Wang, S. Gao, T. P. Jung, and X. Gao, “Filter bank canonical correlation analysis for implementing a high-speed SSVEP-based brain-computer interface,” *J Neural Eng*, vol. 12, no. 4, p. 046008, 2015, doi: 10.1088/1741-2560/12/4/046008.

[79] M. Nakanishi, Y. Wang, X. Chen, Y. Te Wang, X. Gao, and T. P. Jung, “Enhancing detection of SSVEPs for a high-speed brain speller using task-related component analysis,” *IEEE Trans Biomed Eng*, vol. 65, no. 1, pp. 104–112, 2018, doi: 10.1109/TBME.2017.2694818.

[80] Y. Wang, M. Nakanishi, Y. Te Wang, and T. P. Jung, “Enhancing detection of steady state visual evoked potentials using individual training data,” *2014 36th Annual International Conference of the IEEE Engineering in Medicine and Biology Society, EMBC 2014*, pp. 3037–3040, 2014, doi: 10.1109/EMBC.2014.6944263.

[81] M. Nakanishi, Y. Wang, Y. Te Wang, and T. P. Jung, “A comparison study of canonical correlation analysis based methods for detecting steady-state visual evoked potentials,” *PLoS One*, vol. 10, no. 10, pp. 1–18, 2015, doi: 10.1371/journal.pone.0140703.

[82] P. Yuan, X. Chen, Y. Wang, X. Gao, and S. Gao, “Enhancing performances of SSVEP-based brain-computer interfaces via exploiting inter-subject information,” *J Neural Eng*, vol. 12, no. 4, 2015, doi: 10.1088/1741-2560/12/4/046006.

[83] R. Zerafa, T. Camilleri, O. Falzon, and K. P. Camilleri, "To train or not to train? A survey on training of feature extraction methods for SSVEP-based BCIs," *J Neural Eng*, vol. 15, no. 5, p. 051001, 2018, doi: 10.1088/1741-2552/aaca6e.

[84] O. Faust, Y. Hagiwara, T. J. Hong, O. S. Lih, and U. R. Acharya, "Deep learning for healthcare applications based on physiological signals: A review," *Comput Methods Programs Biomed*, vol. 161, pp. 1–13, 2018, doi: 10.1016/j.cmpb.2018.04.005.

[85] A. Craik, Y. He, and J. L. (Pepe) Contreras-Vidal, "Deep learning for Electroencephalogram (EEG) classification tasks: A review," *J Neural Eng*, 2019, doi: 10.1088/1741-2552/ab0ab5.

[86] Y. Roy, H. Banville, I. Albuquerque, A. Gramfort, T. H. Falk, and J. Faubert, "Deep learning-based electroencephalography analysis: A systematic review," Aug. 14, 2019, *Institute of Physics Publishing*.

[87] V. J. Lawhern, A. J. Solon, N. R. Waytowich, S. M. Gordon, C. P. Hung, and B. J. Lance, "EEGNet: a compact convolutional neural network for EEG-based brain–computer interfaces," *J Neural Eng*, vol. 15, no. 5, p. 056013, 2018, doi: 10.1088/1741-2552/aace8c.

[88] A. Supratak, H. Dong, C. Wu, and Y. Guo, "DeepSleepNet: A model for automatic sleep stage scoring based on raw single-channel EEG," *IEEE Transactions on Neural Systems and Rehabilitation Engineering*, vol. 25, no. 11, pp. 1998–2008, Nov. 2017.

[89] N. S. Kwak, K. R. Müller, and S. W. Lee, "A convolutional neural network for steady state visual evoked potential classification under ambulatory environment," *PLoS One*, vol. 12, no. 2, pp. 1–20, 2017, doi: 10.1371/journal.pone.0172578.

[90] T.-H. Nguyen and W.-Y. Chung, "A Single-Channel SSVEP-Based BCI Speller using Deep Learning," *IEEE Access*, vol. 7, pp. 1–1, 2018, doi: 10.1109/ACCESS.2018.2886759.

[91] N. Waytowich *et al.*, “Compact convolutional neural networks for classification of asynchronous steady-state visual evoked potentials,” *J Neural Eng*, vol. 15, no. 6, p. 066031, 2018, doi: 10.1088/1741-2552/aae5d8.

[92] A. Ravi, N. Heydari, and N. Jiang, “User-Independent SSVEP BCI Using Complex FFT Features and CNN Classification,” *2019 IEEE International Conference on Systems, Man, and Cybernetics, SMC 2019*, pp. 4175–4180, 2019.

[93] M. Jochumsen, M. S. Navid, U. Rashid, H. Haavik, and I. K. Niazi, “EMG- Versus EEG-Triggered Electrical Stimulation for Inducing Corticospinal Plasticity,” *IEEE Trans Neural Syst Rehabil Eng*, vol. 27, no. 9, pp. 1901–1908, 2019, doi: 10.1109/TNSRE.2019.2932104.

[94] S. Tortora, L. Tonin, C. Chisari, S. Micera, E. Menegatti, and F. Artoni, “Hybrid Human-Machine Interface for Gait Decoding Through Bayesian Fusion of EEG and EMG Classifiers,” *Front Neurorobot*, vol. 14, Nov. 2020, doi: 10.3389/fnbot.2020.582728.

[95] J. L. Contreras-Vidal *et al.*, “Neural Decoding of Robot-Assisted Gait during Rehabilitation after Stroke,” *Am J Phys Med Rehabil*, vol. 97, no. 8, pp. 541–550, 2018, doi: 10.1097/PHM.0000000000000914.

[96] M. Jaqueline da Cunha, K. D. Rech, A. P. Salazar, and A. S. Pagnussat, “Functional electrical stimulation of the peroneal nerve improves post-stroke gait speed when combined with physiotherapy. A systematic review and meta-analysis,” Jan. 01, 2021, *Elsevier Masson s.r.l.* doi: 10.1016/j.rehab.2020.03.012.

[97] M. Jochumsen *et al.*, “Investigation of optimal afferent feedback modality for inducing neural plasticity with a self-paced brain-computer interface,” *Sensors (Switzerland)*, vol. 18, no. 11, pp. 1–13, 2018, doi: 10.3390/s18113761.

[98] N. Mrachacz-kersting, S. R. Kristensen, I. K. Niazi, and D. Farina, “Precise temporal association between cortical potentials evoked by motor imagination and afference

induces cortical plasticity," vol. 7, pp. 1669–1682, 2012, doi: 10.1113/jphysiol.2011.222851.

[99] P. Wei, J. Zhang, P. Wei, B. Wang, and J. Hong, "Different sEMG and EEG Features Analysis for Gait phase Recognition," *Proceedings of the Annual International Conference of the IEEE Engineering in Medicine and Biology Society, EMBS*, vol. 2020-July, pp. 1002–1006, 2020, doi: 10.1109/EMBC44109.2020.9175655.

[100] N. Kaneko, H. Yokoyama, Y. Masugi, K. Watanabe, and K. Nakazawa, "Phase dependent modulation of cortical activity during action observation and motor imagery of walking: An EEG study," *Neuroimage*, vol. 225, Jan. 2021, doi: 10.1016/j.neuroimage.2020.117486.

[101] S. Solnik, P. Rider, K. Steinweg, P. Devita, and T. Hortobágyi, "Teager-Kaiser energy operator signal conditioning improves EMG onset detection," *Eur J Appl Physiol*, vol. 110, no. 3, pp. 489–498, 2010, doi: 10.1007/s00421-010-1521-8.

[102] A. Gramfort *et al.*, "MEG and EEG data analysis with MNE-Python," *Front Neurosci*, p. 267, 2013, doi: 10.3389/fnins.2013.00267.

[103] A. Shakeel, M. S. Navid, M. N. Anwar, S. Mazhar, M. Jochumsen, and I. K. Niazi, "A review of techniques for detection of movement intention using movement-related cortical potentials," 2015, *Hindawi Limited*. doi: 10.1155/2015/346217.

[104] G. Pfurtscheller and F. H. Lopes Da Silva, "Event-related EEG/MEG synchronization and desynchronization: Basic principles," *Clinical Neurophysiology*, vol. 110, no. 11, pp. 1842–1857, 1999, doi: 10.1016/S1388-2457(99)00141-8.

[105] K. Aono *et al.*, "Relationship between event-related desynchronization and cortical excitability in healthy subjects and stroke patients," *Tokai Journal of Experimental and Clinical Medicine*, vol. 38, no. 4, pp. 123–128, 2013.

[106] E. Maris and R. Oostenveld, "Nonparametric statistical testing of EEG- and MEG-data," *J Neurosci Methods*, vol. 164, no. 1, pp. 177–190, 2007, doi: 10.1016/j.jneumeth.2007.03.024.

[107] S. M. Smith and T. E. Nichols, “Threshold-free cluster enhancement: Addressing problems of smoothing, threshold dependence and localisation in cluster inference,” *Neuroimage*, vol. 44, no. 1, pp. 83–98, Jan. 2009, doi: 10.1016/j.neuroimage.2008.03.061.

[108] F. Ferreri and P. M. Rossini, “TMS and TMS-EEG techniques in the study of the excitability, connectivity, and plasticity of the human motor cortex,” *Rev Neurosci*, vol. 24, no. 4, pp. 431–442, 2013, doi: 10.1515/revneuro-2013-0019.

[109] J. L. Neva, A. M. Singh, M. Vesia, and W. R. Staines, “Selective modulation of left primary motor cortex excitability after continuous theta burst stimulation to right primary motor cortex and bimanual training,” *Behavioural Brain Research*, vol. 269, pp. 138–146, Aug. 2014, doi: 10.1016/j.bbr.2014.04.041.

[110] S. Ge, H. Liu, P. Lin, J. Gao, C. Xiao, and Z. Li, “Neural basis of action observation and understanding from first- and third-person perspectives: An fMRI study,” *Front Behav Neurosci*, vol. 12, no. November, pp. 1–10, 2018, doi: 10.3389/fnbeh.2018.00283.

[111] A. D. Nordin, W. D. Hairston, and D. P. Ferris, “Faster Gait Speeds Reduce Alpha and Beta EEG Spectral Power from Human Sensorimotor Cortex,” *IEEE Trans Biomed Eng*, vol. 67, no. 3, pp. 842–853, Mar. 2020, doi: 10.1109/TBME.2019.2921766.

[112] F. Pedregosa *et al.*, “Scikit-learn: Machine Learning in Python,” Jan. 2012, [Online]. Available: http://arxiv.org/abs/1201.0490

[113] O. Ledoit and M. Wolf, “Honey, I Shrunk the Sample Covariance Matrix,” 2003.

[114] G. Thut, A. Nietzel, S. A. Brandt, and A. Pascual-Leone, “α-Band electroencephalographic activity over occipital cortex indexes visuospatial attention bias and predicts visual target detection,” *Journal of Neuroscience*, vol. 26, no. 37, pp. 9494–9502, Sep. 2006, doi: 10.1523/JNEUROSCI.0875-06.2006.

[115] D. Tang, L. Hu, Y. Lei, H. Li, and A. Chen, “Frontal and occipital-parietal alpha oscillations distinguish between stimulus conflict and response conflict,” *Front Hum Neurosci*, vol. 9, no. AUGUST, pp. 1–12, Aug. 2015, doi: 10.3389/fnhum.2015.00433.

[116] M. Ahn, H. Cho, S. Ahn, and S. C. Jun, “High theta and low alpha powers may be indicative of BCI-illiteracy in motor imagery,” *PLoS One*, vol. 8, no. 11, Nov. 2013, doi: 10.1371/journal.pone.0080886.

[117] S. Biswal, H. Sun, B. Goparaju, M. Brandon Westover, J. Sun, and M. T. Bianchi, “Expert-level sleep scoring with deep neural networks,” *Journal of the American Medical Informatics Association*, vol. 25, no. 12, pp. 1643–1650, Dec. 2018.

[118] S. Chambon, M. N. Galtier, P. J. Arnal, G. Wainrib, and A. Gramfort, “A Deep Learning Architecture for Temporal Sleep Stage Classification Using Multivariate and Multimodal Time Series,” *IEEE Transactions on Neural Systems and Rehabilitation Engineering*, vol. 26, no. 4, pp. 758–769, Apr. 2018, doi: 10.1109/TNSRE.2018.2813138.

[119] G. M. Clements, M. Gyurkovics, K. A. Low, D. M. Beck, M. Fabiani, and G. Gratton, “Dynamics of alpha suppression and enhancement may be related to resource competition in cross-modal cortical regions,” *Neuroimage*, vol. 252, May 2022, doi: 10.1016/j.neuroimage.2022.119048.

[120] X. Zhang, G. Xu, A. Ravi, W. Yan, and N. Jiang, “Fusing Frontal and Occipital EEG Features to Detect ‘brain Switch’ by Utilizing Convolutional Neural Network,” *IEEE Access*, vol. 7, pp. 82817–82825, 2019, doi: 10.1109/ACCESS.2019.2924185.

[121] R. Meers, H. E. Nuttall, and S. Vogt, “Motor imagery alone drives corticospinal excitability during concurrent action observation and motor imagery,” *Cortex*, vol. 126, pp. 322–333, May 2020, doi: 10.1016/j.cortex.2020.01.012.

[122] D. Liu, W. Chen, Z. Pei, and J. Wang, “A brain-controlled lower-limb exoskeleton for human gait training,” *Review of Scientific Instruments*, vol. 88, no. 10, 2017, doi: 10.1063/1.5006461.

[123] S. Tortora *et al.*, "Effect of Lower Limb Exoskeleton on the Modulation of Neural Activity and Gait Classification," *IEEE Transactions on Neural Systems and Rehabilitation Engineering*, vol. 31, pp. 2988–3003, 2023, doi: 10.1109/TNSRE.2023.3294435.

[124] Z. Lin, C. Zhang, W. Wu, and X. Gao, "Frequency recognition based on canonical correlation analysis for SSVEP-Based BCIs," *IEEE Trans Biomed Eng*, vol. 54, no. 6, pp. 1172–1176, 2007, doi: 10.1109/TBME.2006.889197.

[125] A. Ravi, N. Heydari, and N. Jiang, "User-Independent SSVEP BCI Using Complex FFT Features and CNN Classification," *2019 IEEE International Conference on Systems, Man, and Cybernetics, SMC 2019*, pp. 4175–4180, 2019.

[126] A. Ravi, "Enhancing the Decoding Performance of Steady-State Visual Evoked Potentials based Brain-Computer Interface," *Thesis*, 2019.

[127] S. Ioffe and C. Szegedy, "Batch Normalization: Accelerating Deep Network Training by Reducing Internal Covariate Shift," *32nd International Conference on Machine Learning*, vol. 37, pp. 448–456, 2015, doi: 10.1080/17512786.2015.1058180.

[128] H. Si-Mohammed *et al.*, "Towards BCI-based Interfaces for Augmented Reality: Feasibility, Design and Evaluation," *IEEE Trans Vis Comput Graph*, vol. 26, no. 3, pp. 1608–1621, 2018, doi: 10.1109/tvcg.2018.2873737.

[129] Y. Ono *et al.*, "Hand Motor Rehabilitation of Patients with Stroke Using Physiologically Congruent Neurofeedback," *Proceedings - 2018 IEEE International Conference on Systems, Man, and Cybernetics, SMC 2018*, pp. 39–44, 2019, doi: 10.1109/SMC.2018.00016.

[130] A. Vourvopoulos *et al.*, "Effects of a Brain-Computer Interface With Virtual Reality (VR) Neurofeedback: A Pilot Study in Chronic Stroke Patients," *Front Hum Neurosci*, vol. 13, no. June, pp. 1–17, 2019, doi: 10.3389/fnhum.2019.00210.

[131] G. Koch, “The new era of TMS-EEG: Moving towards the clinical practice,” *Clinical Neurophysiology*, vol. 130, no. 5, pp. 791–792, 2019, doi: 10.1016/j.clinph.2019.02.004.

Appendix A

A.1 Open Sourced Code Related to the Thesis

1. Github codebase to generate the CAMS stimulus

   URL: https://github.com/uwnrelab/cams_bci_stimulus_generation

2. Github codebase of the C-CNN architecture

   URL: https://github.com/aaravindravi/Brain-computer-interfaces/tree/master/scripts

3. Github repo of codebase used to develop the experiment data collection and stimulus presentation interface

   URL: https://github.com/WILLSNIU186/EEG-Online-Experiment-GUI